Degradation of Dye Using Compounds Having Barium Titanium Constituent

Petdaw Karoh

A Thesis Submitted in Partial Fulfillment of the Requirements for the Degree of
Master of Science in Inorganic Chemistry
Prince of Songkla University

2014

Thesis Title   Degradation of dye using compounds having barium titanium constituents

Author   Miss Petdaw Karoh

Major Program   Inorganic Chemistry

Major Advisor

………………………………………

(Assoc. Prof. Dr. Sumpun Wongnawa)

Examining Committee

………………………….Chairperson

(Dr. Anob Kantacha)

………………………………………

(Assoc. Prof. Dr. Sumpun Wongnawa)

………………………………………

(Assoc. Prof. Dr. Sumetha Suwanboon)

………………………………………

(Dr. Uraiwan Sirimahachai)

The Graduate School, Prince of Songkla University, has approved this thesis as partial fulfillment of the requirements for the Master of Science Degree in Inorganic Chemistry.

………………………………………

(Assoc. Prof. Dr. Teerapol Srichana)

Dean of Graduate School

This is to certify that the work here submitted in the result of the candidate's own investigations. Due acknowledgement has been made of any assistance received.

……………………………….Signature

(Assoc. Prof. Dr. Sumpun Wongnawa)

Major Advisor

……………………………….Signature

(Miss Petdaw Karoh)

Candidate

I hereby certify that this work has no already been accepted in substance for any degree, and is not being currently submitted in candidature for any degree.

……………………………….Signature

(Miss Petdaw Karoh)

Candidate

ชื่อวิทยานิพนธ์	การกำจัดสีย้อมโดยใช้สารประกอบที่มีแบเรียมไทเทเนียมเป็นองค์ประกอบ
ผู้เขียน	นางสาวเพชรดาว กาเราะ
สาขาวิชา	เคมีอนินทรีย์
ปีการศึกษา	2556

บทคัดย่อ

งานวิจัยนี้ทำการเตรียมสารประกอบสามชนิดที่มีแบเรียมและไทเทเนียมเป็นองค์ประกอบ คือ BTO (แบเรียมไทเทเนียมออกซาเลต), TiO_2-BaC_2O_4 (สารผสมระหว่างไทเทเนียมไดออกไซด์และแบเรียมออกซาเลต), TiO_2-BT (สารผสมระหว่างไทเทเนียมไดออกไซด์และแบเรียมไทเทเนต) (สารผสมสองชนิดหลังนี้มักเป็นที่รู้จักกันในชื่อ ตัวเร่งร่วม) ทำการศึกษาลักษณะของสารตัวอย่างด้วยเทคนิค XRD, SEM, UV-DRS, FT-IR และ UV-Vis พร้อมทั้งทดสอบความสามารถในการเป็นโฟโตคะตะลิสต์ด้วยการสลายสีย้อม orange II sodium salt ภายใต้ช่วงแสงอัลตร้าไวโอเลตและช่วงแสงที่มองเห็น โดยทำการทดลองที่ความเข้มข้นต่างๆดังนี้ 2.0×10^{-5} , 2.5×10^{-5} , 3.0×10^{-5} M และเปรียบเทียบกับสารไทเทเนียมไดออกไซด์ทางการคือ อนาเทส สำหรับที่ความเข้มข้น 2.5×10^{-5} M ใช้ดีกัสซ่า P25 ร่วมเปรียบเทียบด้วย เนื่องจากจากการทดสอบที่ 2.5×10^{-5} M พบว่าอนาเทส และ ดีกัสซ่า P25 มีประสิทธิภาพใกล้เคียงกัน ดังนั้นที่ความเข้มข้นอื่นๆจึงใช้เฉพาะอนาเทสเป็นตัวเปรียบเทียบเนื่องจากอนาเทสหาง่ายและราคาถูกกว่า

สารตัวอย่างที่สังเคราะห์เมื่อนำมาใช้ในกระบวนการโฟโตคะตะไลติก มีข้อดีกว่าการใช้ไทเทเนียมไดออกไซด์ทางการค้า เนื่องจากไม่มีการฟุ้งของสารละลายเป็นคอลลอลยด์เหมือนไทเทเนียมไดออกไซด์ทางการค้า จึงง่ายในการเก็บตัวอย่างเมื่อเสร็จสิ้นการทดลอง นอกจากนี้ยังได้ศึกษาผลของค่าพี-เอช ที่เหมาะสมที่สามารถสลายสีย้อมได้ดีขึ้น รวมทั้งได้ศึกษาการนำกลับมาใช้ใหม่ด้วย

Thesis Title   Degradation of dye using compounds having barium titanium constituents

Author   Miss Petdaw Karoh

Major Program   Inorganic Chemistry

Academic Year   2013

Abstract

In this study three compounds having barium and titanium constituents were prepared: BTO (barium titanium oxalate), TiO_2-BaC_2O_4 (mixture of titanium dioxide and barium oxalate), TiO_2-BT (mixture of titanium dioxide and barium titanate). (Mixture of two compounds usually has been known as co-catalyst). The prepared samples were characterized by XRD, SEM, UV-DRS, FT-IR, and UV-Vis techniques. The photocatalytic activity was evaluated by decolorizing orange II sodium salt under UV and visible light. The photocatalytic efficiency of the three samples were compared with commercial TiO_2 (anatase) at 3 concentrations: 2.0×10^{-5}, 2.5×10^{-5}, and 3.0×10^{-5} M. Degussa P25 was compared at only one concentration (2.5×10^{-5} M) because the efficiencies of anatase and Degussa P25 were very similar so anatase was chosen and used in other concentrations due to its less expensive and readily available.

The BTO and co-catalyst (TiO_2-BaC_2O_4 and TiO_2-BT) have advantage over the commercial titanium dioxide in one aspect that the catalyst could be easily collected after the completion of photocatalytic study. Unless the co-catalyst was used, the solution was usually cloudy due to colloid formation. The optimum pH and recycling usage were also investigated.

Acknowledgements

The relevance of the research work to Thailand

Synthetic dyes are extensively used in the industries because of their simple dyeing procedure and good stability but the release of these coloring agents into the eco-system has caused a big pollution problem of water contamination. The techniques used for color removal such as activated carbon, filtration, and coagulation. Each method has both advantages and disadvantages. For example, the use of charcoal is technically easy but has high waste disposal cost. Coagulation using alums, ferric salts or limes is a low cost process, but all these methods have a major disadvantage of simply transferring the pollutants from one phase to another phase rather than destroying them and sometime the by-products may be more toxic than the dye itself. Biological treatment is a proven method and cost effective. However, it has been reported that majority of dyes are adsorbed on the sludge and very long degraded times, due to the biorecalcitrant nature of these dyes molecules. In recent years, semiconductor photocatalysis has been intensively investigated for its application to environmental pollutants degradation. Titanium dioxide (TiO_2) has been the most widely use and investigated photocatalyst and not toxic but TiO_2 in waste water treatment is limited due to colloid formation and difficult to collect. The purpose of this thesis is to find the method to improve property of TiO_2 by preparing BTO and cocatalyst TiO_2. The photocatalyst model pollutant was orange II sodium salt dye. The co-catalyst and BTO was synthesized to improve the photocatalytic activity and the possible application of wastewater treatment in Thailand.

CONTENTS

CONTENTS (Continued)

CONTENTS (Continued)

List of Figures

List of Figures (Continued)

List of Figures (Continued)

List of Figures (Continued)

List of Figures (Continued)

List of Tables

List of Abbreviation

BTO	=	Barium titanium oxalate
BT	=	Barium titanate
eV	=	Electron volt
G	=	Gram
H	=	Hour
FWHM	=	The full width at half-maximum
Nm	=	Nanometer
Min	=	Minute
mL	=	Milliliter
Mol/L	=	Mole per liter
^{o}C	=	Degree Celsius
T	=	Temperature
λ	=	Wavelength
λ_{Max}	=	Maximum wavelength
TiO_2-BaC_2O_4	=	Coupled of Titanium dioxide and barium titanium oxalate
TiO_2-BT	=	Coupled of Titanium dioxide and barium titanate
TiO_2	=	Titanium dioxide
E_g	=	Band gap energy
Pzc	=	Point of zero charge
CB	=	Conduction band
VB	=	Valence band
BET	=	Brunauer-Emmett-Teller
DRS	=	Diffused reflectance spectroscopy
FT-IR	=	Fourier-transformed infrared spectroscopy
SEM	=	Scanning electron microscopy
UV-Vis	=	Ultraviolet-Visible absorption spectroscopy
XRD	=	X-ray diffraction

CHAPTER 1

Introduction

1.1 Introduction

Dye pollutants from the textile industry are an important source of environmental contamination. Large quantities of dyes are extensively used in the fundamental processing step of textile industries. It is estimated that *ca.* 1-15% of the dye is lost during the dying processes and released as wastewater (Zainal, *et al*., 2005). The colour is usually the first contaminant to be recognized in wastewater, which generated by using synthetic dyes in the industrials. Considering both volumes discharged and effluent compositions, the wastewater generated by the textile industry is rated as one of the most polluting among all industry sectors. Given the great variety of fibres, dyes, process aids and finishing products in use, the textile industry generated wastewater of great chemical complexity, diversity and volume (Bizani, *et al.,* 2006). Synthetic dyes are extensively used in the textile industries because of their simple dyeing procedure and good stability during washing process. Synthetic dyes, classified by their chromophores have different and stable chemical structures to meet various coloring requirements (Torr, *et al.,* 2006). The release of the wastewater into the ecosystem, for instance, as much as many million gallons discharged per year to wastewater treatment systems, is a dramatic source of aesthetic pollution, eutrophication, and perturbation in aquatic life. Therefore, the removal of colored wastewater is a necessary before being released to the environmental (Sauer, *et al.,* 2002).

The other techniques used for color removal such as activated carbon, filtration, and coagulation. Each method has few advantages and disadvantages. For example, the use of charcoal is technically easy but has high waste disposal cost. Coagulation using alums, ferric salts or limes is a low cost process, but all these methods have a major disadvantage of simply transferring the pollutants from one

phase to another phase rather than destroying them and sometime the by-products may be more toxic than the dye itself. Biological treatment is a proven method and cost effective. However, it has been reported that majority of dyes are adsorbed on the sludge having very long degraded times, due to the biorecalcitrant nature of the molecule of these dyes. This leads to the search for highly effective method to degrade the dye into environmentally compatible products (Torr, *et al.,* 2006).

Semiconductor photocatalysis has received intensive attention in environmental purification due to its simplicity, mild reaction conditions, and low energy consumption (Yu, *et al*., 2011). Barium titanium oxalate (BTO) is semiconductor that is widely employed as a precursor used to obtain barium titanate (BT) with better physical and chemical characteristics. BT is an environmentally friendly material and is a good candidate for various applications including capacitor, ultrasonic transducer, piezoelectric device, and semiconductor (Khollam, *et al.,* 2002). Research on BTO in the decomposition of dye has appeared only a few. The implementation of the decomposition of dye with BTO is interesting because of the relatively simple synthetic method and similar band gap energy to titanium dioxide which is the prevailing photocatalyst used for this purpose.

To improve its photocatalytic performance two methods have been developed. The first is to cause changes in its physical property, such as morphology and particle size. The second method for enhancing its photocatalytic efficiency is by noble metal deposition, metal ion doping, semiconductor coupling or nonmetal element doping (Yu, *et al*., 2011). Semiconductor oxides such as ZnO and TiO_2 have been recognized to be preferable materials for photocatalytic processes, due to their high photosensitivity, non-toxic nature, low cost and chemical stability. However, ZnO and TiO_2 can only absorb a small portion of solar spectrum in the UV region, because of their wide band gaps. Therefore, the effective utilization of solar energy still remains a challenge in photocatalytic applications. There have been various attempts to extend the absorption range of ZnO and TiO_2 to visible light region, which include noble metal deposition, transition-metal ions doping, coupled semiconductor systems, etc. In the past several years, coupled semiconductors formed by ZnO and other metal oxides or sulfides such as TiO_2, SnO_2, Fe_2O_3, WO_3, CdS, ZnS, CuO and

so on, have been reported. The results showed that coupling of different semiconductor oxides can reduce its band gap, extend its absorption range to visible light region, promote electron-hole pair separation under irradiation and, consequently, achieve a higher photocatalytic activity (Chao, *et al.*, 2010).

The aim of our study is to prepare the compounds having barium titanium constituents such as 1) barium titanium oxalate (BTO) and study their photocatalytic activities, 2) TiO_2 photocatalyst combination with barium oxalate and barium titanate for improvement photocatalyst of TiO_2 and study their photocatalytic activities. Orange II sodium salt, a mono-azo dye soluble in water and widely used in industry (Maruska, *et al.,* 1978), was chosen as model pollutant.

1.2 Review of literatures
1.2.1 Heterogeneous Photocatalysis

Heterogeneous photocatalysis is a rapidly expanding technology for water and air treatment. It can be defined as the acceleration of photoreaction in the presence of a catalyst. The initial interest in the heterogeneous photocatalysis was started when Fujishima and Honda discovered in 1972 the photochemical splitting of water into hydrogen and oxygen with TiO_2 (Fujishima, *et al.,* 1972). In recent years interest has been focused on the use of semiconductor materials as photocatalysts for the removal of organic and inorganic species from aqueous or gas phase. This method has been suggested in environmental protection due to its ability to oxidise the organic and inorganic substrates (Fox, *et al.,* 1993).

In heterogeneous photocatalysis two or more phases are used in the photocatalytic reaction. A light source with semiconductor material is used to initiate the photoreaction. The catalysts can carry out substrate oxidations and reductions simultaneously. UV light of long wavelengths can be used, possibly even sunlight. Heterogeneous photocatalysis using semiconductors such as titanium dioxide can be more interesting than conventional methods for removing organic species in the environment. Because the process gradually breaks down the contaminant molecule, no residue of the original material remains and therefore no sludge requiring disposal

to landfill is produced. The catalyst itself is unchanged during the process and no consumable chemicals are required. This result in considerable savings and a simpler operation of the equipment involved. Additionally, because the contaminant is attracted strongly to the surface of the catalyst, the process will continue to work at very low concentrations allowing sub part-per-million contents to be achieved. Taken together, these advantages mean that the process results in considerable savings in the water production cost and keeping the environment clean (Al-rasheed, *et al.,* 2005).

The basic process of photocatalysis is initiated by the absorption of a photon with energy equal to, or greater than band gap of semiconductor. The electron will ejected from the valence band (VB) to the conduction band (CB) of the semiconductor thus creating a h^+ hole in the valence band. This is followed by the formation of extremely reactive radicals such as $^\bullet OH$ at the semiconductor surface or by direct oxidation of the polluting species by h^+. As for the ejected electrons, they react with electron acceptor such as adsorbed oxygen or dissolved in water. However, one of the factor limiting the efficiency of photocatalysis is the rapid recombination of photogenerated electrons and holes in semiconductor particle. Currently, many research teams are working on ways to limit the recombination of charges. For example, to achieve higher efficiency for photocatalytic one may consider the following possibilities : 1. the coupling with another appropriate semiconductor, 2. metal doped with silver or gold, 3. adding electron acceptor such as dissolved oxygen or employing organic sacrificial agents (electron donors) such as methanol (Bassiad, *et al.,* 2009).

A wide range of semiconductors may be used for photocatalysis, such as TiO_2, ZnO, MgO, WO_3, Fe_2O_3, CdS. The ideal photocatalyst should possess the following properties (i) photoactivity, (ii) biological and chemical inertness, (iii) stability toward photocorrosion, (v) suitability towards visible or near UV light, (vi) low cost, and (vi) lack of toxicity (Bhatkhande, *et al.,* 2001).

1.2.2 The coupled semiconductor photocatalyst

Photocatalysis over titanium dioxide (TiO_2) is initiated by the absorption of a photon with energy equal to or greater than the band gap of TiO_2 (3.2 eV), producing electron-hole (e^-/h^+) pairs. Consequently, following irradiation, the TiO_2 particle can act as either an electron donor or acceptor for molecules in the surrounding media. However, the photoinduced charge separation in bare TiO_2 particles has a very short lifetime because of charge recombination. Therefore, it is important to prevent electron-hole recombination before a designated chemical reaction occurs on the TiO_2 surface. TiO_2 and high recombination rate of the photogenerated electron-hole pairs hinder its further application in industry. Having recognized that charge separation is a major problem, numerous efforts have been attempted to improve its photo catalytic activity by modifying the surface or bulk properties of TiO_2, such as deposition of metals, doping , surface chelation, and coupling of two semiconductors (Chatterjee, *et al*., 2002).

Kawahara, *et al.,* (2003) prepared rutile-anatase coupled TiO_2 particles and showed that the photocatalytic activity of rutile-anatase coupled TiO_2 particles was higher than P-25. In the preparation of rutile-anatase coupled TiO_2 particles, rutile TiO_2 particles of 7.2 g were added into 200 mL of H_2SO_4 aqueous solution and refluxed at the boiling temperature to be partly dissolved. After the solution was cooled to room temperature, the dissolved Ti^{4+} ions were reprecipitated by controlling the pH at *ca*.10.5 with the addition of 14% NH_3 solution. The solids recovered from the suspension by centrifugal separation were rinsed repeatedly with distilled water until the pH of the supernatant reached *ca.* 7 and then dried overnight *in vacuo*. The resulting particles were heated in air at various temperatures (400-900 ^{o}C) for 1 h. For the purpose of comparison, some samples were made without the dissolution process. Titanyl sulfate ($TiOSO_4$-3.1H_2O, TAYCA) was dissolved in 200 mL of pure water, and 7.2 g of rutile particles was added into the solution. Then Ti^{4+} ions were precipitated by adding 14% NH_3 solution and the suspension was processed the same way as mentioned above. The crystal structure of the particles was determined by powder X-ray diffraction (XRD, RIGAKU- RINT2500) using Ni-filtered CuK_{α} radiation in the range of 2θ from 15 to 75°. The average sizes of anatase and rutile

crystallites were calculated from the width at half the height of the diffraction peaks from the (101) plane of anatase ($2\theta = 25.4^{\circ}$) and from the (110) plane of rutile ($2\theta = 27.4^{\circ}$), respectively, using Scherrer's equation. The photocatalytic activity of the sample was evaluated for the gas-phase oxidation of CH_3CHO.

Keller, *et al.,* (2003) prepared the composite ternary catalyst WO_3/SiC-TiO_2. TiO_2 and SiC are two semiconductors, which can be photoexcited simultaneously in the near UV region because of their close energy band gap of 3.2 and 3.0 eV, respectively. Furthermore, the redox energy level of their corresponding valence and conduction bands are suitably disposed. The mixed ternary semiconductor oxide photocatalysts used in this study were prepared in two successive steps, the first one consisting of the simultaneous coating of SiC and TiO_2 on the glass on the inside radius of the annular reactor. $SiC+TiO_2$ mechanical mixtures (150-250 µm) were prepared from an aqueous slurry of TiO_2 (Degussa P25) (specific area around 50 m^2/g) and adding appropriate amounts of SiC (specific area around 25 m^2/g). The amount of TiO_2 was calculated in order to obtain a theoretical covering of 1 mg/cm^2 on the reactor used as support. The TiO_2+SiC slurry was deposited on the glass reactor by heating until complete evaporation of the aqueous solvent. After that it was dried in an oven at 120 °C for 30 min. The second step was the wet impregnation of WO_3 with an aqueous solution of ammonium paratungstate, $(NH_4)_{10}W_{12}O_{41}.5H_2O$, in order to cover the surface of the TiO_2+SiC carrier with monolayer thickness. After impregnation on the TiO_2+SiC carrier, already coated on the photo-reactor, the system was heated to dryness. Finally, the catalyst was calcined on air at 420 °C for 1 h.

Maolin, *et al.,* (2005) synthesized the coupled $ZnO-SnO_2$ by homogeneous co-precipitation method. All of the chemical reagents used in the experiments were analytical grade without further purification and treatment. The synthesis procedures of the coupled $ZnO-SnO_2$ are as follows: 10 mol/L NaOH aqueous solution was added dropwise into 100 mL of 0.5 mol/L $Zn(NO_3)_2$ aqueous solution under vigorous stirring until the solution became transparent, and then 100 mL of 0.5 mol/L Na_2SnO_3 solution and a certain volume of distilled water were added. As a result, 300 mL of the mixture solution containing Na_2SnO_3 and

$Na_2[Zn(OH)_4]$ was obtained. Subsequently, 200 mL of H_2O, CH_3COCH_3 and $CH_3COOC_2H_5$ mixture solution with 3: 3: 2 volume ratio was added into the above mixture solution at room temperature (*ca.*25°C) under vigorous stirring, and the resulting solution was subjected to precipitation by the hydrolysis of ethyl acetate until the reaction mixture attained a pH value between 9 and 10. The precipitate obtained was separated and washed 3 times with distilled water, and dried at 80 °C, then calcined at different temperatures in air to synthesize $ZnO-SnO_2$ particles. The result of this study, the nanosized coupled oxide $ZnO-SnO_2$ had a better photo catalytic activity than that of either single oxides, ZnO or SnO_2, and its photocatalytic activity was slightly higher than commercial P25 TiO_2.

Wang, *et al.,* (2008) prepared ZnO-anatase-rutile semiconductor by impregnating ZnO nano particle on Degussa P25 surface. $Zn(NO_3)_2 \cdot 6H_2O$ as analytical grade was used, and 4 g TiO_2 powder was impregnated with aqueous solutions containing the required amounts of the zinc ions. After aging at room temperature for 1 h, the pH value of the suspension was adjusted to 10.0 by the addition of NH_3 solution (1.0 mole/L), while the suspension was stirred by a magnetic stirrer. Immobilization was carried out by the dip coating method. The TiO_2 suspension was gradually dropped and the catalyst was coated on the woven glass fabric (pretreatment: 500 °C for 1 h) over an area of 4 cm $\times$ 80 cm. The coated woven glass fabric was treated with a desiccation process in a convection oven at 80 °C for 12 h. Finally, the woven glass fabric was calcined at 400 °C for 1 h. The amount of coated TiO_2 was determined by the mass increase of the woven glass fabric after the coating. In all experiments, the weight of TiO_2 coated was kept at 0.5 g $\pm$ 10%.

Yin, *et al.,* (2011) synthesized $BiVO_4/TiO_2$ hetero-junction nanocatalysts using a simple coupling method. In a typical procedure, 0.02 mol of $Bi(NO_3)_3 \cdot 5H_2O$ and 0.02 mol of NH_4VO_3 were respectively dissolved into 20 mL of concentrated nitric acid and 20 mL of 6 M NaOH aqueous solution to form two transparent solutions with agitation for 2 h. The above solutions were mixed together with the Bi/V molar ratio of 1:1. The mixture was stirred for 1 h under ambient air. The orange slurry was obtained by adjusting pH to 11–12 with diluted sodium

hydroxide, which was transferred into a teflon lined stainless steel autoclave with a capacity of 100 mL. And then the sealed reactor was heated to 180 ^{o}C and maintained at this temperature for 6 h. The final products were filtered and washed with deionized water and ethanol several times, and finally dried at 60 ^{o}C for several hours. A mixture of 1.3 mL of HNO_3, 180 mL of H_2O, and 15 mL of $Ti(OC_3H_7)_4$ was peptized at 40 ^{o}C for 24 h to form a highly dispersed TiO_2 colloidal solution. Finally, the as prepared $BiVO_4$ powder was added into self-made TiO_2 colloid with ultrasonic dispersed for 0.5 h and sustained stirring for 12 h, and then dried by using a microwave oven. The resultant samples were all calcined at 500 ^{o}C for 3 h (2 ^{o}C/min) to remove solvents and other organic species.

Bi_2WO_6 and TiO_2, the two most extensively studied photocatalysts, were successfully coupled via a facile one step hydrothermal process (Jiehui, *et al.,* 2012). The as-prepared Bi_2WO_6/TiO_2 possessed enhanced visible-light-induced activity in photocatalytic degradation of contaminants in aqueous/gaseous phases compared with those of the sole Bi_2WO_6 or TiO_2. The versatile Bi_2WO_6/TiO_2 photocatalyst also exhibited long-time recyclable ability for the contaminants degradation under visible irradiation ($\lambda > 420$ nm) of xenon lamp or household fluorescent lamp. The photoluminescence and electrochemical impedance spectroscopy were used to analyze the physical properties of the photogenerated carriers and it was found that the separation of photogenerated carriers of Bi_2WO_6 was largely promoted after being coupled with wide-band-gap semiconductor TiO_2. This work could be extended to the design of other composite photocatalyst with the purpose of enhancing activity by coupling suitable wide and narrow band gap semiconductors, which was inspiring for the practical environmental purification. All the chemicals were analytical grade reagents from Shanghai Chemical Company and used without further purification. P25 titanium dioxide (approximately 80% anatase and 20% rutile structure) was provided by the Degussa Company. The composite catalysts were synthesized by a facile one step hydrothermal process. Since P25 is a commercial catalyst, the powders were activated in the nitric acid solution before use. In a typical hydrothermal synthesis procedure, different mass ratios of TiO_2 (15%, 25% and 35%) were well dispersed in diluted nitrite acid (HNO_3) by

sonication. $Bi(NO_3)_3 \cdot 5H_2O$ and $Na_2WO_4 \cdot 2H_2O$, in a molar ratio of 2:1, were added in the TiO_2 suspension in turn. After sufficient reaction, pH value of the mixed solution was adjusted to 5 by sodium hydroxide solution. Then the suspension was added into a 50 mL Teflon lined autoclave with a stainless steel tank and heated at 160 ^{o}C for 18 h. Afterwards, the samples obtained were rinsed with deionized water and anhydrous ethanol and then oven dried at 60 ^{o}C for 4 h.

1.2.3 Titanium dioxide (TiO$_2$)

Titanium dioxide (TiO_2) also known as titanium (IV) oxide or titania, is the naturally occurring oxide of titanium. It exists in three polymorphous structures, namely, anatase, brookite and rutile. The most common structures are anatase and rutile, since brookite is rather unstable. Both anatase and rutile are tetragonal, whereas brookite is orthorhombic. In all three oxide modifications, each titanium atom is coordinated to six almost equidistant oxygen atoms, and each oxygen atom to three titanium atoms (Clark, *et al.,* 1968). The structure of anatase, brookite and rutile can be discussed in term of (TiO_6^{2-}) octahedral. The three crystal structures differ by the distortion of each octahedral and by the assembly patterns of the octahedral chains. In the case of anatase, the TiO_6^{2-} octahedron is slightly distorted, with two Ti-O bond slightly greater than the other four, and with some of the O-Ti-O bond angles deviating form 90º. The distortion is greater in anatase than rutile. The third form of TiO_2, brookite, the interatomic distances and the O-Ti-O bond angles are similar to those of rutile and anatase. The essential difference is that there are six different Ti-O bonds ranging from 1.87 to 2.04 Aº. Accordingly, there are 12 different O-Ti-O bond angles ranging from 77º to 105º. Brookite is formed by joining together the distorted TiO_6^{2-} octahedral sharing three edges. All three oxide modifications are birefringent; anatase is uniaxial negative, brookite is biaxial positive and rutile is uniaxial positive. Further data are given in Table 1. Crystallographic data on the three oxide modifications are summarized in Table 2.

Table 1 Properties of the three modifications of TiO_2 (Clark, *et al.,* 1968)

	Anatase	Brookite	Rutile
Density (g/cm^3)	3.90	4.13	4.27
Hardness (Mohs'scale)	5.5-6.0	5.5-6.0	6.0-6.5
Melting Point (ºC)	change to rutile	change to rutile	1840 ± 10
Entropy $S^o_{298.16}$ (Cal/deg/m)	11.93	-	12.01
Refractive Index (25ºC) (λ=5893 ºA)	n_ω 2.512 n_ω 2.4880	n_α 2.5831 n_β 2.5843	n_ω 2.6124 n_ω 2.8993 n_γ 2.7004
Dielectric Constant	$\varepsilon = 48$ (powder)	$\varepsilon = 78$	$\varepsilon_{av} \approx 110$ $\varepsilon_{II} = 180$ at 3×10^5 c/s 25 ºC $\varepsilon_\perp = 89$, at 3×10^5 c/s 25 ºC

Table 2 X-ray data on TiO_2 modifications (Clark, *et al.,* 1968 : 268)

Space group	Z	Cell Parameters Aº			Ti-O (Aº)[a]
		A	B	C	
Anatase C_{4h}^{19} = C4/amc	8	5.36	-	9.53	1.91 (2) 1.95 (4)
Brookite D_{2h}^{15} = *Pbca*	8	9.15	5.44	5.14	1.84 - 2.03
Rutile D_{4h}^{14} = *P4$_2$ / mnm*	2	4.954	-	2.959	1.944 (4) 1.988 (2)

[a] The numbers in parentheses refer to the number of equivalent oxygen atoms at the stated distance from a titanium atom.

Of the three forms, the most common structures are anatase and rutile since brookite is rather unstable. The brookite type cannot be used in industrial because of its instability at room temperature.

The anatase type has the problems of poor light, heat resistance, and gradually decreasing in whiteness due to weather. It also has drawbacks for applications involving adsorption technology owing to its low surface energy. The rutile type has outdoor applicability because of its good light resistance and can be applied to surfaces by the use of adsorption technology without advanced skills or sophisticated equipment (Clark, *et al.,* 1968).

TiO_2 is extensively used as a white permanent pigment with good covering power in paint, paper, printing ink, plastic, polymer and cosmetic products. Paints made with TiO_2 are excellent reflectors of infrared radiation and are used in exterior paints. It is also used as strengthening filler in paper and cement. Recently, there has been increasing interest in application of nanocrystalline materials for catalyst, supports, ceramics, inorganic membranes, gas sensing, water purification, and solar energy conversion (Yanqing, *et al.,* 2001). Furthermore, photocatalysis of nanocrystalline TiO_2 has a great many advantage on waste water treatment such as high catalysis efficiency, energy saving, no pollution, etc. and can degrade all kinds of organic pollutants from water effectively. Organic pollutants from water effectively. All of those merits make photocatalysis of water treatment and it is supposed to be used widely in the future (Baolong, *et al.,* 2003).

1.2.4   Barium titanium oxalate (BTO)

Louer, *et al.,* (1992) synthesized barium titanyl oxalate $BaTiO(C_2O_4)_2.4.5H_2O$ using $BaCl_2.2H_2O$, $TiCl_4$, and $H_2C_2O_4$ as starting materials. The samples were heated in air with a slow heating rate of 10 ^oC hr^{-1} in range 18-800 ^oC. The result of crystallographic data showed the crystal system as monoclinic $P2_1/n$ space group. The structure was determined from Patterson and Fourier syntheses. The refinement was done by the method of least squares. The final R values were $R = 0.056$ and $R_w = 0.079$ for 3261 unique reflections. The structure was characterized by a body-centered arrangement of finite groups consisting of four vertex-sharing TiO_6 distorted octahedral. These groups were connected by barium polyhedra and oxalate groups. The study showed that the water molecule number was 4.5 by formula rather than 4 reported previously. This conclusion supported by TG measurements.

Rhine, *et al.,* (1992) synthesized single crystal barium titanyl oxalate BaTiO$(C_2O_4)_2$.5H$_2$O using ammonium titanyl oxalate solution (NH$_4$)$_2$TiO(C$_2$O4)$_2$.H$_2$O and added to barium nitrate solution, and the mixture remained free of precipitate. Water was allowed to evaporate slowly from open Erlenmeyer flask, and crystals of BaTiO$(C_2O_4)_2$.5H$_2$O nucleated, grew, and became visible after several months. The crystals, which begin to loss water even at room temperature, were isolated by filtration and air dried at room temperature. Elemental analysis for BaTi(O)(C$_2$O$_4$)$_2$.4.5H$_2$O *calcd* C, 10.48(found,10.48); H, 1.98(1.95); Ba, 29.96 (29.59), Ti, 10.45 (10.28); Ba/Ti mol ratio = 1.003. Sample that were analyzed for water content after shorter drying times contained more water with 5 waters being the upper limit. The structure was solved by a combination of the Patterson method and difference Fourier methods. In this effort, they prepared BTO via reaction of ammonium titanyl oxalate solution (NH$_4$)$_2$Ti(O)(C$_2$O4)$_2$.H$_2$O with barium salts under a variety of conditions, but they encountered difficulty obtaining a precipitate with 1.00:1.00 stoichiometry (i.e., BTO free of other byproducts). However, by working at room temperature in dilute solution at pH 0-1.5, they were able to achieve slow crystallization of stoichiometric BTO. In the method used to grew crystals for this work, a clear solution was obtained when a stoichiometric amount of Ba(NO$_3$)$_3$ was added to a dilute solution ($<10^{-3}$M) of ammonium titanyl oxalate as long as the pH was less than 1.5. If the pH was not adjusted by adding acid, a precipitate formed immediately and did not redissolve. X-ray diffraction patterns of precipitates obtained at pHs of precipitates obtained at pHs of 4-5 indicated the precipitates were amorphous. When the initial pH was below 0, crystals of Ba(NO$_3$)$_2$ were isolated instead of BTO. Recently, aqueous stability diagrams were calculated for the Ba-Ti-C$_2$O$_4$-H$_2$O system based on thermodynamic modeling (Osseoasara, *et al*., 1990). According to that work, BTO showed be thermodynamically unstable relative to titanium oxide or hydrous oxide, especially at low ($<10^{-2}$) metal ion concentrations; its existence was suggested to be due to complexation with chloride ion or to its precipitation as a metastable phase. The fact that the crystals of BTO grew slowly out of solution over several months suggesting that BTO was a thermodynamically stable compound. The results suggested that the precipitate which initially forms, as observed in that work and reported by Clabaugh *et al*., (1956) was the kinetically

controlled product and dissolves under acidic conditions (pHs less than 1.5). From their results, the products isolated immediately after combining reagents are titanium-rich. Similar result was reported by Orlyaski, and most successful preparations use a 1-5% excess of barium in the solutions. X-ray diffraction from single crystal showed that BTO crystallizes in the monoclinic space group $P2_1/n$. To account for the number of unique atoms in the structure, BTO is formulated as $Ba_2Ti_2O_4(C_2O_4)_4.10H_2O$. The overall structure of BTO was rather complex and not easily viewed in its entirety. The IR spectra of BTO agreed with the crystal structure and showed that it did not contain isolated Ti=O bonds. Titanyl compounds possess a Ti=O stretching frequency in the range 1050-950 cm^{-1}. The vibrational frequencies of BTO were observed at 1705, ν_{as} (C=O); 1424, ν_s (C-O, C-C); 1279, ν_s (C-O) + δ (O-C=O); 910, ν_s (CPO) + δ (O-C=O); and 824 cm^{-1}, δ (O-C=O) + ν (M-O). The vibrational frequencies of ammonium titanyl oxalate were observed at 1690, ν_{as} (C=O); 1401, ν_s (C-O, C-C); 1244, ν_s (C-O) + δ (O-C=O); 896, ν_s(C-O) + δ (O-C=O); 880, 778 cm^{-1}, δ (O-C=O) + ν (M-O). The conversion of BTO to $BaTiO_3$ requires heating 6 h at 600 ^{o}C, 1h at 700 ^{o}C, and less than 0.5 h at 800-900 ^{o}C. Although the TGA indicates that decomposition is complete by 700 ^{o}C at a heating rate of 10 ^{o}C /min, they have observed that the decomposition products obtained after heating BTO to 850 ^{o}C at 10 ^{o}C/min (no hold) contained both phase pure $BaTiO_3$ and a small amount of amorphous material as shown by the broad peak between 15 and 35° in the X-ray diffraction pattern. Heating to 900 ^{o}C at 10 ^{o}C/min (no hold) resulted incomplete conversion to barium titanate.

In the report by Potdar, *et al*., (2001) the starting materials used in the synthesis of BTO were barium hydroxide, titanium tetrabutoxide, oxalic acid, isopropanol, nitric acid. Initially titanium tetrabutoxide was dissolved in 200 mL of isopropanol (pH~3.5). Then 0.1 M of oxalic acid was made by dissolving 12.607 g of oxalic acid in 350 mL of isopropanol alcohol containing 3.6 mL distilled water (pH~1.9). This solution was taken in a 5 L capacity beaker and stirred continuously. A 0.1 M solution of ammonium oxalate was made by dissolving 14.211 g of ammonium oxalate in 350 mL distilled water (pH~6.5). Butyl titanate monomer (BTM) solution in IPA was added with continuous stirring to oxalic acid solution in IPA, when a

white precipitate was obtained. To this, 0.1 M solution of ammonium oxalate was added and solution was diluted by adding 1050 mL distilled water when clear solution containing soluble titanium species Ammonium titanyl oxalate (ATO) (pH~4.2) was obtained. In order to avoid pH variation during precipitation, (0.1 M) barium precursor solution was made by dissolving (31.548 g) of barium hydroxide in 400 mL of distilled water, the pH of which was adjusted to 4.25 by partial neutralization with dilute (1.1 M) HNO_3 solution. This freshly prepared barium precursor solution was further added to the clear solution of ATO with continuous stirring, to precipitate barium titanyl oxalate (BTO). The precipitation was complete within 5 min and the precipitate was filtered through a Buchner funnel assembly using whatman filter paper no. 41. The precipitate was washed with distilled water several times and finally air dried at room temperature. The filtrate (pH~3.15) was evaporated to dryness to obtain dissolved material.

Khollam, *et al.,* (2002) prepared barium titanium oxalate by self-sustaining controlled acid–base reaction between oxalotitanic acid $[H_2TiO(C_2O_4)_2]$(HTO) and barium hydroxide $[Ba(OH)_2.8H_2O]$ at room temperature. For this purpose, an intermediate soluble oxalotitanic acid precursor was generated by reacting 0.1 M solution of titanium tetrabutoxide in isopropanol (IPA) with 0.2 M solution of oxalic acid in IPA. Equimolar suspended $Ba(OH)_2$ particles in IPA were mixed with the above-mentioned oxalotitanic acid solution. The self-sustaining acid-base reaction between $Ba(OH)_2$ and $H_2TiO(C_2O_4)_2$ was initiated only when necessary amount of water was added. This shift from non-aqueous to semi-aqueous condition allowed a required solubility of $Ba(OH)_2$ to make Ba^{2+} ions available for the exchange reaction. The solubility of $Ba(OH)_2$ and its dissociation governed the kinetics of the reaction leading to the precipitation of BTO with yield ≥99%. The controlled pyrolysis of BTO at 750°C/4 h in air produced agglomerated cubic $BaTiO_3$ powders having spherical particles with size ≈ 100 nm. These powders were sintered in the form of pellets at 1300°C/4 h to obtain compacts with density ≈ 95%. These compacts showed dielectric constant $\varepsilon_{RT} = 1680$ (tan δ ≤ 2%), $\varepsilon_{max} \approx 7780$ at $T_C = 121°C$.

$$H_2TiO(C_2O_4)_2 + Ba(OH)_2 \xrightarrow{\text{IPA + Water}} BaTiO(C_2O_4)_2.4H_2O + 2H_2O \quad \text{(I)}$$
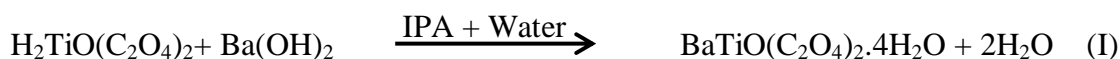
The main reaction (I) actually occursed in the following manner. Initially dispersed solid $Ba(OH)_2$ dissolved to produce Ba^{2+} ions as given below by reaction (1).

$$Ba(OH)_2 \xrightarrow{\text{IPA + Water}} Ba^{2+} + OH^- \tag{1}$$

$$H_2TiO(C_2O_4)_2 \xrightarrow{\text{IPA + Water}} 2H^+ + TiO(C_2O_4)_2^{2-} \tag{2}$$
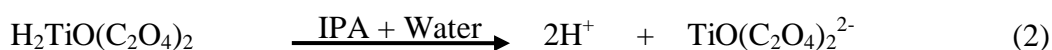
Similarly, oxalotitanic acid dissociated to form H^+ and $TiO(C_2O_4)_2^{2-}$ species as shown in Eq. (2). When ionic product of Ba^{2+} and $TiO(C_2O_4)_2^{2-}$ exceeded the solubility product of BTO, the neutralization reaction occurred to precipitate BTO. As soon as Ba^{2+} ions were consumed to precipitate BTO, more and more $Ba(OH)_2$ solid dissolved to maintain equilibrium concentration of Ba^{2+} ions depending on its solubility at ambient conditions. This overall reaction is represented by Eq. (3) as given below.

$$Ba^{2+} + 2OH^- + 2H^+ + TiO(C_2O_4)_2^{2-} \longrightarrow BaTiO(C_2O_4)_2.4H_2O + 2H_2O \tag{3}$$
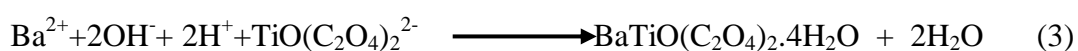
Thus, the reactions (1) and (2) occurred simultaneously till all $Ba(OH)_2$ and oxalotitanic acid was consumed. In this way, the main react ion (I) was driven to its completion. Thus, the reaction (I) was kinetically controlled and gave the precipitate yield $\geq$ 99%. The IR spectrum of BTO formed by reaction (I) showed the characteristics absorption bands at 1640, 1420 and 1280 cm^{-1} corresponding to the different modes of vibration of oxalate group. The broad band centered around 3550 cm^{-1} was assigned to anti symmetric and symmetric stretching vibration of OH group and that of 1600 cm^{-1} could be due to H-O-H bending of coordinated water. The band at 1600 cm^{-1} was overlapped with that of ν_{asy} (C = O) of oxalate group.

Gotar, *et al.,* (2003) prepared barium titanium oxalate using $BaCl_2.2H_2O$, $TiCl_4$ and $H_2C_2O_4.2H_2O$ as raw materials. High resolution X-ray diffraction studies of this precursor showed that the Clabaugh synthesis method led to a single-phase product with a Ba/Ti ratio equal to one. Pure and stoichiometric

BaTiO$_3$ powders were obtained from the thermal decomposition of the BTO precursor as checked by X-ray fluorescence analysis.

Malghe, *et al.,* (2004) synthesized BTO from the aqueous solution of Ba(NO$_3$)$_2$ (BN) and K$_2$TiO(C$_2$O$_4$)$_2$ (KTO). Both the chemicals were of analytical grade. The method consisted of mixing of equimolar aqueous solutions of BN and KTO with constant stirring. The white BTO precipitate obtained was filtered, washed with distilled water and dried in an oven at 50°C for 24 h. From chemical analysis, the product could be assigned the molecular formula, BaTiO(C$_2$O$_4$)$_2$.4H$_2$O.

1.2.5   Barium oxalate

Christensen, *et al.,* (1992) prepared BaC$_2$O$_4$.3.5H$_2$O and BaC$_2$O$_4$.0.5H$_2$O. The compounds were made from CO$_2$ free solutions of BaCl$_2$.2H$_2$O, (NH$_4$)$_2$C$_2$O$_4$.H$_2$O, and H$_2$C$_2$O$_4$.H$_2$O. For BaC$_2$O$_4$.3.5H$_2$O, 50 mL of a 0.05 M solution of BaCl$_2$.2H$_2$O were added dropwise to 250 mL of a 0.007 M solution of (NH$_4$)$_2$C$_2$O$_4$.H$_2$O. The white crystalline precipitate was BaC$_2$O$_4$.3.5H$_2$O. The precipitate barium oxalate was washed by decanting, filtered and dried on the filter at room temperature. For BaC$_2$O$_4$.0.5H$_2$O, 500 mL of a 0.20 M solution of BaCl$_2$.2H$_2$O were added dropwise to 500 mL of a 0.20 solution of (NH$_4$)$_2$C$_2$O$_4$.H$_2$O. The white crystalline precipitate was BaC$_2$O$_4$.0.5H$_2$O. The precipitate barium oxalate was washed by decanting, filtered and dried on the filter at room temperature.

Christensen, *et al.,* (1994) prepared barium oxalates from CO$_2$ free solutions of BaCl$_2$.2H$_2$O, (NH$_4$)$_2$C$_2$O$_4$.H$_2$O, and H$_2$C$_2$O$_4$.H$_2$O. The purity of the barium oxalates was investigated with Guinier photographs which were taken with a Nonius Guinier camera using CuK$_\alpha$ radiation (λ = 1.540598 °A) and silicon as an internal standard (a$_{si}$ = 5.43050 A). The positions and intensities of the Bragg reflections on the Guinier films were measured on a photometer and were compared with the values on the respective JCPDS data cards. The powder sample of BaC$_2$O$_4$.2H$_2$O was obtained in attempts to make samples of BaC$_2$O$_4$.3.5H$_2$O: solutions of 12.2g BaCl$_2$.2H$_2$O in 500 mL water and of 4.5 g H$_2$C$_2$O$_4$.H$_2$O in 500 mL water were cooled to 5 °C in an ice bath. A solution of

oxalic acid was added drop wise to the barium chloride solution which was stirred with a magnetic stirrer and kept at 5 °C. The white crystalline precipitate of $BaC_2O_4.3.5H_2O$ was filtered on a Buchner funnel, washed with water and ethanol and stored in a polyethylene flask. $BaC_2O_4.3.5H_2O$ was unstable at room temperature. It could be kept in a refrigerator or over dry ice in a dewar for some days, but at room temperature it would convert to $BaC_2O_4.2H_2O$ in a few days and in weeks to $BaC_2O_4.H_2O$. The single crystal sample of $BaC_2O_4.2H_2O$ was obtained as reported previously.

Nayak, *et al.,* (2000) prepared barium oxalate prepared by precipitation from oxalic acid (AR grade) and barium nitrate (AR grade) in a dilute aqueous solution and the crystals were dehydrated in vacuum at 493 K to a constant weight. Purity (99.9%) of the sample was checked by estimating barium by flame photometrically and oxalate by chemical analysis.

Dalal, *et al.,* (2006) synthesized barium oxalate single crystal in agar gel. Barium oxalate was grown in agar gel at ambient temperature. The effect of various parameters like gel concentration, gel setting time, and concentration of the reactants on the growth of these crystals were studied. Prismatic plate shaped spherulites and dendrites were obtained. The grown crystals were characterized by X-ray powder diffractometry, infrared spectroscopy, thermogravimetric and differential thermal analysis. An attempt was made to explain the spherulitic growth mechanism. The starting material barium chloride, oxalic acid, acetic acid, and agar-agar were of AR grade. In that work, agar-agar gel was preferentially used for the growth of crystals by single and double diffusion techniques. A test tube having 25 cm in length and 2×5 cm in diameter was employed. In single diffusion, hot aqueous agar gel and oxalic acid solution were thoroughly mixed and kept in the test tube for setting. After setting and aging, the gel, barium chloride, was added to the above gel. Now on reversing the reactants, in single diffusion, hot aqueous agar gel and barium chloride solutions were thoroughly mixed and kept in the test tube for setting. After setting and aging the gel, oxalic acid, was added. In double diffusion, the U tube was filled up to proper heights with hot agar-agar solution and kept for setting and aging. Oxalic acid solution was poured into one limb and barium chloride solution was poured into the

other limb of the U tube. The reaction to the growth of crystals. IR absorption spectrum of barium oxalate crystals showed a well pronounced broad intense peak at 3556.72 cm^{-1}, which was assigned to anti-symmetric and symmetric O-H stretching and the peak at 1615.67 cm^{-1} relating to O-H bending vibration which confirmed the presence of water of crystallization. The sharp peak at 782.84 cm^{-1} was attributed to metal-oxygen bond.

Sharma, *et al.,* (2009) prepared spherical barium oxalate (BaC_2O_4) nanoparticles. Nanoparticles of BaC_2O_4 was synthesized *in situ* from barium nitrate and ammonium oxalate by reverse micelle method. These particles were characterized using transmission electron microscope (TEM), Fourier-transformed infrared (FT-IR) and x-ray diffraction (XRD). The results indicated spherical barium oxalate (BaC_2O_4) nanoparticles could be fabricated with high crystallinity. The XRD pattern of BaC_2O_4 displays a number of diffraction peaks corresponding to 2θ: 18.36, 23.75, 26.17, 28.18, 29.01, 35.53, 39.68, 41.16, 43.28, with most prominent peak at 28.18 ^{o}. This peak correlated to (200) hkl indices, predicting a monoclinic structure of BaC_2O_4 and growth of nanoparticles along the face (200). FT-IR spectrum of BaC_2O_4 showed a well pronounced peak at 1600.4 cm^{-1} due to O-H bending vibration indicating the presence of water molecule associated with nanocrystals. The IR band at 1313.4 cm^{-1} corresponded to the asymmetric stretching mode of C-O bond. The sharp peak at 867.6 cm^{-1} confirmed the bonding of metal-oxygen (M-O bond).

1.2.6   Barium titanate (BaTiO$_3$)

Xia, *et al.,* (1995) prepared $BaTiO_3$ by hydrothermal method. The results of hydrothermal preparation of $BaTiO_3$ fine powder were reported. The effects of reaction temperature, the molar ratio of Ba/Ti in the precursors, the chemical form of the precursors on the phase composition, the size and morphology of products were presented. The higher the temperature, the higher basicity, and the greater the molar ration of Ba/Ti in the precursor, the easier was the formation of perovskite type $BaTiO_3$ crystallite. It was found that $BaTiO_3$ microcrystals (150-300 nm) could be synthesized through the hydrothermal reaction of commercial TiO_2 with $Ba(OH)_2$

aqueous solution, while the hydrothermal reaction of the newly prepared Ti(OH)$_4$ gel with the Ba(OH)$_2$ solution produced highly crystallized, well dispersed perovskite type BaTiO$_3$ crystallites with very fine (<100 nm) particles. The newly prepared Ti(OH)$_4$ gel proved to be suitable precursor for the hydrothermal preparation of BaTiO$_3$ fine powders. X-ray diffraction (XRD) of the hydrothermal BaTiO$_3$ powders reveals a simple cubic perovskite structure. Above that, the lattice constant decreased with the increase of the reaction temperature. These abnormal crystallographic features were assumed to result from lattice defects, due to OH$^-$ incorporation in the perovskite lattice. The precursors and the medium used in this study are shown in Table 3. The products were filtered and washed with dilute acetic acid to remove any excess Ba(OH)$_2$, and then washed with deionized water and alcohol and then airdried at 120 mL capacity, which was then put into the autoclave and heated at 75-400 °C for various durations. The pressure remained close to the vapour pressure curve of H$_2$O in this temperature range. The products were filtered and washed with dilute acetic acid to remove any excess Ba(OH)$_2$, and then washed with deionized water and alcohol and then air dried at 120 °C. The extent of reaction was determined by analyzing the amount of OH$^-$ in the residual solution. The influence of temperature on the phase composition and morphology. Equimolar Ba(OH)$_2$.8H$_2$O and commercial TiO$_2$ powder were hydrothermally processed at various temperatures for different durations showed the XRD spectrum of product of 75 °C for 8 h. The BaTiO$_3$ peaks appeared besides the peaks of TiO$_2$ was formed. The products were nearly single phase BaTiO$_3$ when the precursors were treated at 400 °C for 8 h. It was found by the analysis of the products synthesized at other temperatures (100, 150, 180, 200, 250 and 300 °C) that the (101) peak of anatase was presented in all the products synthesized at the temperatures below 300 °C.

Table 3. Precursors and solutions selected for hydrothermal synthesis of $BaTiO_3$ powders (Xia, *et al.,* 1995).

NO.	Ba precursor	Ti precursor	Reaction medium
1	$Ba(OH)_2.8H_2O$	Commercial TiO_2	Aqueous solution
2	$Ba(CH_3COO)_2$ + NaOH	Commercial TiO_2	Aqueous solution
3	$Ba(OH)_2.8H_2O$	Tetrabutyl titanate	Aqueous solution
4	$Ba(OH)_2.8H_2O$	Tetrabutyl titanate	Ethanol 50 vol% aqueous solution

The TEM morphologies of the powders prepared at different temperature for 8 h. The morphologies of the powders were strongly dependent on the temperature. The increase temperature, the morphology of the powders changed from spheric cluster to porous spheric cluster, and finally formed well crystallized or spheres. The crystallites also increased slightly with the increase of reaction temperature. A typical IR spectrum of hydrothermal $BaTiO_3$ showed broad absorption in the region of 3200-3600 cm^{-1}, a shallow band around 1640 cm^{-1} and a strong band at 650 cm^{-1}. The 1640 cm^{-1} band (bending mode of H_2O) indicated that some H_2O was present. The characteristic strong band at 650 cm^{-1} of the vibration mode of OH^{-1} groups was more distinct than the OH^{-1} stretching which was masked by the corresponding H_2O bands around 3600 cm^{-1}.

A chemical coprecipitation route was developed to synthesize a mixed oxalates (BaC_2O_4 + $TiO(C_2O_4)(H_2O)_2$) precursor by Potdar, *et al.,* 1999. In this route, titanyl oxalate, $TiOC_2O_4.nH_2O$ was prepared by reaction between alcoholic solutions of butyl titanate monomer and oxalic acid. This was further converted into soluble sodium titanyl oxalate, $Na_2TiO(C_2O_4)_2$ by reaction with sodium oxalate solution. The anionic $TiO(C_2O_4)_2^{2-}$ species (stable over narrow pH range) thus produced were destabilized by maneuvering pH conditions with the addition of aqueous solution of barium acetate to form insoluble $TiOC_2O_4(H_2O)_2$ and oxalic acid. The *in situ*

regenerated oxalic acid reacted with Ba^{2+} ions to precipitate BaC_2O_4 simultaneously. The mixed oxalate $[BaC_2O_4 + TiOC_2O_4(H_2O)_2]$ on pyrolysis in air produced $BaTiO_3$ powders. Various physicochemical techniques were used to characterize the mixed oxalate and BT powders. The precipitation of mixed oxalates/formation of BT powders in presently described route could be understood on the basis of following four steps which controlled the nature of chemical species available during precipitation.

Step I: Formation of $TiOC_2O_4$ (Potdar, *et al.,* 1999)

Ti(IV) formed complex compounds with oxalate ions in both aqueous and alcoholic media. All complexes were shown to be titanyl compounds with formula $TiOC_2O_4.nH_2O$ if the Ti : C_2O_4 ratio was 1 : 1 and pH $\leq$ 2 was maintained. In our experiment, when BTM (0.1 M) solution was added to solution containing 0.1 M oxalic acid with 0.2 M of H_2O and pH= 1.3, it was reasonable that the hydrolysis followed by reaction with acid would form a precipitate of titanyl oxalate $TiOC_2O_4.nH_2O$.

$$(C_4H_9O)_4Ti + H_2C_2O_4.2H_2O \quad \xrightarrow[2H_2O]{in\ IPA} \quad TiOC_2O_4 + 4C_4H_9OH \qquad (1)$$
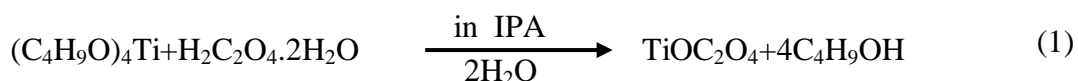
Formation of $TiOC_2O_4$ by reaction (1) was in agreement with previously reported observations that the synthesized 1 : 1 complex was $TiOC_2O_4.nH_2O$ with n $\leq$ 2.

Step II: Conversion of $TiOC_2O_4$ to soluble $Na_2TiO(C_2O_4)_2$

With excess oxalate concentration where Ti : C_2O_4 ratio was maintained as 1 : 2, the precipitate formed by reaction (1) was converted to $Na_2TiO(C_2O_4)_2$ by following reaction:

$$TiOC_2O_4 + Na_2C_2O_4 \quad \xrightarrow{\hspace{2cm}} \quad Na_2TiO(C_2O_4)_2 \qquad (2)$$
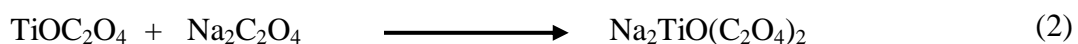
It was reasonable to expect the formation of $Na_2TiO(C_2O_4)_2$ by reaction (2) as titanium had tendency to form anionic oxalate complex species with a large number of coordinated oxalate ions. It was reported in the literature that the fraction of $TiOC_2O_4$

species decreased rapidly with increasing pH whereas the complex $TiO(C_2O_4)_2^{2-}$ built up and approached 100% in the pH range 2.5-3.5. The pH of the solution was increased to 3.3 after addition of $Na_2C_2O_4$. Therefore, it was reasonable to expect the formation of soluble sodiumtitanyl oxalate by reaction (2) given earlier. Such observations were separately reported by Velde that the complex titanyl ion was monomeric 1 : 2 chelate with charge -2 and stable over pH range of 2.5-3.5.

Step III: Destabilization of $TiO(C_2O_4)_2^{2-}$ due to pH change on addition of Ba precursor solution resulting in simultaneous precipitation of (Ba + Ti) in the form of oxalates

When barium acetate solution with pH = 6.9-7.1 was added to solution containing anionic $TiO(C_2O_4)_2^{2-}$ species (pH = 3.3), white precipitate was formed due to destabilization of anionic species. The pH after precipitation was ≈5.2. The destabilization can occurred by following reactions:

$$Na_2TiO(C_2O_4) \rightleftharpoons 2Na^+ + TiO(C_2O_4)_2^{2-} \tag{3}$$

$$TiO(C_2O_4)_2^{2-} + 2H_2O + C_2O_4^{2-} \xrightarrow{\text{destabilization}} TiOC_2O_4(H_2O)_2 \downarrow \tag{4}$$

$$Ba(CH_3COO)_2 \rightleftharpoons Ba^{2+} + 2CH_3COO^- \tag{5}$$

$$Ba^{2+} + C_2O_4^{2-} \longrightarrow BaC_2O_4 \downarrow \tag{6}$$

$$2Na^+ + 2CH_3COO^- \xrightarrow{\text{crystallization}} 2CH_3COONa \tag{7}$$
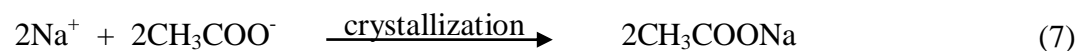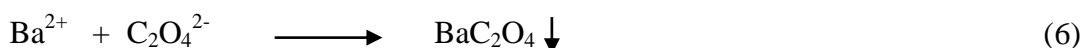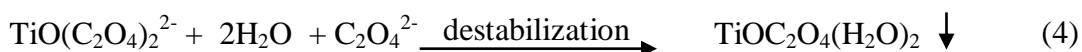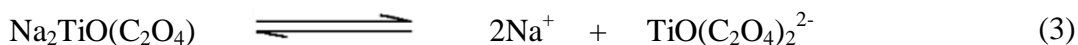
The precipitate after drying was subjected to IR analysis. The IR spectrum indicated strong characteristic absorption bands (1650, 1425, 1270 and 780 cm^{-1}) corresponding to oxalate ligand. The DTA/TG/DTG curves obtained for the as-dried precipitate indicated decomposition in three steps with total weight loss of 56.07%. Since the as dried precipitate was used, it might contain some adsorbed water (Y) in addition to the hydrated water. Assuming final product as TiO_2 and total weight loss 56.07%, the weight loss occurring at each step was calculated from the equation below (Potdar, *et al.,* 1999):

$$TiO_2C_2O_4(H_2O)_2 \ + \ Y \quad = \quad TiO_2 \ + \ [C_2O_3 + (H_2O)_2 + Y \ ]$$

The initial weight loss (16.4%) in the temperature range 35-200 °C may be attributed to the liberation of surface adsorbed and hydrated water, which was accompanied by an endothermic peak in DTA. The marked weight loss of 39.6% in the temperature range 200-600 °C in the TGA curve was due to the decomposition of oxalate to form TiO_2. The interruption occurred in the down slope of TGA curve at about 450 °C was related to the conversion of TiO to TiO_2 formed during the decomposition of oxalate by two simultaneous processes:

1. By air oxidation $TiO + \frac{1}{2}O_2 \longrightarrow TiO_2$
2. By CO_2 reduction $TiO \ + \ CO_2 \longrightarrow TiO_2 + CO$

A chemical coprecipitation route is developed to synthesize a mixed (Ba + Ti) oxalate precursor at room temperature. The pyrolysis of mixed oxalates at $T \geq 750$ °C in air produced submicron-sized BT powder (size range 0.2-0.5 mm) with spherical morphology.

Golubko, *et al.,* (2000) reported the preparation of barium titanate and related materials by the alkoxide-hydroxide route. Formation of perovskites $MTiO_3$ (M = Ba, Sr) at low temperature (<100 °C) by heterogeneous reactions of $M(OH)_2$ aqueous solutions with hydrolysis products of $Ti(OBu)_4$ was discussed. Reaction products were characterized by means of chemical and X-ray analysis, and electron microscopy. Reaction rate is enhanced by hydroxide concentration and reaction temperature, and increased drastically when $Sr(OH)_2$ was used instead of $Ba(OH)_2$. Particles shape and size of the perovskites formed was independent of morphology of $Ti(OBu)_4$ hydrolysis product. The main factor of perovskites morphology regulation lied in the rate of $M(OH)_2$ absorption. Lowering the absorption rate allowed to prepare uniform perovskite powders which could be readily sintered to ceramic bodies with high dielectric permittivity. The worked by Golubko, *et al.,* 2000 concerned the study of the impact of the reaction conditions on the phase formation and morphology of perovskite powders in the course of $M^{II}TiO_3$ preparation by the alkoxide hydroxide method. Golubko and coworker used titanium butoxide $Ti(OBu)_4$ as a starting

reagent. Reagent-grade barium and strontium hydroxides were dissolved in the calculated amounts of distilled water free of CO_2 at 65-75 °C, the hot solutions were decanted from the insoluble impurities into the heated dry flasks in dry argon atmosphere. Hydroxide concentration was determined by titration of the weighed samples by 0.1 M HCl. Solutions were stored at 65 °C under argon. Reagent-grade strontium formate was also used in certain experiments. Titanium butoxide solutions in butyl alcohol were hydrolyzed on vigorous stirring at different temperature conditions, the precipitates were aged under the mother liquor for certain time periods, and then aqueous solutions of alkaline-earth hydroxides were added to the reaction mixtures. Absorption of alkaline-earth cations from the aqueous solutions by the precipitates of $Ti(OBu)_4$ hydrolysis products occurred. Formation of crystalline perovskites might occur as a result of the reaction between titanium butoxide and aqueous solutions of $M(OH)_2$. On the other hand, $M^{II}TiO_3$ also crystallized in the course of a two step process when at first $Ti(OBu)_4$ was hydrolyzed by water or water-butanol mixture, and then the suspension was treated by aqueous solutions of alkaline-earth hydroxides. Stoichiometry and phase composition of $M^{II}TiO_3$ in the two cases were the same, however morphology of the powders was dependent on the way chosen for perovskite preparation. The product had a strong trend to agglomeration, and many rough agglomerates higher than 10 μm in size were formed. Therefore, all their further experiments were performed with a two-step process (Golubko, *et al.,* 2000). Formation of crystalline $BaTiO_3$ occurred only if $Ba(OH)_2$ concentration exceeded 5 mass.%.

Hu, *et al.,* (2000) developed a low-temperature hydrothermal reaction scheme to produce pure, ultrafine, uniform-sized, nanocrystalline barium titanate ($BaTiO_3$) microspheres from two inorganic precursors: synthesized titania microspheres and barium hydroxide solutions. Monodispersed titania microspheres approximately 0.1–1 mm in diameter were successfully synthesized for the further conversion to barium titanate. Barium titanate and titania microspheres were characterized by scanning electron microscopy SEM and room temperature X-ray diffraction RTXRD. High-temperature XRD HTXRD was also utilized for *in situ* study of the phase transformations and changes of crystallite size with calcination

temperatures. The titania microspheres were predominant in the anatase plus some brookite phase at room temperature and were converted to the rutile phase when the calcination temperature was increased from 650 °C to 900 °C. Monodispersed barium titanate microspheres were successfully synthesized from optimized titania via a hydrothermal reaction ($\leq$ 100 °C) in barium hydroxide solutions. The size and morphology of the barium titanate particles remained the same as the precursor titania particles, indicating a ''shrinking-core'' diffusion reaction mechanism. Barium carbonate in the form of witherite was also found along with the formation of barium titanate, especially under conditions with higher Ba/Ti ratios, but a formic acid washing procedure effectively removed this impurity phase from the barium titanate samples. The as-prepared barium titanate was in the cubic nanocrystalline form and did not change when the temperature was increased from room temperature to as high as 750 °C. The cubic phase was also stable at high temperatures for over 5 h. They explored various low-temperature-induced homogeneous coprecipitation processes using only inorganic precursor chemicals and devised a ''two-stage''approach for preparing monodispersed barium titanate: 1.dielectric-tuning solution (DTS) precipitation of titania microspheres and 2. Low temperature hydrothermal conversion of titania microspheres in barium hydroxide solutions. They prepared near perfect microspheres of titania and barium titanate under optimized conditions and focused on an investigation of TiO_2 to $BaTiO_3$ hydrothermal conversion processes by X-ray diffraction techniques (XRD). This route coupled two low-temperature hydrothermal processing steps: 1) DTS precipitation of monodispersed titania microspheres and 2) hydrothermal conversion of the prepared titania microspheres to nanocrystalline barium titanate. In particular, using titania microspheres prepared in their laboratory, they studied the titania-to-$BaTiO_3$ conversion process by characterizing the converted samples with XRD. Their results showed that high-purity $BaTiO_3$ could be obtained by hydrothermal conversion plus the formic acid washing step without the need for KOH addition or the requirement of CO_2 free water or argon atmosphere. The experimental evidence supported the *in situ* transformation diffusion reaction mechanism for the TiO_2 to $BaTiO_3$ conversion process.

A simple chemical route was developed by Potdar, *et al*., 2001 to obtain an important molecular precursor (leading to barium titanate powders), namely barium titanyl oxalate (BTO) with nearly theoretical yield. In this route, 0.1 M alcoholic solution of titanium tetrabutoxide was reacted with 0.1 M alcoholic solution of oxalic acid to form titanyl oxalate ($TiOC_2O_4$). This was further converted to soluble ammonium titanyl oxalate (ATO); $(NH_4)_2TiO_2(C_4O_2).H_2O$ by reacting with an equimolar aqueous solution of ammonium oxalate (pH 4.25). Instead of using available barium salts (halide / nitrate / acetate) solution, a modified barium precursor solution with controlled pH (5.42) was prepared for carrying out cation-exchange reaction with ATO. For this purpose the modified Ba-precursor solution was freshly prepared by partial neutralization of a 0.1 M aqueous solution of barium hydroxide with controlled addition of dilute HNO_3 (1.1 M) solution. The pH of this solution was the same as that of the ATO solution. The exchange reaction between equimolar ATO and modified Ba-precursor solution precipitated barium titanyl oxalate (BTO) with a quantitative yield at room temperature. Submicron-sized, stoichiometric, pure $BaTiO_3$ powders were obtained by the controlled pyrolysis of BTO in air. The present communication deals (Potdar, *et al*., 2001) with the detailed analysis of this simplifiied method in producing BTO / BT powders and their characterization employing various physicochemical techniques. The starting materials used in the synthesis of BTO were barium hydroxide, titanium tetrabutoxide, oxalic acid, isopropanol, nitric acid. The modified method of precipitation of BTO had the following advantages:

1. Complete exchange with 100% yield giving single phase BTO.

2. The procedure was simple, fast and gave reproducible results.

3. The pH adjustment was done prior to precipitation of BTO which helped to overcome limitation of local pH variation thus leading to homogeneous precipitation of BTO.

4. No excess reagents was required.

5. Unwanted impurity contamination (Na^+, K^+, and Cl^-) ions were avoided and stoichiometric agglomerated BT powders were obtained.

BaTiO$_3$ powder obtained by calcination of BTO at 750 ^{o}C for 5 hour and at 1300 ^{o}C for 4 hour were shown in Figure 1.2.6.1 and 1.2.6.2, respectively.
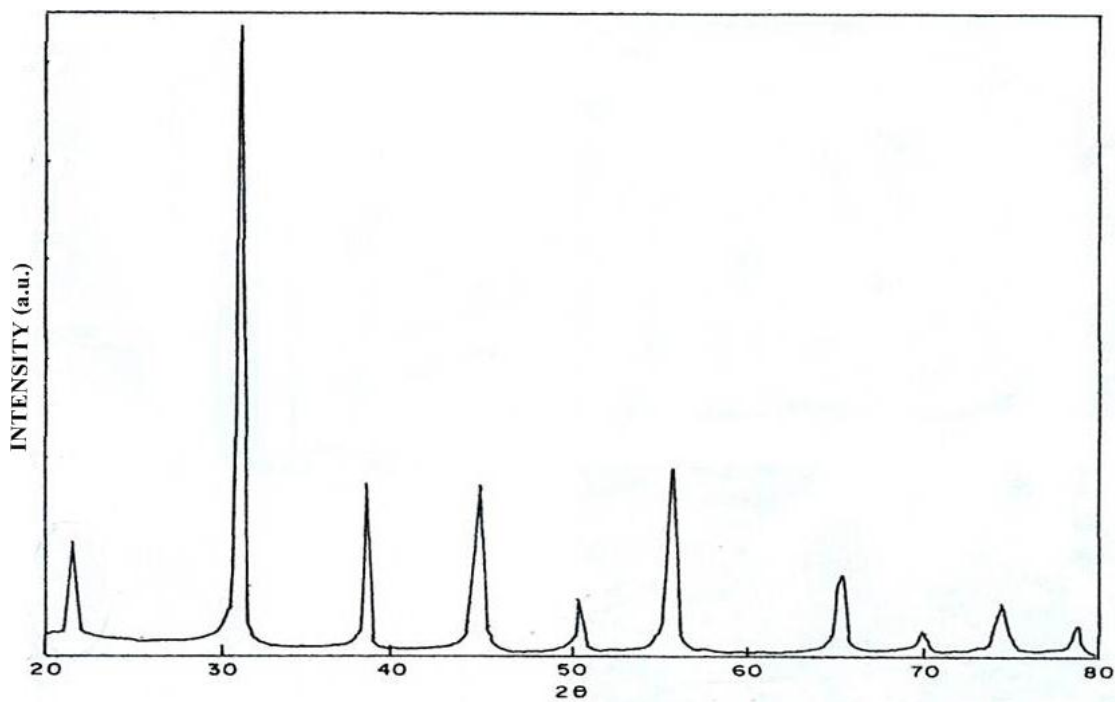
Figure 1.2.6.1 XRD patern of BaTiO$_3$ (calcined at 750°C/5h) (Potdar, *et al.,* 2001)
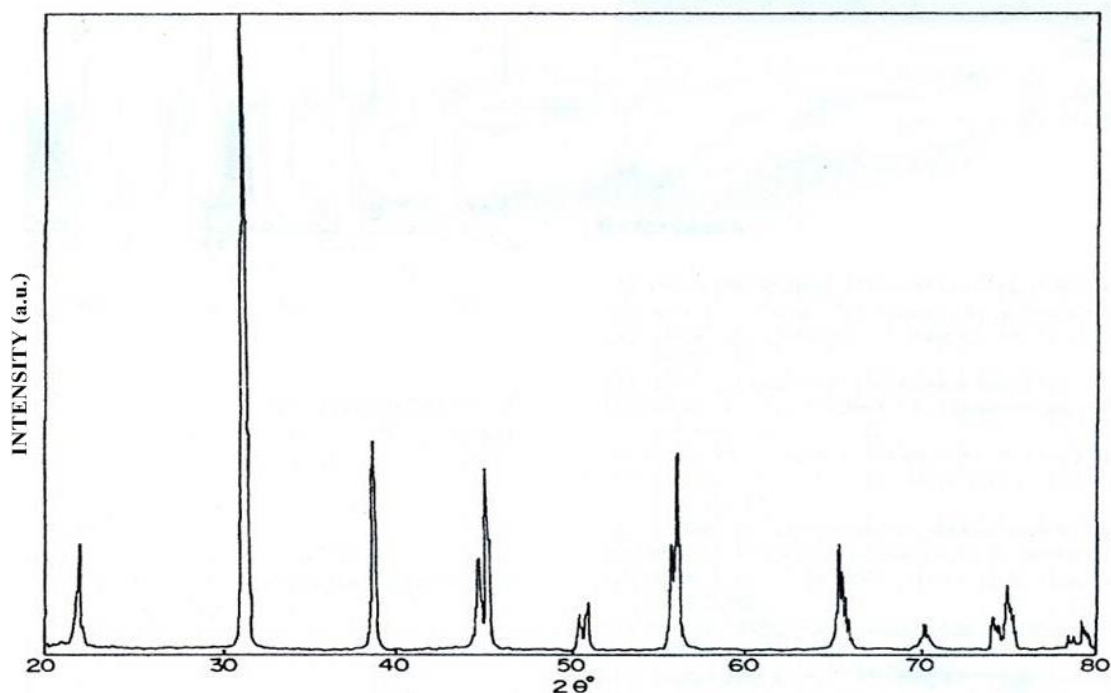
Figure 1.2.6.2 XRD patern of BaTiO$_3$ (calcined at 1300°C/4h) (Potdar, *et al.,* 2001)

Bera, *et al.,* (2003) prepared barium titanate powder via a semi-oxalate method. The starting materials used in the present work included Ba(NO$_3$)$_2$, TiO$_2$, and (COOH)$_2$·2H$_2$O. An aqueous solution of 0.12 molar Ba(NO$_3$)$_2$ was prepared using deionized water. Required amount (Ba/Ti = 1:1) of TiO$_2$ powder was added to the Ba(NO$_3$)$_2$ solution with constant stirring. The suspension was ultrasonicated (10 minutes) to break TiO$_2$ agglomerates. Required amount of oxalic acid (0.4 molar solution) was added drop wise into the mixture under vigorous stirring. The pH of the resultant mixture was adjusted to 6–7 by adding ammonia solution. This process precipitated barium oxalate on the surface of fine TiO$_2$ (seed) particles by heterogeneous nucleation. It was well known that heterogeneous nucleation was used in coating of ceramic particles with another ceramics. Barium oxalate was precipitated from nitrate solution onto the surface of TiO$_2$ powders. Crystallization of BaTiO$_3$ from the precursors was investigated by TGA, DTA and XRD analysis. It was evident that an intermediate barium oxycarbonate along with BaCO$_3$ formed between 450-500 ^{o}C and that decomposed to BaCO$_3$ again at high temperature. Decomposition of BaCO$_3$ occurred at much lower temperature, from 600 ^{o}C onwards, due to the

presence of TiO_2. The precursor completely transformed into $BaTiO_3$ at 900 $^{\circ}$C. Nanometer size $BaTiO_3$ crystallites were produced during this synthesis due to the lower calcination temperature. The crystalline morphology of $BaTiO_3$ was controlled mainly by the morphology of $BaCO_3$, which formed in the intermediate stage.

Malghe, *et al.,* (2004) synthesized cubic barium titanate ($BaTiO_3$) powder by heating barium titanyl oxalate hydrate, $BaTiO(C_2O_4)_2.4H_2O$ (BTO) precursor in microwave heating system in air at 500 °C. Heating BTO in microwave above 600 °C yielded tetragonal form of $BaTiO_3$. Experiments repeated in silicon carbide furnace showed that $BaTiO_3$ was formed only above 700 °C. The product obtained was cubic. BTO used in the present work was synthesized from the aqueous solution of $Ba(NO_3)_2$(BN) and $K_2TiO(C_2O_4)_2$(KTO). Both the chemicals were of analytical grade. The method consisted of mixing of equimolar aqueous solutions of BN and KTO with constant stirring. The white BTO precipitate obtained was filtered, washed with distilled water and dried in an oven at 50 °C for 24 h. From chemical analysis, the product could be assigned the molecular formula, $BaTiO(C_2O_4)_2.4H_2O$. The BTO precursor was heated to different temperatures in the range 400-700 °C employing the microwave heating system fabricated indigenously. The microwave oven used could supply maximum 750 watts input power. The power to the unit could be maintained to a constant set value to fix the desired temperature needed for the experiments, employing the proportional type (PID) temperature controller coupled to a solid state relay (SSR). A shielded chromel-alumel thermocouple was used as a sensor for controlling the input power to the microwave oven at the set temperature. The thermocouple shield had to be grounded to obtain steady temperature values at the set point. The temperature of the sample could be maintained constant to $\pm$ 1 °C and measured by a separate calibrated chromel-alumel thermocouple. For the influence of microwave field on the measured temperature, it was checked by momentarily putting off the microwave oven. No difference was observed in the temperature displayed on the indicator. The sample contained in a cylindrical zirconia crucible was surrounded symmetrically by four silicon carbide rods, which acted as a preheater for the samples poorly interacting with the microwaves at ambient temperature. The X-ray diffraction patterns of the product of thermal decomposition

of BTO in microwave heating system in the temperature range 500–700 °C revealed that formation of $BaTiO_3$ from BTO was complete at 500 °C. The product at 500 °C consisted of pure cubic $BaTiO_3$. The product obtained at 600 °C, however, indicated that the cubic form possibly transformed to tetragonal structure as revealed by asymmetric peaks at the 2θ values corresponding to 45.25, 50.90, 56.12, 74.87and 79.5^o, respectively. The splitting of these peaks in the sample heated at 700 °C and above confirmed the transformation of cubic phase to a tetragonal form. The results obtained in this investigation showed that $BaTiO_3$ in the cubic form could be synthesized from BTO at temperature as low as 500 °C. Thermal decomposition of BTO presumably yields hypostoichiometric TiO_2 by virtue of the presence of evolved CO in the reaction, which in the presence of the microwave field combines with BaO to yield the cubic phase. The cubic $BaTiO_3$ transformed completely to the tetragonal form on heating it in the microwave field above 700 °C. In the recent studies (Potdar, *et al.,* 1999; Khollam, *et al*., 2002), it was reported that BTO on heating in the resistance heated furnace above 700°C in air produced cubic form of BT. Their observations were in agreement with these results. The cubic form was transformed to tetragonal structure in the pellets sintered in air above 1250 °C (Potdar, *et al.,* 1999; Khollam, *et al*., 2002). The production of tetragonal form of $BaTiO_3$ at low temperatures following the present procedure could provide considerable edge over other existing processes and made it economically much more viable for commercial exploitation.

Shut, *et al.,* (2008) prepared barium titanate powders with average crystallite sizes of 68–2000 nm by the calcination of barium titanyl oxalate (BTO) at temperatures of 700–1150 °C. The morphology and recrystallization kinetics of the powders were studied using the SEM and X-ray methods.

Sreekantan, *et al.,* (2008) prepared barium titanate powder at temperature 80 °C by reacting TiO_2 sol in aqueous solutions that contained $BaCl_2$ and NaOH at atmospheric pressure. Well-crystallized (cubic phase), spherical barium titanate powder with average size of 35 nm was formed by this method at 80 °C. As for sintered barium titanate, observation via SEM showed bimodal distribution of

grain size. The fine grains were in the range of 0.3–0.5 μm whereas the large ones were approximately 1.5–2.0 μm. Sintering at 1300 °C, led to the formation of a tetragonal structure $BaTiO_3$ with a secondary phase of $BaTi_2O_5$ and $Ba_6Ti_{17}O_{40}$. Based on the research done, it is apparent that the most of the investigations placed their aim mainly on the preparation of fine powders with high purity at low temperature. On the other hand, there had been few studies dealing with electrical characterization of sintered ceramics prepared by wet chemical methods. In the study by Sreekantan, *et al.,* 2008, the structural and electrical characteristic of barium titanate powder and the sintered body which was prepared by a simple chloride aqueous method at low temperatures 80 ^{o}C at atmospheric pressure was reported. The chloride aqueous method was established to produce barium titanate by reacting titania sol in alkaline aqueous solutions of $BaCl_2$ and NaOH. As shown in the paper, the chloride aqueous method resulted in nanosized, crystalline particles with the formation of a metastable phase under certain condition. They demonstrated the possibility of obtaining well-crystallized, cubic and nano-sized barium titanate at 80 ^{o}C using chloride aqueous method. Sintering at 1300 ^{o}C, led to tetragonal phase and crystallite growth. Evidence was obtained for the existence of the wedge shaped domains and it appeared to have stopped not only by grain boundaries but also by the other domains and {111} twin. The response of barium titanate sintered at 1300 ^{o}C indicated the presence of two elements in this material.

In order to enhance the tetragonality of $BaTiO_3$ derived from barium titanyl oxalate (BTO), various treatments were carried out by considering the thermal decomposition mechanism of BTO in air (Kim, *et al.,* 2007). A multi-step heat treatment process and the addition of carbon black, as a particle growth inhibitor, were effective in increasing the tetragonality, whilst maintaining a particle size smaller than 200 nm. The synthesized $BaTiO_3$ powder with a mean particle size of 177 nm showed a tetragonality and K-factor of 1.0064 and approximately 3, respectively.

Jung, *et al.,* (2011) examined the formation of $BaTiO_3$ from degassed barium titanyl oxalate (degassed BTO), which was heat treated at 500 °C for 2 h

followed by 20 min of aqueous milling, upon further heating. The evolution of $BaCO_3$ by Ti-based inter phase was formed $BaTiO_3$ at various temperatures. The examined by X-ray diffraction, high-resolution scanning transmission electron microscopy, and electron energy loss spectroscopy. When the degassed BTO was exposed to an aqueous milling, significant amounts of needle-shaped $BaCO_3$ crystals formed preferentially, which made this system similar to that of a solid-state reaction. However, the formation mechanism of $BaTiO_3$ observed in this study was found to be different from that of a solid-state reaction due to the different nature of the Ti-based phase.

$BaTiO_3$ has band gap (Eg) 3.2 eV (Cox, 1995) which almost equals to that of TiO_2 anatase. It is interesting to see this effect when $BaTiO_3$ is coupled with TiO_2 in term of photocatalytic activity. One sample in this work (TiO_2-BT) is the one that coupling $BaTiO_3$ and TiO_2 for this purpose.

1.2.7   Classification of dyes and treatment method for dye pollutant

Dyes are classified according to their chemical constitution on the basis of their dyeing properties. Thus members of the great group classified constitutionally as azo dyes are found amongst several of the classes based on application. The practical dyer is primarily interested in classification according to application. The constitutional groups will therefore only be classified briefly (Suwanchawalit, 2008).

-Acid dye

Acid dye is a member of a class of dye that is applied from an acidic solution. In textiles, acid dyes are effective on protein fibers, i.e. animal hair fibers like wool, alpaca and mohair. They are also effective on silk. They are effective in dyeing the synthetic fiber nylon but of minimal interest in dyeing any other synthetic fibers. Acid dye are thought to fix to fibers by hydrogen bonding, van der waals forces and ionic bonding. Animal protein fiber and synthetic Nylon fibers contain many cationic sites therefore there is an attractive of anionic dye molecule to a

cationic site on the fiber. The chemistry of acid dyes is quite complex. Dyes are normally very large aromatic molecules consisting of many linked rings. Acid dyes usually have a sulfo or carboxy group on the molecule making them soluble in water. Water is the medium in which dyeing takes place (http://en. Wikipe dia. org/ wiki/ Acid_dye).

- Basic dyes

Basic dyes is a class of dyes, usually synthetic, that act as bases, and which are actually aniline dyes. Their color base is not water soluble but can be made so by converting the base into a salt. The basic dyes, while possessing great tincrotrial strength and brightness, are not generally light-fast; therefore their use in the dyeing of archival materials is largely restricted to those materials not requiring this and methylene blue. It is applied to wool, silk, cotton and modified acrylic fibers. Basic dyes perform poorly on natural fibers, but work very well on acrylics. Basic dyes are also used in the coloration of paper (http://www.jagson.com/paper_dyes.htm).

- Direct dyes

Direct dyes are a class of hot water dyes for use on cellulose fibers, such as cotton, rayon, and linen, but they will also color silk and wool. Direct dyes are applied in hot water, typically between 175 ^{o}F and 200 ^{o}F. They can be applied in the same boiling-water dye bath with acid dye. Direct dyes are only loosely associated with the fiber molecule through the property called substantivity, which is the tendency of the dye to associate with the dye without strong bonds that used the relatively weak van der waals forces and some hydrogen bonding (http:// www. pburch.net/dyeing/directdye.shtml).

- **Mordant dyes**

Mordant dyes require a mordant, which improves the fastness of the dye on the fiber such as water, light and perspiration fastness. Mordants are substance of organic or inorganic origin which combine with the coloring matter and are used to

fix the same in the production of the color. The mordant substances include such acids as tannic acid, sumac, gall nuts, bark extracts, oleic and stearic acids, and metallic substances such as various combinations or soluble salts of chromium, aluminum, iron, copper, and tin. The latter, the metallic mordants are more used than the acid mordants. The choice of mordant is very important as different mordants can change the final colour significantly. The most commonly used mordant dyes have hydroxyl and carboxyl groups and are negatively charged, i.e. anionic. It is convenient to view these as a specialized subgroup of acid dye. Some other mordant dyes may possess amino groups, and are cationic overall. Despite this, they must still have hydroxyl or carboxyl groups, since lake formation requires it. Mordant dyes can usually stain by ionic interaction in the same way as other ionisable dyes (http:// www .jagsom .com/ mordant_dyes.htm). In addition, these dyes have no natural affinity for textiles but are applied to cellulosic or protein fibers which have been mordanted previously with a metallic oxide. The acid mordant dyes are a special class of dyes applied to wool or polyamide fibers as if they were acid dyes, and then given very high wet-fastness by subsequent mordanting (Trotman, 1975).

- **Vat dyes**

Vat dyes are an ancient class of dyes, based on the natural dye, indigo, which is now produced synthetically. Most vat dyes are less suitable than fiber reactive dyes, as they are difficult to work with; they require a reducing agent to solubilize them. The dye is soluble only in its reduced (oxygen-free) from. (http://en.wikipedia.org/wiki/Vat_dye). Vat dyes are used in cotton dyeing where high wash and boil fastness required. Because of the high alkali concentration in the dye bath, pure vat dyes cannot be used on animal fibers (wool, natural silk, and various hairs) (http://www.dyeman.com/Dye%20summary.h tml).

-Reactive dyes

In a reactive dye a chromophore contains a substituent that is activated and allowed to directly react to the surface of the substrate. Reactive dyes are used to dye cellulosic fibers. The dyes contain a reactive group, either a halo- heterocycle or

an activated double bond, that, when applied to fiber in an alkaline dye bath forms a chemical bond with an hydroxyl group on the cellulosic fiber. Reactive dyes can also be applied on wool and nylon; in the latter case they are applied under weakly acidic condition (http://en.wikipedia.Org / wiki / Reactive_dye).

-Disperse dyes

Disperse dyes were originally developed for dyeing of cellulose acetate, and are water insoluble. The dyes are finely ground in presence of a dispersing agent and then sold as paste, or spray-dried and sold as a powder. Their main use is to dye polyester but they can also be used to dye nylon, cellulose triacetate, and acrylic fibers (http://en.wikipedia. org/wiki/Dye)

-Azoic dyes

A dye in which the azo group (N=N) is the chromophore and joins benzene or naphthalene rings. These dyes are insoluble pigments built up within the fiber by padding with a soluble coupling component and then treating with a diazotized base. They are used for dyeing colors on cellulosic fibers when comparatively good wet-fastness combined with brightness of shade is required at a reasonable cost (Trotman, 1975).

-Sulfur dye

Sulfur dyes are dyed from a dye bath containing sodium sulphide and common or Glauber's salt, and are oxidized by airing or with some oxidizing agents (sodium bichromate or hydrogen peroxide) in fresh bath. The main advantage lays in their cheapness, ease of application and good wash-fastness. In their normal state sulphur dyes are insoluble in water but are readily soluble in the solution of sodium sulphide. In this from they have high affinity to the all cellulose fibers (http://www . dyeman.com/com/Dye%20summary.html).

In the present work, orange II sodium salt (Acid dye or anionic dye) was selected as a model of dye pollutant with which the degradation efficiencies of the as prepared catalyst are to be investigated. The structure is shown in Figure 7 (http://www.sigmaaldrich.com).
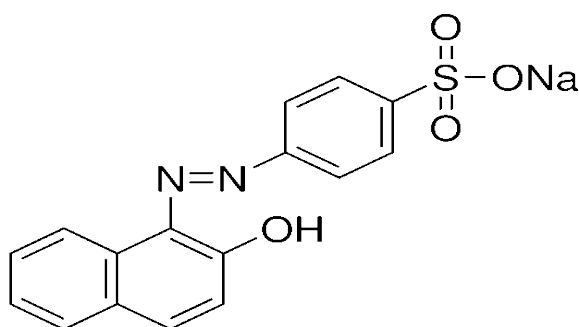
Figure 7. Structure of orange II sodium salt.

Orange II sodium salt

Orange II sodium salt or also called acid orange 7 (AO7), (4-(2-hydroxy naphthylazo) benzenesulfonic acid sodium salt), $C_{16}H_{11}N_2NaO_4S$, is a molecule with N=N bonds that is widely used in the dyeing of textiles and cosmetics, and thus found in the wastewaters of the related industries. Acid orange has been used in several research articles. Stylidi, *et al.*, (2004) studied photocatalytic degradation of acid orange 7 in TiO_2 suspensions using solar light simulating source. Konstantinou, *et al.,* (2004) investigated kinetic and mechanistic of photocatalytic degradation of AO7 using TiO_2 as photocatalyst. Fernandez, *et al.*, (2004) investigated the effect of pH and H_2O_2 addition using using TiO_2-coated glass rings as immobilized photocatalyst. Azam and Hamid (2006) investigated effects of the reactor gap size and UV dosage on decolorization of AO7 using UV/H_2O_2 process. Hammami, *et al.,* (2008) studied the degradation of AO7 aqueous solutions by electro-Fenton process using Pt or boron-doped diamond (BDD) anode. Zhang, *et al.*, (2008) investigated the roles of active oxygen species in photodegradation of AO7 in TiO_2 photocatalysis illuminated by microwave electrodeless lamp. The degradation pathway of AO7 was

determined by a careful identification of intermediate product. The oxidative attack of AO7 led to benzene sulfonate and naphthoquinone as primary degradation products. The obtained quinine forms were unstable in the oxidative medium of the experience and underwent ring opening reactions leading to the formation of short chain aliphatic acids such as succinic, formic, maleic, oxalic and acetic acids which were the last by products before mineralization. Meneralization of AO7 led to the conversion of nitrogen and sulphur heteroatoms present in the molecule into inorganic ions, such as nitrate, ammonium and sulphate ions (Konstantinou, *et al.,*2004; Hamami,et al.,2008).

Treatment of dye pollutant

Textile dyes and other industrials dyestuffs constitute one of largest group of organic compounds that represent an creasing environmental danger. About 15% of the total world production of synthetic textile dyes is lost during the dyeing process and is released in the textile effluents. The release of these colored wastewaters in the ecosystem is dramatic source of aesthetic pollution, eutrophication and perturbations in aquatic life. Therefore, it is important to develop effective wastewater remediation technologies for these compounds (Houas, *et al.,* 2001; Konstantinou, *et al.,* 2004)

A variety of physical, chemical and biological methods are presently available for treatment of textile wastewater. Biological treatment is a proven technology and is cost-effective. However, it has been reported that the majority of dyes are only adsorbed on the sludge and are not degraded. Physical methods such as ion-exchange, adsorption, air stripping, *etc.,* are also ineffective on pollutants which are not readily adsorbable or volatile, and have the further disadvantage that they simply transfer the pollutants to another phase rather than destroying them (Senthilkumarr, *et al.,* 2006). This leads to search for highly effective method to degrade the dyes into environmentally compatible products. It has been revealed from several literatures that the heterogeneous photocatalysis can be used to destroy the dyes using semiconductor catalyst under light irradiation (Muruganandham, *et al.,* 2005).

Among the semiconductors used, TiO$_2$ has been successfully used to decolorize and mineralize many organic pollutants including several dyes and their intermediates present in aqueous system using both artificial light and under sunlight using solar technology. TiO$_2$ is the most widely used photocatalyst because of its good activity, chemical stability, commercial availability and inexpensiveness. It is generally used as a photocatalyst for environmental applications such as air purification, water disinfection, hazardous waste radiation and water purification (Houas, *et al.,* 2001; Nagaveni, *et al.,* 2004; Muruganandham, *et al.,* 2005).

The major advantages of this heterogeneous photocatalysis are as follows. (i) Photocatalysis offers a good substitute for the energy-intensive conventional treatment methods with capacity for using renewable and pollution-free solar energy. (ii) Unlike conventional treatment measures, which transfer pollutants from one medium to another, photocatalysis leads to the formation of innocuous products. (iii) This process can be used to destroy a variety of hazardous compound in different wastewater streams. (iv) It can be applied to aqueous and gaseous-phase treatment, as well as soild-phase treatment to the same extent. (v) The reaction conditions for photocatalysis are mild, the reaction time is modest, and a lesser chemical input is required. (vi) Secondary waste generation is minimal. (vii) The option for recovery can also be explored for metals, which are converted to their less-toxic/nontoxic metallic states (Kabra, *et al.,* 2004).

Recently, many works have been reported on the degradation of organic dyes induced by visible light by photosensitization. The interest is to use solar visible light which is free and inexhaustible (Houas, *et al.,* 2001). The electron-hole pair (e$^-$-h$^+$ pair) thus created migrates to the photocatalyst surface where it either recombines, producing thermal energy, or participates in redox reactions with the compounds adsorbed on the photocatalyst. The lifetime of an e$^-$-h$^+$ pair is a few nanoseconds, but this is still long enough for promoting redox reactions in the solution or gas phase in contact with the semiconductor (Kabra, *et al.,* 2004).

Generally, the hole oxidizes water to hydroxyl radicals (which subsequently initiate a chain of reactions leading to the oxidation of organics), or it

can be combined with the electron from a donor species, depending on the mechanism of the photoreaction. Similarly, the electron can be donated to an electron acceptor such as an oxygen molecule (leading to formation of superoxide radical) or a metal ion (with a redox potential more positive than the band gap of photocatalyst). This metal ion can be reduced to its lower valence states and deposited on the surface of the catalyst. The electron-transfer process is more efficient if the species are pre adsorbed on the catalyst surface (Kabra, *et al.,* 2004).

Many studied revealed that heterogeneous photocatalytic oxidation process could be used for removing coloring material from dye effluent. Zhang, *et al.,* (1998) demonstrated the TiO_2-doping on the photocatalytic degradation of Acid Orange 7 (AO7). Zhang, *et al.,* (2000) investigated the effect of calcination on the photocatalytic properties of nanosized TiO_2 powders prepared by $TiCl_4$ hydrolysis. Zhu, *et al.,* (2000) studied the photocatalytic degradation of azo dyes by reported TiO_2 + UV in aqueous solution. Hachem, *et al.,* (2001) studied the photocatalytic degradation of various dyes (orange II, orange G, Congo Red, Indigo Carmine, Crystal violet, Malachite Green, Remazol Blue and Methyl Yellow) using P25 Degussa as catalyst. Grzechulska, *et al.,* (2002) investigated the effect of operational parameters, i.e., pH, photocatalyst content, initial dye concentration on the photocatalytic decomposition of azo-dye acid black 1 in water over modified titanium dioxide. Zhao, *et al.,* (2002) studied the influence of Pt doping on photodegradation of sulforhodamine-B dye under visible irradiation. Sauer, *et al.,* (2002) studied the kinetics of photocatalytic degradation of reactive dyes in a TiO_2 slurry reactor. Ferendez-Ibanez, *et al.,* (2002) reported photo-discolouration of orange II solutions at different concentrations irradiated with a 254 nm mercury lamp (125 W) in the presence of Degussa P25-TiO_2 dispersions. Daneshvar, *et al.,* (2003) studied the photocatalytic degradation of azo dye acid red 14 in water and investigated the effect of operational parameters. Gomes da silva and freire (2003) investigated effect of kinetic on photodegradation of azo dye (Solophenyl Green: SG) by TiO_2 under UV irradiation. Xie and Yuan (2003) reported the photocatalytic activity and recycle application of titanium dioxide sol for X-3B photodegradtion. Konstatinou, *et al.,* (2004) investigated the effect of kinetic on the photocatalytic degradation of azo dye

in an irradiated titanium dioxide aqueous suspension. Shifu, *et al.,* (2005) reported the role of primary active species and TiO_2 surface characteristic in UV-illuminated photodegradation of acid orange 7. Zhang, *et al.,* (2006) revealed the effect of Pt doped on the TiO_2 thin film under visible irradiation. Venkatachalam, *et al.,* (2007) reported the varied reaction parameters: hydrolyzing agent, molar ratio, aging time, calcination during the synthesis of nano size TiO_2 and revealed its photocatalytic activity higher than P25-TiO_2 on photocatalytic oxidation of bisphenol-A.

1.3 Objectives

The objectives of this research are as follows.

(1) To prepare compounds containing barium and titanium constituents; barium-titanium-oxalate (BTO), mixture of titanium dioxide and barium oxalate (or coupled TiO_2-BaC_2O_4), and mixture of titanium dioxide and barium titanate (or coupled TiO_2-BT) by oxalate route.

(2) To study photocatalytic activity under UV and visible light of BTO, coupled TiO_2-BaC_2O_4, and coupled TiO_2-BT and compare them with the commercial TiO_2 powder catalyst (Degussa P25) under the same condition.

(3) To study the effect of pH and concentration of dye on the photocatalytic degradation of BTO, coupled TiO_2-BaC_2O_4, and coupled TiO_2-BT.

(4) To study recyclability of BTO, coupled TiO_2-BaC_2O_4, and coupled TiO_2-BT.

CHAPTER 2

Experimental and characterization techniques

2.1 Synthesis of BTO, TiO$_2$-BaC$_2$O$_4$, and TiO$_2$-BT by oxalate route

2.1.1 Materials

(1) Barium chloride, BaCl$_2$, A.R., code no. 2827 39 85, MERCK, Germany.

(2) Hydrochloric acid, HCl, A.R., code no. 9535-03, J.T. Baker, U.S.A.

(3) Potassium oxalate, (COOK)$_2$.H$_2$O, A.R., code no. A413, Ajax Finechem, Australia.

(4) Silver nitrate, AgNO$_3$, A.R., code no. 102333J, BDH, England.

(5) Sodium chloride, NaCl, A.R., code no. 479686, CARLO ERBA REAGENTI, Italy.

(6) Titanium dioxide (anatase), TiO$_2$, A.R., code no. 488257, CARLO ERBA REAGENTI, Italy.

(7) Titanium dioxide (Degussa P25), code no. D-60287, Degussa AG, Frankfurt, Germany.

(8) Titanium oxysulfate, TiOSO$_4$.xH$_2$O, A.R., Sigma Aldrich, Germany.

(9) Oxalic acid, (COOH)$_2$.H$_2$O, A.R., code no. O/0650/60, Fisher Scitific, UK.

(10) Orange II sodium salt, C$_{16}$H$_{11}$N$_2$O$_4$S, A.R.,code no.08126-256, Fluka, U.S.A.

2.1.2 Instruments

Department of Chemistry, PSU.

1. Centrifuge, EBA 20, Hettich, Germany.

2. Diffused reflectance spectrophotometer, DRS, UV- 2401, Shimadzu, Japan.

3. Fourier-transformed infrared spectrophotometer, FT- IR, Spectrum

GX, Perkin-Elmer, U.S.A.

4. Ultraviolet-visible spectrophotometer, SPECORDS 100, Analytik Jena GmbH, Germany.

5. Reaction compartment (UV light, 0.75m × 0.75m × 0.75m; Visible light, 0.70m × 0.70m × 0.70m).

6. pH meter, pH Tester 10, Eutech Instruments/ Oakton Instruments, U.S.A.

Scientific Equipment Center, PSU.

1. X-ray diffractometer, XRD, PHILIPS X'Pert MPD, the Netherlands.

2. Scanning electron microscopy, SEM, JEOL JSM - 5800LV, Japan.

3. Scanning electron microscopy, SEM, QUANTA 400, Japan.

National Metal and Materials Technology Center, MTEC

1. BET surface area, Quantachrome/ Autosorb-1.

2.1.3 Method

This work involves syntheses, characterizations, and photocatalytic studies of barium titanium oxalate (BTO), coupled TiO_2-BaC_2O_4, and coupled TiO_2-BT. The coupled TiO_2-BT was obtained by calcination of TiO_2-BaC_2O_4 at 800 ^{o}C. In the photocatalytic study, orange II sodium salt was used as model dye pollutant in wastewater. The light irradiation covered both UV and visible regions. The known commercial TiO_2 photocatalysts (anatase and Degussa P25) were simultaneously studied for comparison of degradation efficiencies. The syntheses and characterizations are given and discussed in sections 3.1-3.3 and the photocatalytic studies in sections 3.4-3.6.

2.1.3.1 Synthesis of BTO

The product was synthesized by the procedure described by Khollam, *et al.*, 2002 and displayed in the flow chart in Fig. 2.1. In the procedure, 1.593 g of $TiOSO_4$ was added to 100 mL of distilled water to give a clear solution and mixed with hot solution of 0.1 M $H_2C_2O_4$ 100 mL. The sulfate ion (SO_4^{2-}) was removed by precipitation with excess 0.1 M $BaCl_2$. The species remained in the solution was $[TiO(C_2O_4)]^{2-}$ which after addition of 0.1 M $BaCl_2$ and evaporation under vigorous stirring the resulting white precipitate (BTO) was formed and then filtered. The product was washed with distilled water until no chloride ion was found by $AgNO_3$ solution test and dried in air.

```
                    ┌─────────────────────────┐
                    │     TiOSO₄ 0.1 M         │
                    └─────────────────────────┘
                                │
                    Hot solution of 0.1 M H₂C₂O₄
                                ↓
                    ┌─────────────────────────┐
                    │     Clear solution       │
                    └─────────────────────────┘
                                │
              Excess 0.1 M BaCl₂ to remove SO₄²⁻
                                ↓
                    ┌─────────────────────────┐
                    │     Precipitation        │
                    └─────────────────────────┘
                         ↙              ↘
   White precipitation          ┌──────────────────────────────┐
   BaSO₄                        │  Clear solution of [TiOC₂O₄]²⁻ │
                                └──────────────────────────────┘
                                            │
                                       0.1 M BaCl₂
                                            ↓
                                ┌──────────────────────────────┐
                                │ Evaporation while vigorous     │
                                │ stirring                       │
                                └──────────────────────────────┘
                                            │
                                            ↓
                                ┌──────────────────────────────┐
                                │        Precipitate             │
                                └──────────────────────────────┘
                                            │
                                  Washing / Filtering / Drying
                                            ↓
                                ┌──────────────────────────────┐
                                │            BTO                 │
                                └──────────────────────────────┘
```
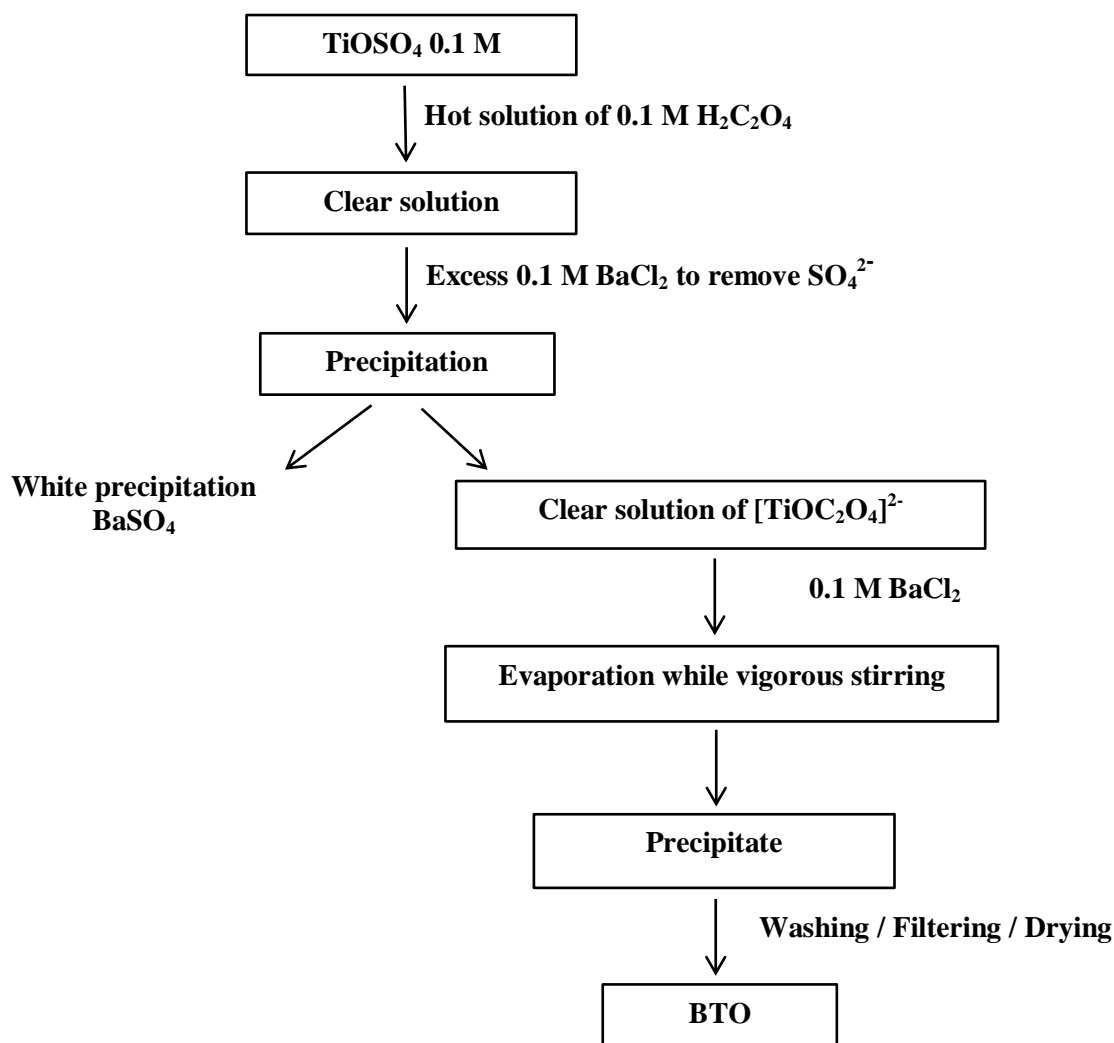
Figure 2.1 Flow chart of BTO synthesis (adapted from Khollam, *et al.,* 2002)

2.1.3.2 Synthesis of coupled TiO_2-BaC_2O_4

All chemicals used in this work were of analytical grade and were used without further purification. Titanium dioxide anatase phase and potassium oxalate were used as starting materials to produce coupled TiO_2-BaC_2O_4. The products was synthesized by the procedure described by Louer, *et al.*, 1992 and displayed in the flow chart in Fig. 2.2. Initially, potassium titanium oxalate, $K_2TiO(C_2O_4)_2$, was prepared by adding a slurry of 0.01 mole of TiO_2 (anatase phase) in 100 mL H_2O to 100 mL of 0.1M potassium oxalate solution. The mixture was stirred and 100 mL of 0.1 M $BaCl_2$ solution was added. The white precipitate formed was filtered and then washed with distilled water until no chloride ion was found by the $AgNO_3$ solution and dried in air.

0.1 M Potassium oxalate solution (100mL)

↓ **Slurry of 0.01 mole TiO_2 in 100 mL**

Potassium titanium oxalate

↓ **0.1 M $BaCl_2$ solution (100 mL)**
Constant stirring

Precipitation

↓

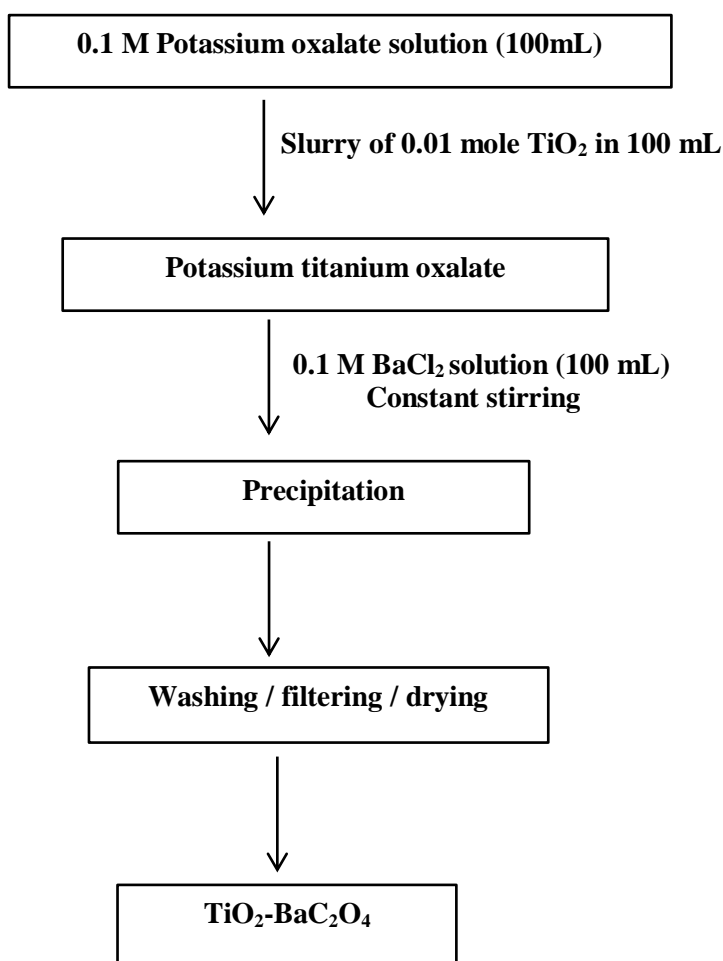| Washing / filtering / drying |
| :---: |

↓

TiO_2-BaC_2O_4

Figure 2.2 Flow chart of TiO_2-BaC_2O_4 synthesis (adapted from Louer, *et al.,* 1992)

2.1.3.3 Synthesis of coupled TiO$_2$-BT

In the synthesis of coupled TiO$_2$-BT, a slurry of 0.01 mole of TiO$_2$ (anatase) in 100 mL H$_2$O and 100 mL of 0.1 M potassium oxalate solution were mixed and stirred and 100 mL of 0.1 M BaCl$_2$ solution was added. The white precipitate formed and was filtered, washed with distilled water until free of chloride ion, and dried in air and then calcined at 800°C. This synthesis was described by Louer, *et al.*, 1992 and displayed in the flow chart in Fig. 2.3.
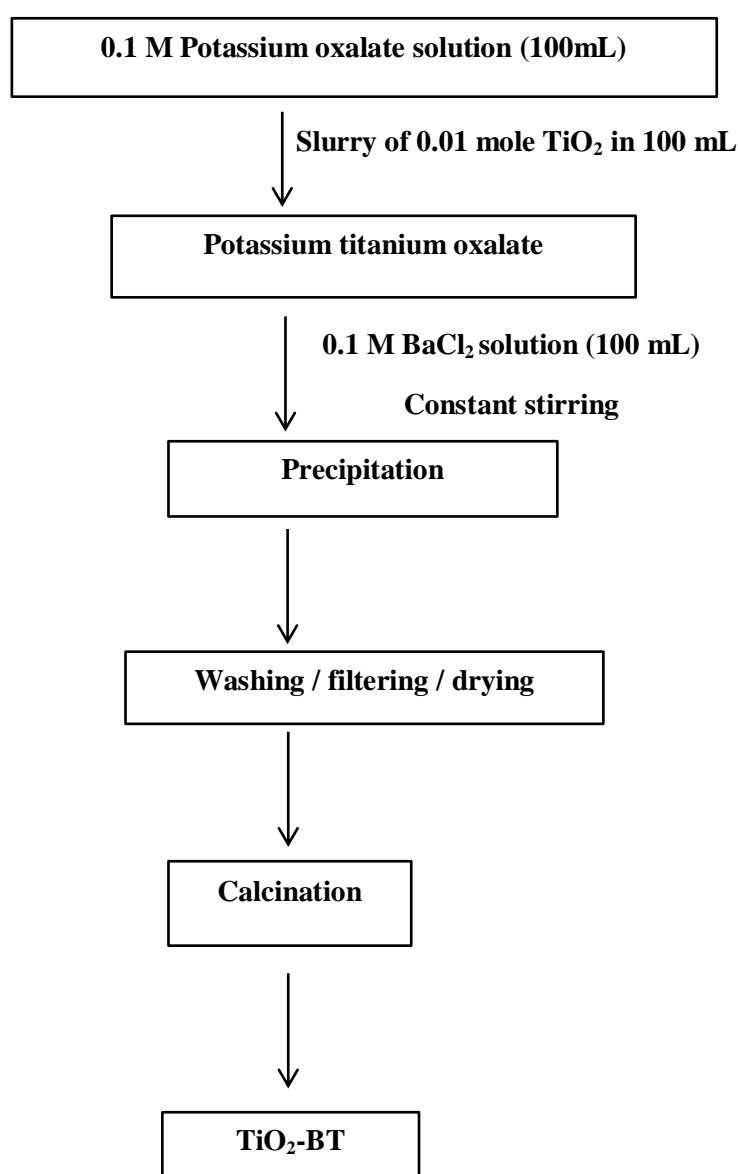
```
┌─────────────────────────────────────────────┐
│   0.1 M Potassium oxalate solution (100mL)   │
└─────────────────────────────────────────────┘
                    │  Slurry of 0.01 mole TiO₂ in 100 mL
                    ▼
        ┌───────────────────────────────┐
        │   Potassium titanium oxalate  │
        └───────────────────────────────┘
                    │  0.1 M BaCl₂ solution (100 mL)
                    │       Constant stirring
                    ▼
        ┌───────────────────────────────┐
        │         Precipitation         │
        └───────────────────────────────┘
                    │
                    ▼
        ┌───────────────────────────────┐
        │   Washing / filtering / drying │
        └───────────────────────────────┘
                    │
                    ▼
        ┌───────────────────────────────┐
        │          Calcination          │
        └───────────────────────────────┘
                    │
                    ▼
        ┌───────────────────────────────┐
        │           TiO₂-BT             │
        └───────────────────────────────┘
```

Figure 2.3 Flow chart of TiO$_2$-BT synthesis (adapted from Louer, *et al.,* 1992)

2.2 Characterization techniques

The synthesized TiO_2 powders were characterized by various techniques like XRD, SEM, UV-Vis DRS, and FT-IR.

2.2.1 X-ray diffraction (XRD)

The XRD technique was used to identify and confirm structure of all samples (BTO, TiO_2-BaC_2O_4, TiO_2-BT) synthesized in this work. The XRD spectra were acquired at the Scientific Equipment Center, Prince of Songkla University, Hat Yai, Songkhla, Thailand, with the Philips PW 3710 powder diffractometer (PHILIPS X'Pert MPD) using Cu K_α radiation and equipped with a Ni filter over the range of 2θ = 5-90° at room temperature. The crystallite size was calculated using the Scherrer's equation(Eq. (2.1)).

$$d = [0.9\lambda /(\beta cos\theta)]\times[180/\pi] \tag{2.1}$$

In Eq. (2.1), d is the crystallite size, β is the full width at half maximum (FWHM, in radians), λ is the wavelength of the X-ray radiation (1.5406 A°) and θ is the diffraction angle of the reflection (Lakshiminarasimhan, *et al.*, 2007).

2.2.2 Scanning electron microscopy (SEM)

In this work, the surface morphology and size of BTO, TiO_2-BC_2O_4, and TiO_2-BT samples were observed with a SEM (JEOL JSM-5800LV and Quanta 400). All data were acquired at the Scientific Equipment Center, Prince of Songkla University, Hat Yai, Songkhla, Thailand.

2.2.3 Surface area measurement

The Brunauer-Emmett-Teller (BET) surface area was determined using BET theory from the N_2 adsorption (Quantachrome/ Autosorb-1, outgas temperature at 300 ^{o}C). The average particle size was estimated by assuming all the particles have same spherical shape and size.

2.2.4 Diffused reflectance UV-Vis spectroscopy (DRS)

The band gap energies of BTO, TiO_2-BaC_2O_4, and TiO_2-BT were determined using UV-Vis DRS spectroscopy with a Shimadzu UV-2401 spectrophotometer (Shimadzu, Japan). The spectra were recorded in diffused reflectance mode using $BaSO_4$ as a reference. The band gap energies (E_g) of the catalyst were calculated according to

$$E_g = \frac{hc}{\lambda} = \frac{1240}{\lambda} \tag{2.4}$$

where E_g is the band gap energy (eV), h is the Planck's constant (6.63×10^{-34} J.s.), c is the light velocity (3×10^8 ms^{-1}), λ is the onset absorption wavelength (nm).

2.2.5 Fourier-transformed infrared spectroscopy (FT-IR)

The FT-IR spectrophotometry technique was used to identify the functional groups in the range 4,000-400 cm^{-1} with Spectrum GX, Perkin Elmer, U.S.A., using KBr as reference material.

2.2.6 UV-Vis spectroscopy

In this work, the concentration of orange II sodium salt in the solution was determined by measuring the absorbance intensity at 480 nm (Specord S100, Analytical Jena GmbH, Germany) and the results were obtained by the use of calibration curves.

2.3 The pH of the point of zero charge (pH$_{pzc}$)

The pH of the point of zero charge (pH$_{pzc}$) was measured by the pH drift method (Utrilla, *et al.,* 2001; Bessekhouad, *et al*., 2004). In the process, 0.05 g of sample was added into 50 mL of 0.01M NaCl solution at various pH values and the suspensions were magnetically stirred for 3h. The pH was adjusted to a value between 2 to 12 by addition of 0.1 M HCl or 0.1M NaOH solution. All solutions were prepared using distilled water. The final pH (reached after 3h) was measured at room

temperature and plotted as a function of initial pH. The pH of the suspension was measured using a pH meter. The method used in this work followed the one described by Besskhouad, *et al.,* 2004. The pH at which the curve crosses the line pH (final) = pH (initial) is the pH_{pzc} of the given catalyst.

2.4 Photocatalytic test

The photocatalytic properties of BTO, TiO_2-BaC_2O_4, TiO_2-BT was studied by decolorizing orange II sodium salt dye in aqueous solutions under UV and visible light irradiations. In the experiment, 0.08 g of sample was dispersed in 50 mL orange II sodium salt solution in each experiment (at 2.0×10^{-5}M, 2.5×10^{-5}M, and 3.0×10^{-5}M). The experiments were performed in a closed compartment (0.75m $\times$ 0.75m $\times$ 0.75m for UV light and 0.70m $\times$ 0.70m $\times$ 0.70m for Visible light). Prior to the illumination, the suspension was stirred for 30 minutes to reach the adsorption equilibrium. Then the mixture was irradiated using 5 tubes of fluorescence blacklight 20 W, λ_{max} 366 nm (Randorn, *et al*., 2004) and using 5 tubes of visible light 20 W. In all studies, the mixture was magnetically stirred, before and during illumination. At given irradiation time intervals (every 1 h), 5 mL of the sample was collected and centrifuged to separate sample powder prior to the absorbance measurement. The residual concentration of orange II sodium salt was monitored by observing the change in absorbance about 485 nm using UV-vis spectrophotometer (Specord S100, Analytik Jena GmbH, Germany and Shimadzu UV2450, UV-Visible spectrophoto-meter). Controlled experiments, without the catalyst, were performed to demonstrate that the degradation of the dye was dependent on the presence of the catalyst. A flow chart of photodegradation of orange II sodium salt is shown in Figure 2.4. The percentage of orange II sodium salt decolorized (adsorption study) or degraded (photocatalytic study) was determined from the following equation;

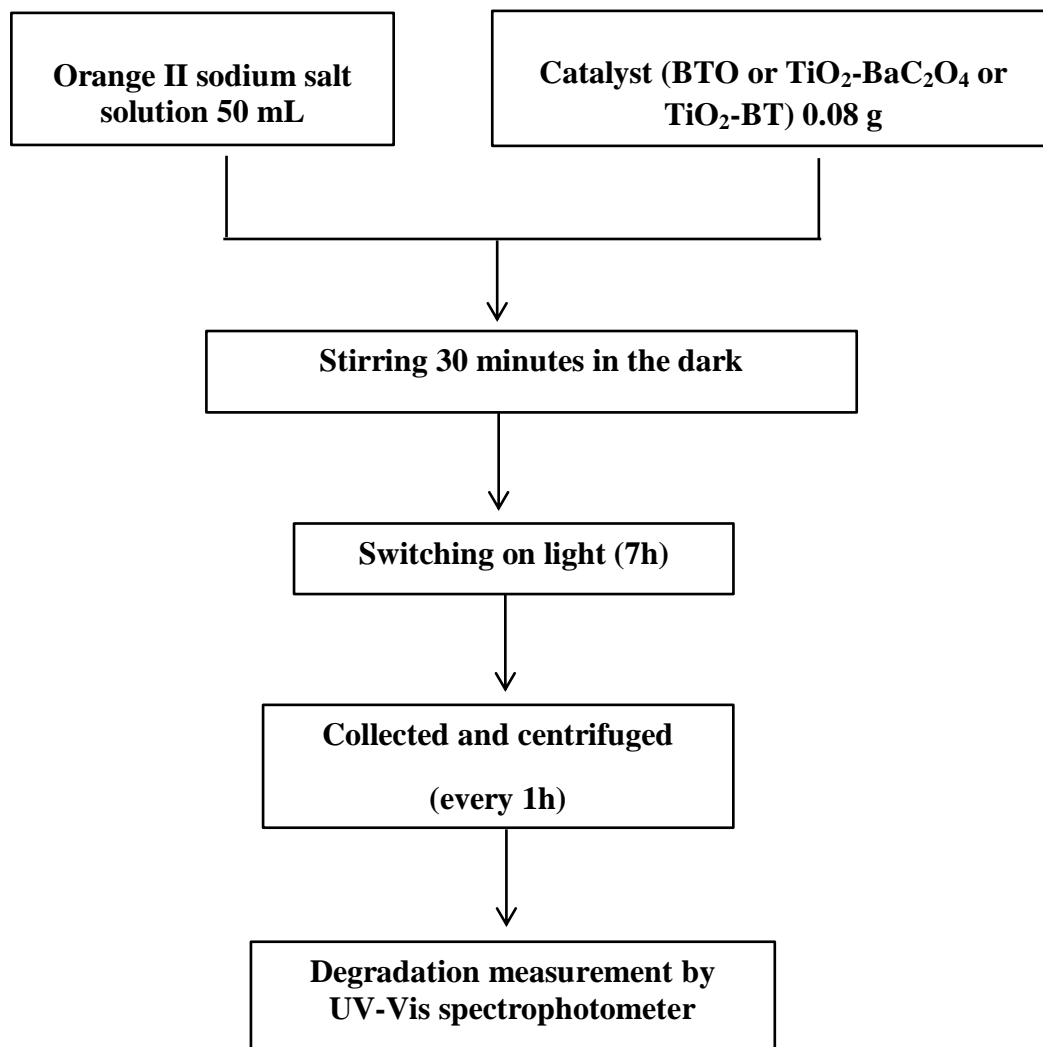$$\% \text{ Decolorization} = \frac{(C_0 - C_t) \times 100}{C_0} \qquad (2.4)$$

```
┌─────────────────────────┐        ┌──────────────────────────────────┐
│  Orange II sodium salt  │        │ Catalyst (BTO or TiO₂-BaC₂O₄ or  │
│   solution 50 mL        │        │        TiO₂-BT) 0.08 g           │
└─────────────────────────┘        └──────────────────────────────────┘
```

$$\text{Orange II sodium salt solution 50 mL} \qquad \text{Catalyst (BTO or TiO}_2\text{-BaC}_2\text{O}_4 \text{ or TiO}_2\text{-BT) 0.08 g}$$

Stirring 30 minutes in the dark

Switching on light (7h)

Collected and centrifuged

(every 1h)

Degradation measurement by
UV-Vis spectrophotometer

Figure 2.4 Flow chart of the photodegradation of orange II sodium salt dye by the catalyst under studied : (BTO, TiO$_2$-BaC$_2$O$_4$, TiO2-BT)

where C$_0$ is the initial concentration of orange II sodium salt solution and C$_t$ is the concentration of orange II sodium salt solution at specific time interval when the aliquot was collected.

2.5 Recyclability studies of BTO, TiO$_2$-BaC$_2$O$_4$, and TiO$_2$-BT.

   Recyclability of the synthesized photocatalysts was studied in 6 cycles of reuses. The concentration of dye in this set of experiment was 2.5×10^{-5} M and irradiated with UV light and visible light. During the course of photodegradation, a fraction of the dye solution was collected for analysis at the intervals 1, 3, 5, and 7 h. After each round of use, the catalyst was recovered and washed with DI water several times prior to the next reuse.

CHARTER 3

Results and discussion

Numerous efforts have been attempted to improve the photocatalytic activity by modifying the surface of TiO_2 such as deposition of metals, doping, surface chelation, and coupling of two semiconductors (Chatterjee, *et al*., 2002). Coupling of TiO_2 with other semiconductor to improve photocatalytic properties of TiO_2 has been reported such as SnO_2-TiO_2 ("combination of TiO_2 with SnO_2" or in another word TiO_2 coupled with SnO_2) and the study of its photocatalytic with 1,2-epoxyoctane. According to the yield of 1,2-epoxyoctane, the photocatalytic activity was concluded as SnO_2-TiO_2 > TiO_2. The SEM of SnO_2-TiO_2 showed the existence of SnO_2 nanoparticles attached on the surface of TiO_2 (Nur, *et al*., 2007). Bassiad, *et al*., 2009 studied to improve the performance of TiO_2 photocatalyst in combination or coupling with calcium oxalate for the elimination of organic compounds in water. Orange II sodium salt was chosen as a model pollutant for comparing the performance of the prepared TiO_2/$Ca(COO)_2$ photocatalytic materials. The result shows the effect of oxalate on photocatalytic decolourization of orange II sodium salt. The oxalate significantly improved the performance of TiO_2 while calcium oxalate alone was not active. The TiO_2 samples used were Degussa P25 and TiO_2 synthesized by sol-gel method. The photocatalytic degradation mechanism of orange II sodium salt in the presence of TiO_2 was described by Stylidi, *et al*., 2004. The mechanisms depend on light wavelength with the wavelength (λ) < 400 nm is usually employed. The basic photocatalytic process begins with ejecting an electron from the valence band (VB) to the conduction band (CB) of the TiO_2 semiconductor, creating a "h^+" hole in valence band. This is due to UV irradiation of TiO_2 with an energy equal or superior to the band gap (>3.2eV)(Eq.(1)). This is followed by the formation of extremely reactive radicals (like $^\bullet OH$) at the semi-conductor surface and/or a direct oxidation of the polluting species (R) (Eqs. (2)-(4)) (Stylidi, *et al*., 2004):

$$TiO_2 + h\nu \longrightarrow e_{cb}^- + h_{vb}^+ \tag{1}$$

$$h_{vb}^+ + H_2O \longrightarrow {}^\bullet OH + H^+ \tag{2}$$

$$h_{vb}^+ + OH_{ads}^- \longrightarrow {}^\bullet OH \tag{3}$$

$$h_{vb}^+ + R_{ads} \longrightarrow R^+ \tag{4}$$

The ejected electrons react with electron acceptors such as oxygen adsorbed or dissolved in water (Eq.(5)):

$$e_{cb}^- + O_2 \longrightarrow O_2^{\bullet-} \tag{5}$$

Also, the electrons and holes may recombine together without electron donors or acceptors (Eq.(6)):

$$e_{cb}^- + h_{vb}^+ \longrightarrow heat \tag{6}$$
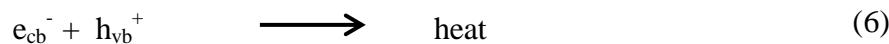
A $\lambda > 400$ nm, TiO_2 is inactive and degradation of orange II sodium salt can be explained by the sensitization of the dye by visible light photons. To summarize, when the dye is excited by visible light there is major formation of singlet exited state orange II sodium salt ($^1OII^*$) (Eq.(7)). Then an electron can be injected from the excited state of the adsorbed dye to the conduction band of TiO_2 (Eq.(8)), and the ejected electron can be scavenged by molecular oxygen to generate the superoxide radical species (Eq.(9)), which can then form other oxidative intermediate species (such as $^\bullet OH$, $OH_2^\bullet$, etc.)(Stylidi, *et al.*, 2004).

$$OII + h\nu \longrightarrow {}^1OII^* \tag{7}$$

$$^1OII^* + TiO_2 \longrightarrow OII^{\bullet+} + TiO_2(e^-) \tag{8}$$

$$TiO_2(e^-) + O_2 \longrightarrow TiO_2 + O_2^{\bullet-} \tag{9}$$

According to Stylidi, *et al.*, 2004, the first step of orange II sodium salt degradation is the cleavage of the active azo bond (-N=N-) which is more liable to oxidation by oxidative species with formation of benzene sulfonate and naphtoquinone derivatives (Eq.(10)).

$$(10)$$
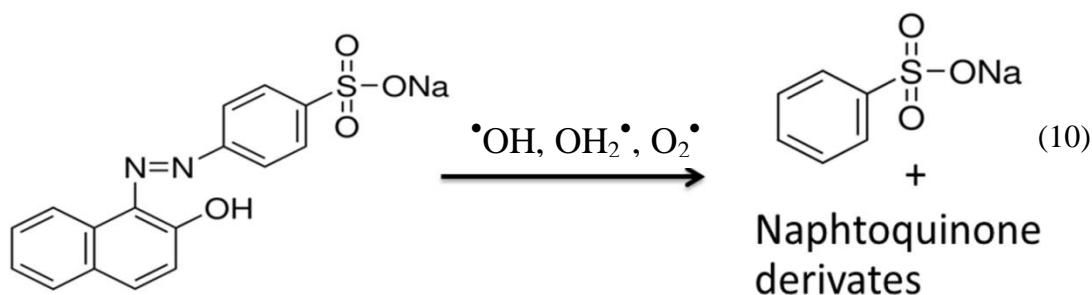
After the cleavage of azo bond, there is a sequence of different reactions leading to total mineralization with formation of CO_2, NH_4^+, NO_3^- and SO_4^{2-} as final products.

3.1) Synthesis and characterization of BTO, TiO$_2$-BaC$_2$O$_4$, and TiO$_2$-BT

The aim of our study is to prepare the compounds having barium and titanium constituents such as TiO_2 (anatase phase) photocatalyst coupled with barium oxalate (TiO_2-BaC_2O_4) or barium titanate (TiO_2-BT) to improve properties of TiO_2 and study their photocatalytic activities using orange II sodium salt as model pollutant. Orange II sodium salt is a mono-azo dye which is soluble in water and widely used in industry (Azam and Hamid., 1978). The properties of TiO_2-BaC_2O_4 and TiO_2-BT were characterized by XRD, SEM, BET, DRS, and FT-IR techniques.

In this work, BTO was synthesized via oxalate route using oxalic acid, titanium oxysulfate and barium chloride as the starting materials. The synthesis can be described by the following chemical reactions as shown in Eq. 3.1-3.3 (adapted from Fang, *et al.*, 1989; Khollam, *et al.*, 2002).

$$TiOSO_{4(aq)} + 2H_2C_2O_{4(aq)} \longrightarrow H_2TiO(C_2O_4)_{2(aq)} + SO_4^{2-} \qquad (3.1)$$

$$SO_4^{2-} + BaCl_{2(aq)} \longrightarrow BaSO_{4(s)} + 2Cl^- \qquad (3.2)$$

$$H_2TiO(C_2O_4)_{2(aq)} + BaCl_{2(aq)} \xrightarrow{\text{Heat}} C_4BaTiO_{9(s)} + 2HCl_{(l)} \qquad (3.3)$$
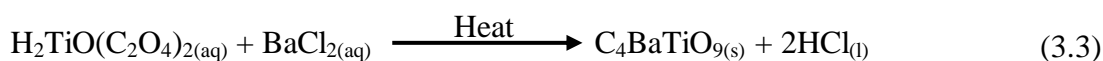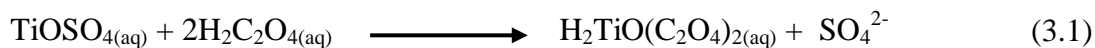
The obtained BTO was characterized by XRD, SEM, DRS, and FT-IR techniques. The BTO was obtained as a white powder as shown in Figure 3.1.4.

Figure 3.1.4 BTO obtained from the synthesis

Many studies on the synthesis of BTO powder have been reported using titanium precursor such as titanium tetrachloride, titanium tetrabutoxide, and potassium titanyl oxalate (Fang, *et al*., 1989; Khollam, *et al.,* 2002; Louer, *et al.,* 1992; Potdar, *et al.,* 2001).

The synthesis of BTO by Fang, *et al*., 1989 and Louder, *et al.,* 1992 is given is Eq.(3.4) while the same is Khollam, *et al.,* 2002 by Eq.(3.5-3.6).

The synthesis of BTO by Fang, *et al*., 1989 and Louder, *et al.,* 1992,

$$TiCl_4 \ + \ 2H_2C_2O_{4(aq)} \xrightarrow{\ BaCl_4\ } C_4BaTiO_{9(s)} \tag{3.4}$$

The synthesis of BTO by Khollam, *et al*., 2002,

$$C_{16}H_{36}O_4TiO_{(aq)} + 2H_2C_2O_{4(aq)} \xrightarrow[\text{Constant stirring}]{\text{In IPA}} C_4H_2TiO_{9(s)} \tag{3.5}$$

$$H_2TiO(C_2O_4)_{2(aq)} + Ba(OH)_{2(aq)} \xrightarrow[\text{Constant stirring}]{\text{Mixture kept overnight}} C_4BaTiO_{9(s)} \tag{3.6}$$
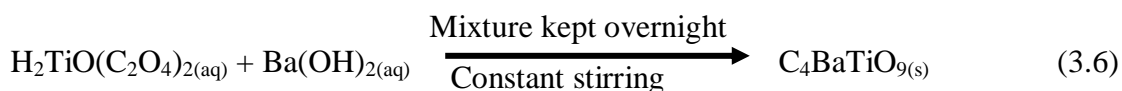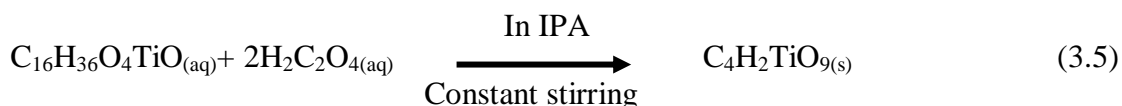
The method of preparing the TiO_2 coupling with BaC_2O_4 was adapted from the method reported by Fang, *et al*., 1989 and Khollam, *et al.,* 2002 (Eq 3.4-3.6). This method used an oxalic acid as source of oxalate ligand. The result from FT-IR Fig.3.1.1 and 3.1.2 showed oxalate which ligand was not attached to TiO_2 because the FT-IR spectrum of the anticipated TiO_2-BaC_2O_4 was similar to that of pure TiO_2 anatase indicating unsuccessful preparation via this method.
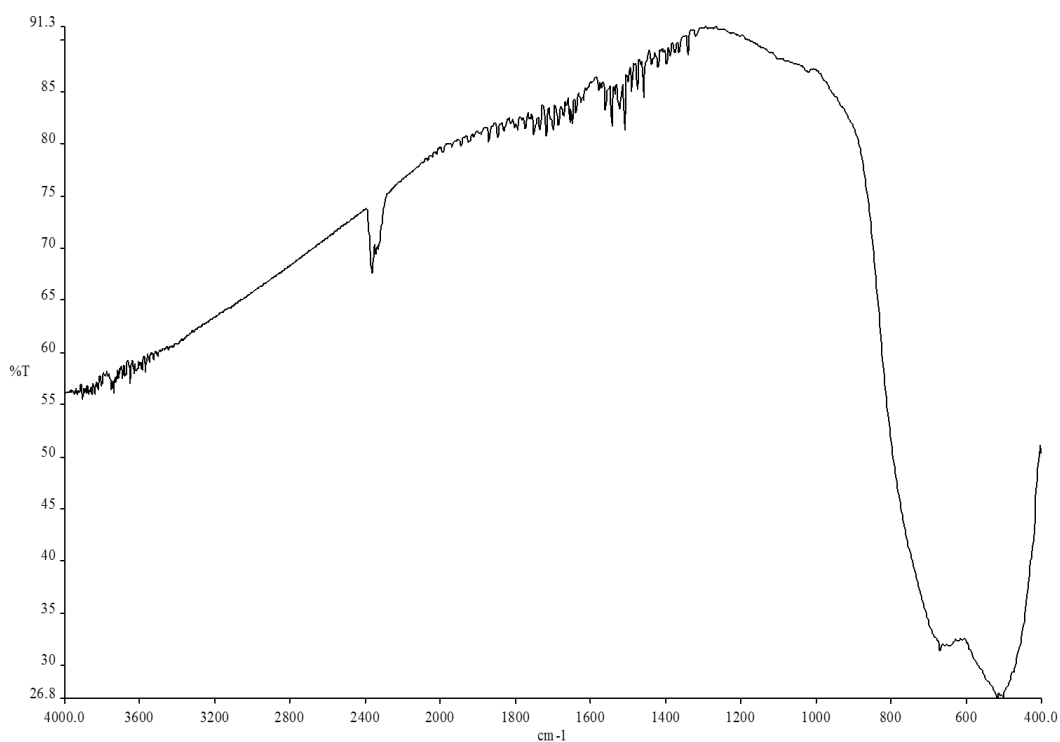
Figure 3.1.1 The FT-IR of TiO_2 (anatase phase)
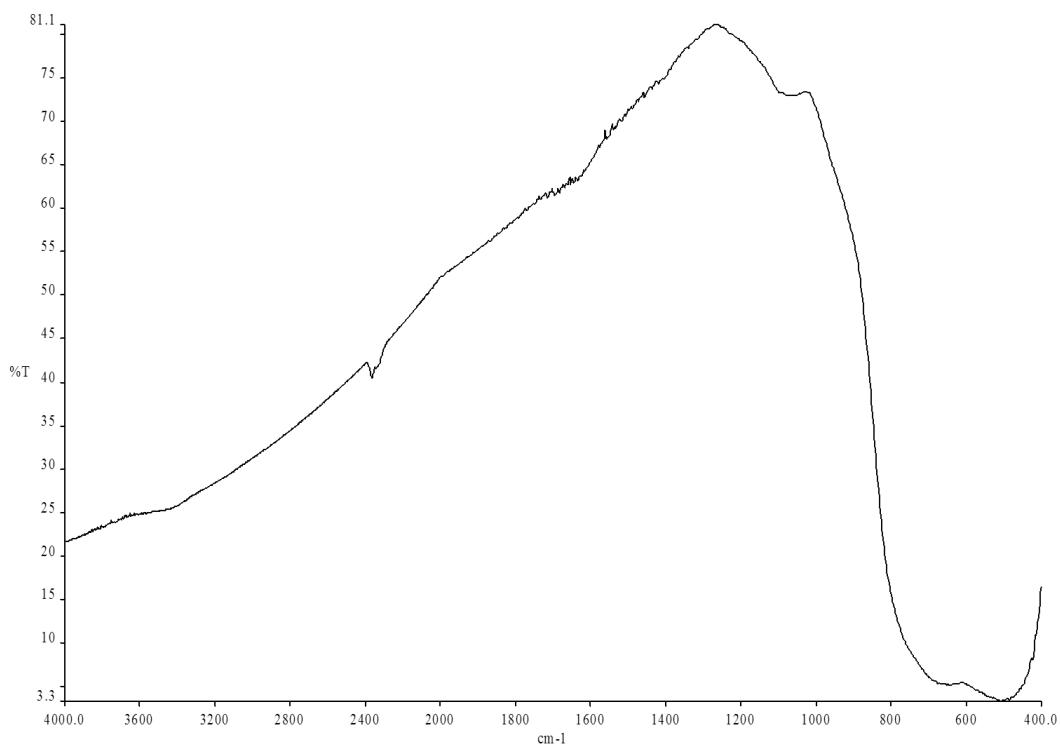
Figure 3.1.2 The FT-IR of the anticipated TiO_2-BaC_2O_4 prepared with oxalic acid

Another method was then attempted by using potassium oxalate as a source of oxalate ligand. This method was adapted from that reported by Louer, *et al*., 1992 (Eq 3.4). The product from this method contained the oxalate ligand as shown by FT-IR spectrum (Figure 3.1.3) with the presence of bands at 1600 and 1300 cm^{-1}. The product, which was prepared by this method, was converted to TiO_2-BT by calcination at 800 ^{o}C.
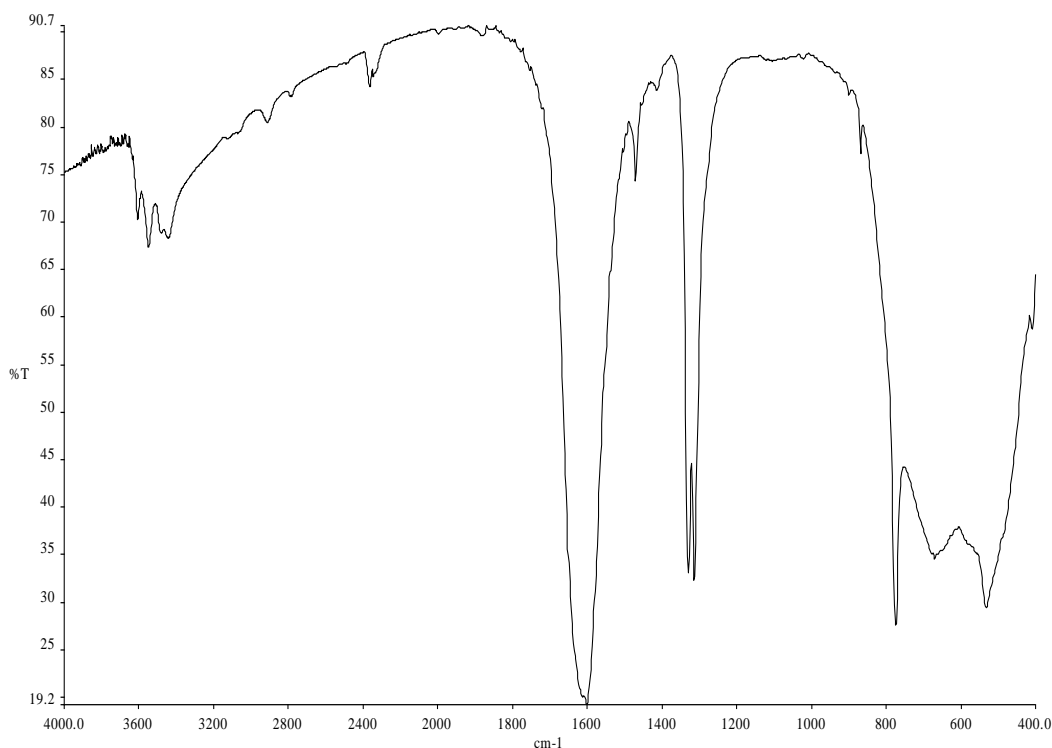
Figure 3.1.3 The FT-IR spectrum of TiO_2-BaC_2O_4 as prepared from potassium oxalate

The coupling products of titanium dioxide with BaC_2O_4 (TiO_2-BaC_2O_4) and BT (TiO_2-BT) were obtained as white powders as shown in Figure 3.1.5 and 3.1.6, respectively. The synthesis can be described by the following chemical reaction as shown in Eq. 3.7-3.9 (adapted from Louer, *et al*., 1992). TiO_2-BaC_2O_4 was synthesized via oxalate route using potassium oxalate, TiO_2 anatase as the precursor Ti atom.

$$TiO_{2(aq)} + K_2C_2O_{4(aq)} \longrightarrow K_2TiOC_2O_{4(aq)} + OH^- \qquad (3.7)$$

$$K_2TiOC_2O_{4(aq)} + BaCl_2 \longrightarrow BaC_2O_{4(s)} + TiO_{2(s)} + KOH_{(aq)} \qquad (3.8)$$

$$BaC_2O_{4(s)} + TiO_{2(s)} \xrightarrow{\text{Calcined at } 800^\circ C} TiO_{2(s)} + BaTiO_3 \qquad (3.9)$$

Figure 3.1.5 TiO_2-BaC_2O_4 obtained from synthesis
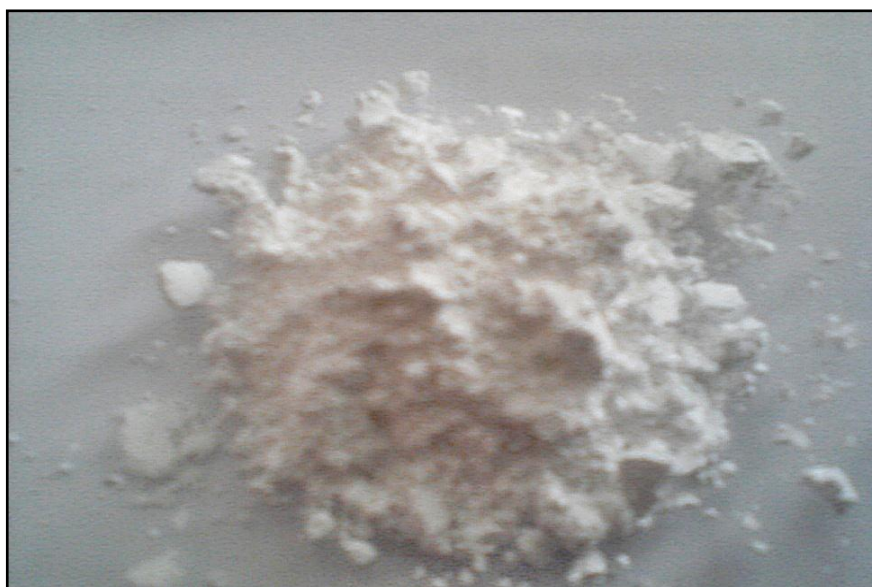
Figure 3.1.6 TiO_2-BT obtained from the synthesis

3.2 Characterization of BTO, TiO$_2$-BaC$_2$O$_4$, and TiO$_2$-BT

3.2.1 X-ray diffractometry (XRD)

XRD measurement was carried out with the Philips PW 3710 powder diffractometer (PHILIPS X'Pert MPD, the Netherlands) using CuK$_\alpha$ radiation (λ=1.5406 °A) and equipped with a Ni filter over the range of 2θ = 5-90° at room temperature. The identification of a species from its powder diffraction pattern is based upon the position of the lines (in terms of 2θ) and their relative intensities (Skoog and Leary, 1992). XRD pattern of BTO is shown in Figure 3.2.1.1 and the pattern was matched with the pattern of barium titanyl oxalate penta hydrate (BTO.5H$_2$O) in the XRD library as shown in Figure 3.2.1.2.
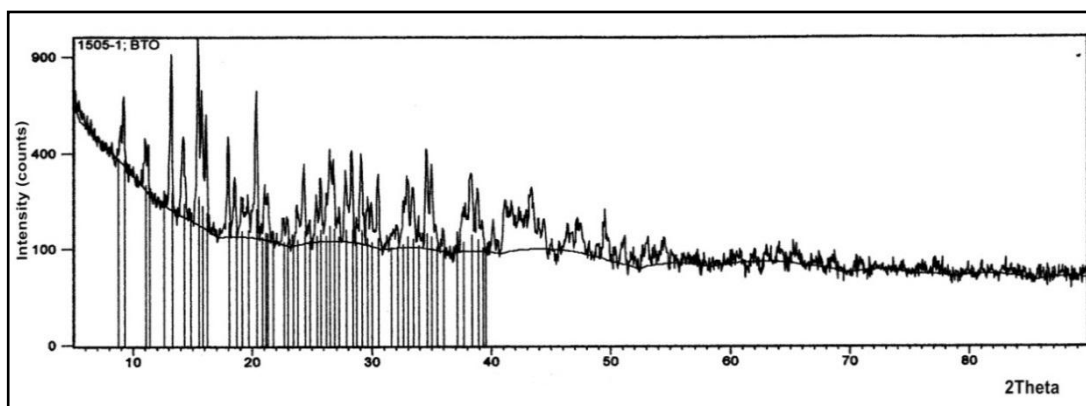
Figure 3.2.1.1 X-ray diffraction patterns of BTO
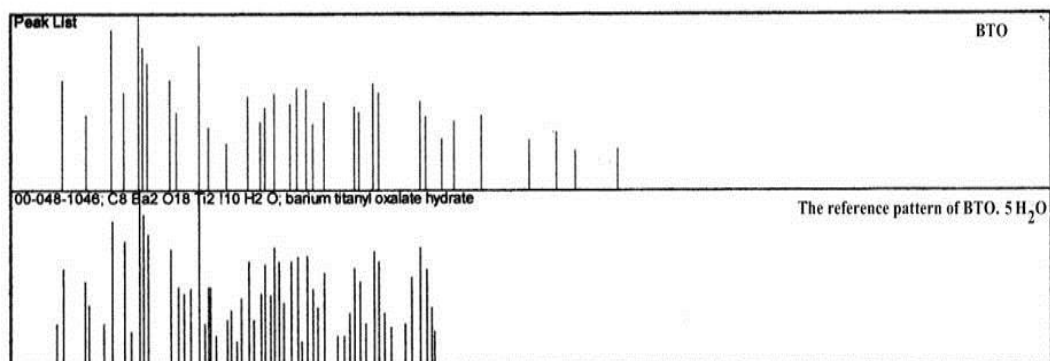
Figure 3.2.1.2 The peak list of BTO comparison with reference pattern of BTO in XRD library

The XRD patterns of TiO_2-BaC_2O_4 is shown in Figure 3.2.1.3. and was matched with the pattern of simple mixture of TiO_2 (anatase) and $BaC_2O_4.5H_2O$ in the XRD library as shown in Figure 3.2.1.4.
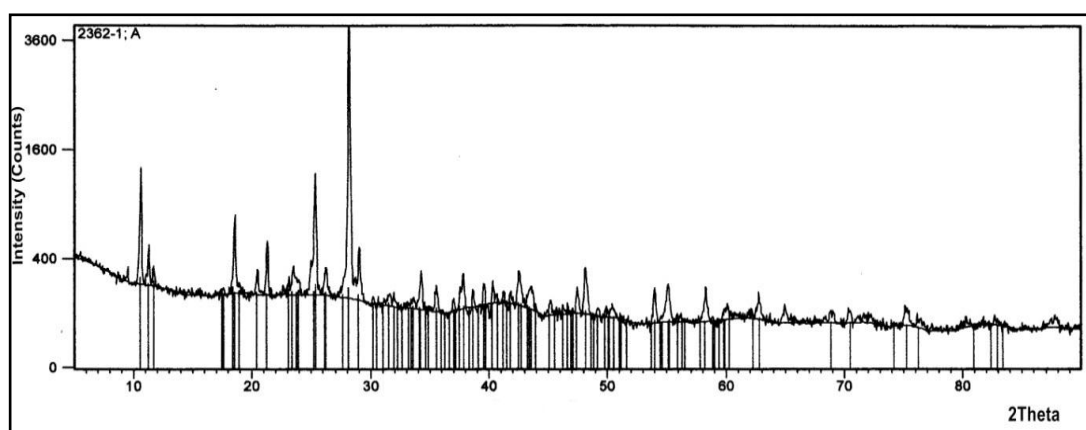
Figure 3.2.1.3 X-ray diffraction patterns of TiO_2-BaC_2O_4 and the reference pattern in XRD library
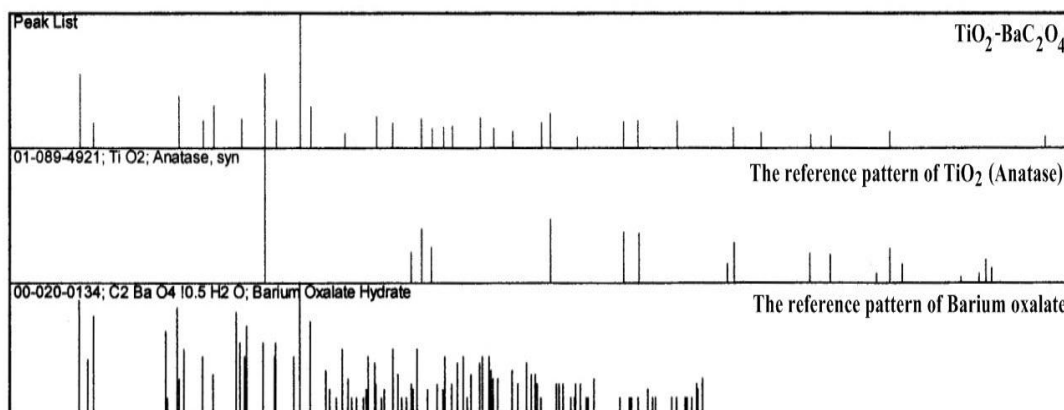
Figure 3.2.1.4 The peak list of TiO_2-BaC_2O_4 comparison with reference pattern of TiO_2 (anatase phase) and BaC_2O_4 in XRD library

The XRD pattern of coupled TiO_2-BT is shown in Figure 3.2.1.5 and was matched with the pattern of simple mixture of TiO_2 (anatase) and BT in the XRD library. The peaks of either perovskite phase barium titanate ($BaTiO_3$ or BT) appear at 22.2, 31.5, 38.9, 45.2, 50.9, 56.2, 65.9 70.4, 75.0, 79.5, and 87.9°. The diffraction peaks of anatase appear at 25.3, 37.8, 48.1, 53.9, 83.4° (Wongkaew, *et al.*, 2010). Pure barium titanate peaks appear at 6.8, 9.8, 22.2, 31.5, 38.9, 44.9, 45.3, 50.9, 51.0, 56.2, 65.8, 66.0, 70.5, 74.5, 75.1, 79.5, and 87°(Thongsang, 2002).
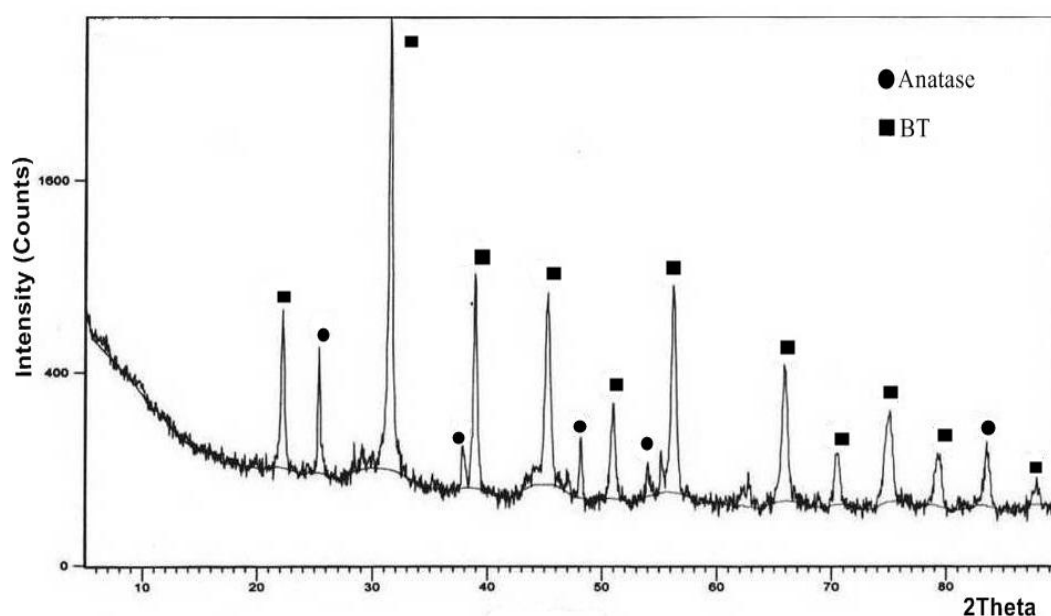
Figure 3.2.1.5 X-ray diffraction patterns of TiO_2-BT

The crystallite size (nm) was calculated from the Scherer equation (Eq. (2.1)).

$$d = [0.9\lambda\ /(\beta\cos\theta)]\times[180/\pi] \qquad (2.1)$$

In Eq. (2.1), d is the crystallite size, β is the full width at half maximum (FWHM, in radians), λ is the wavelength of the X-ray radiation (1.5406 A°) and θ is the diffraction angle of the reflection (Lakshiminarasimhan, *et al.*, 2007). The strongest peak of BTO, TiO_2-BaC_2O_4, and TiO_2-BT were showed at $2\theta = 15.4694^{o}$, $2\theta = 28.2065^{o}$, and $2\theta = 31.5601^{o}$ according with crystallite size are 54, 55, and 34 nm, respectively.

Table 3.2.1 The crystallite size of BTO, TiO_2-BaC_2O_4, and TiO_2-BT

Sample	2θ (The strongest peak)	FWHM	Crystallite size[a] (nm)
BTO	15.4694	0.1476	54
TiO_2-BaC_2O_4	28.2065	0.1476	55
TiO_2-BT	31.5601	0.2460	34

[a]The crystallite size was calculated by using Scherrer's equation

3.2.2 Scanning electron microscopy (SEM)

The external morphology and surface features of BTO were observed on a scanning electron microscope (SEM) model JEOL JSM-5800 LV. Figure 3.2.2.1-3.2.2.3 show magnified images at 500X, 2,00X, and 10,000X, respectively. The surface and textural morphology of BTO appear like leaves of tree.
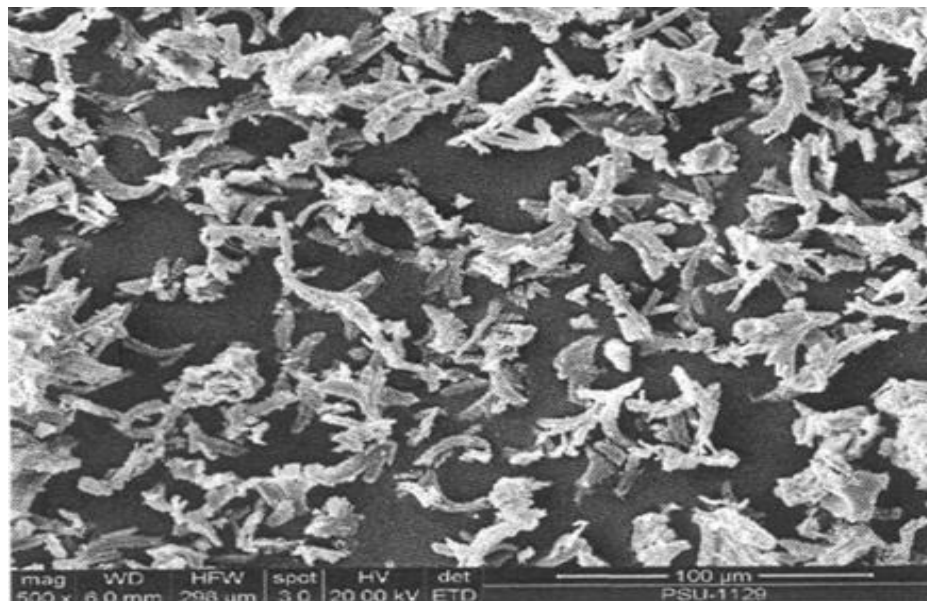
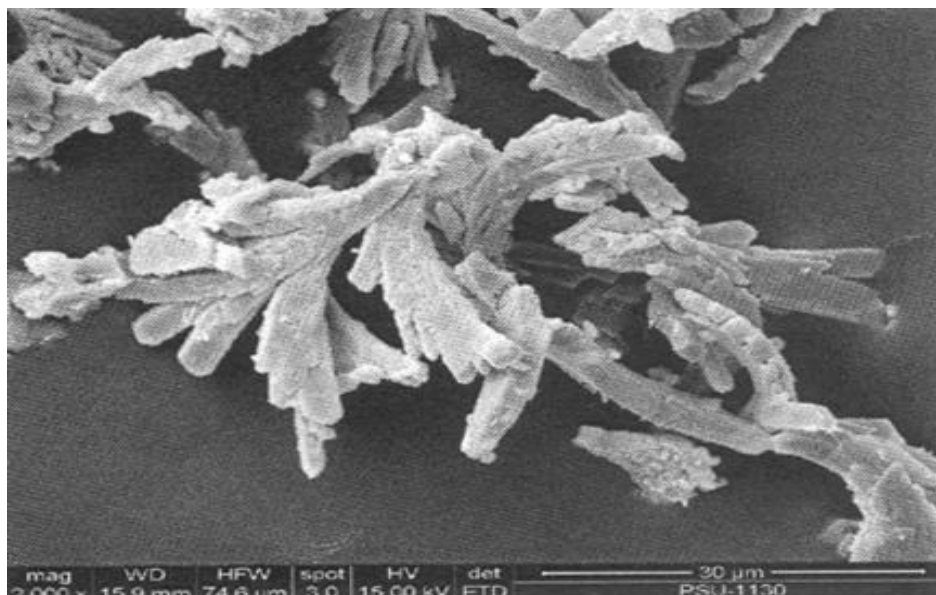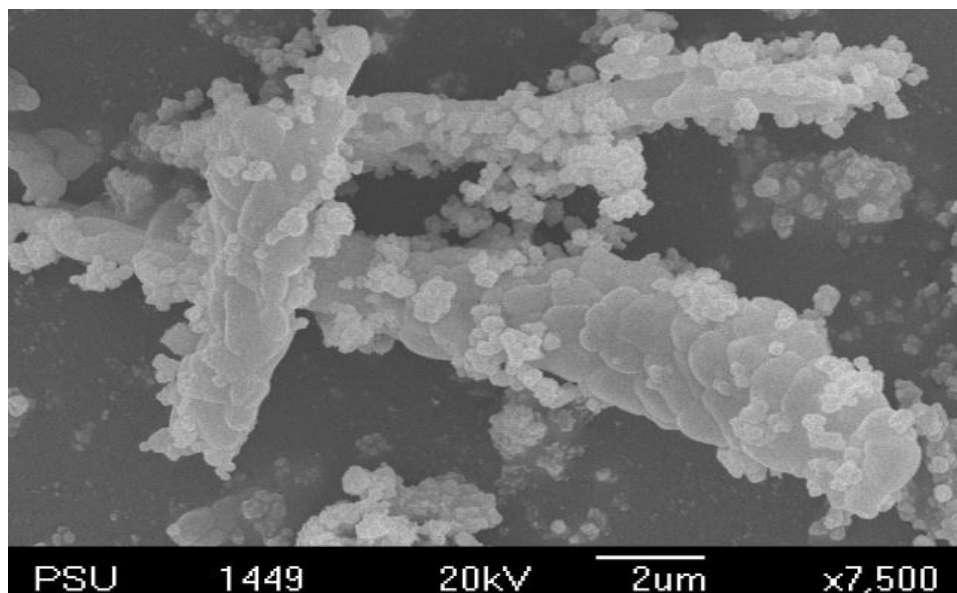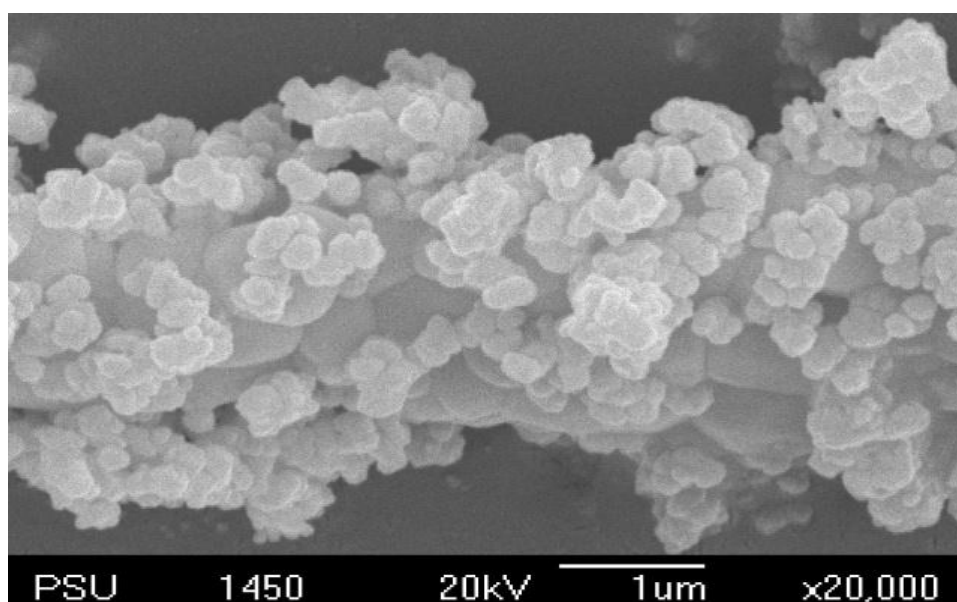**Figure 3.2.2.1** SEM image of BTO at 500X magnification

Figure 3.2.2.2 SEM image of BTO at 2,000X magnification

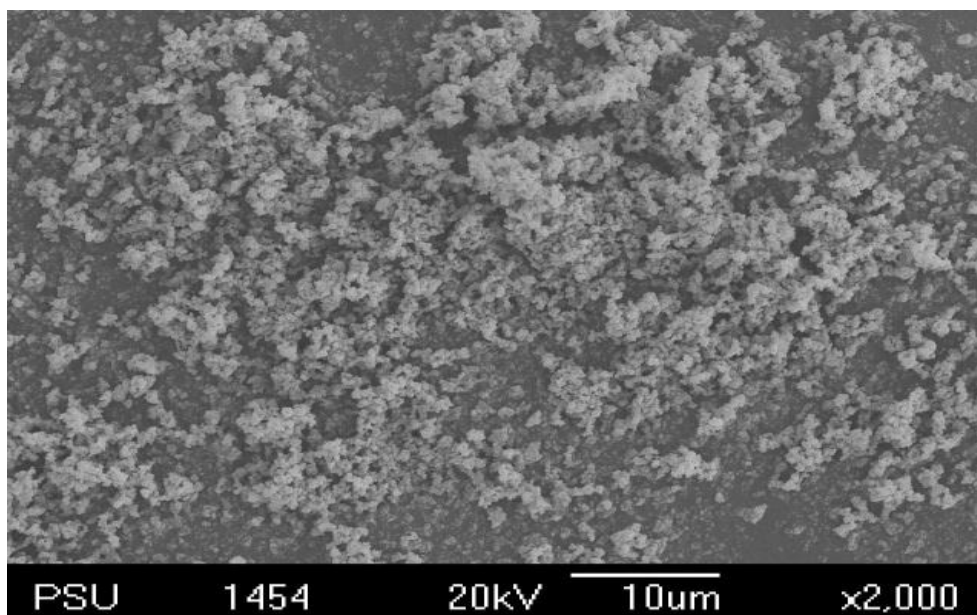**Figure 3.2.2.3** SEM image of BTO at 10,000X magnification

The SEM images of coupled TiO_2-BaC_2O_4 are shown in Figure 3.2.2.4-3.2.2.6. The morphology of BaC_2O_4 alone appears as long rod or micelle (Sharma, *et al.,* 2009). In this work, BaC_2O_4 in TiO_2-BaC_2O_4 also appears as a long rod with its surface was covered with TiO_2. The morphologies of commercial TiO_2 anatase are shown in Figure 3.2.2.7-3.2.2.9 and they are spherical shape.
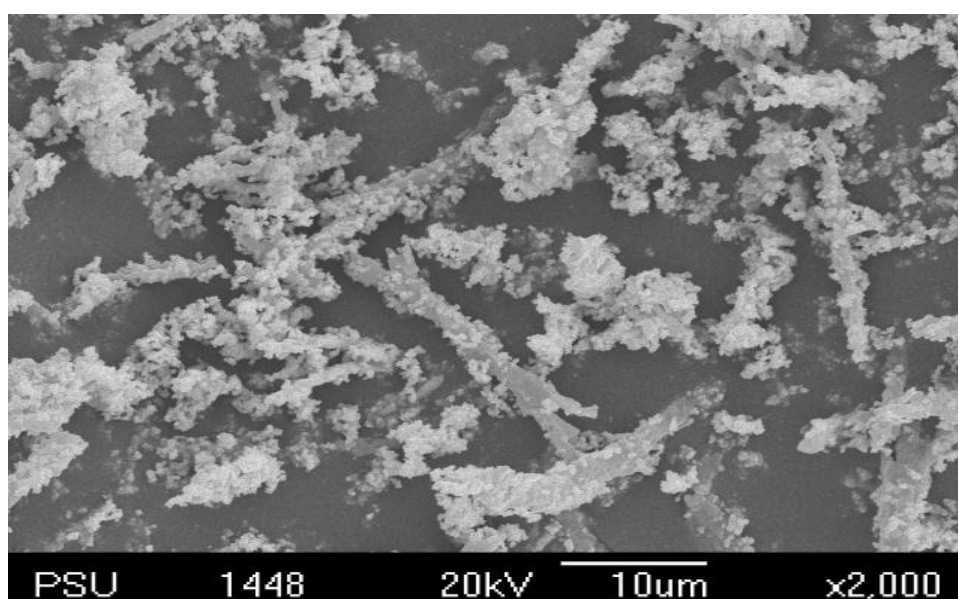
Figure 3.2.2.4 SEM image of TiO_2-BaC_2O_4 at 2,000X magnification

Figure 3.2.2.5 SEM image of TiO_2-BaC_2O_4 at 7,500X magnification

Figure 3.2.2.6 SEM image of TiO_2-BaC_2O_4 at 20,000X magnification

Figure 3.2.2.7 SEM image of TiO$_2$(anatase) at 2,000X magnification
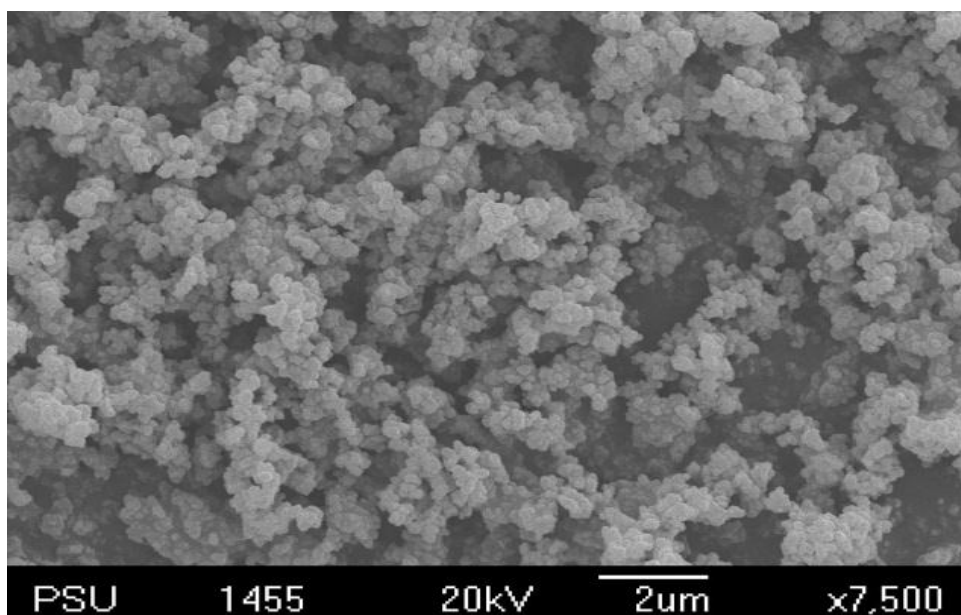

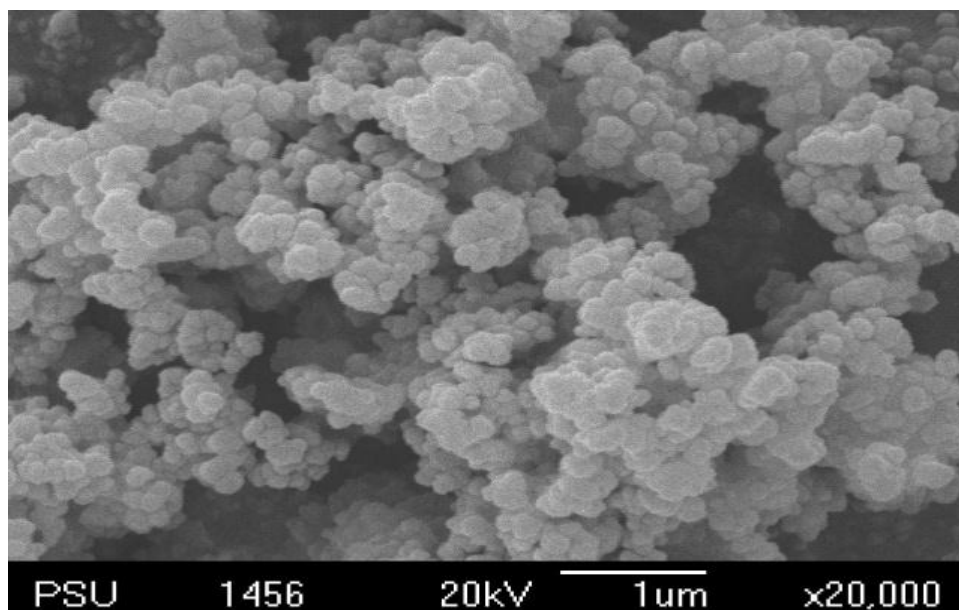**Figure 3.2.2.8** SEM image of TiO$_2$(anatase) at 7,500X magnification

Figure 3.2.2.9 SEM image of TiO_2(anatase) at 20,000X magnification

Figure 3.2.2.10-3.2.2.12 show the SEM images of TiO_2-BT at different magnifications (2,000x, 7500x, 20,000x). TiO_2-BT powders in this work were obtained by calcination of TiO_2-BaC_2O_4 at 800°C for 3h. The pure BT particles are spherical in nature with size about 100 nm (Khollam, *et al*., 2002). TiO_2-BaC_2O_4 after calcination turned to BT as spherical shape which agglomerated with excess TiO_2 (also of spherical shape).
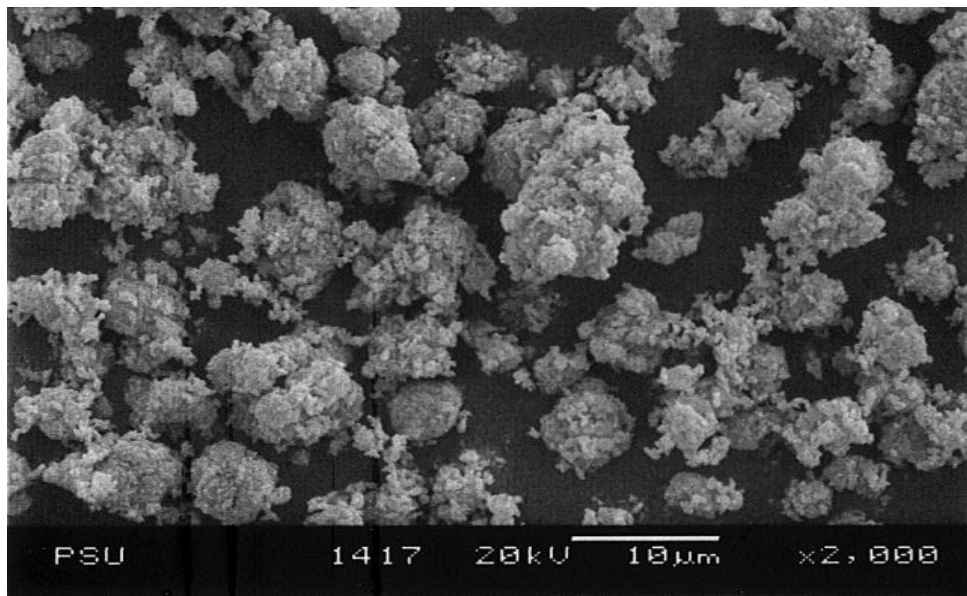
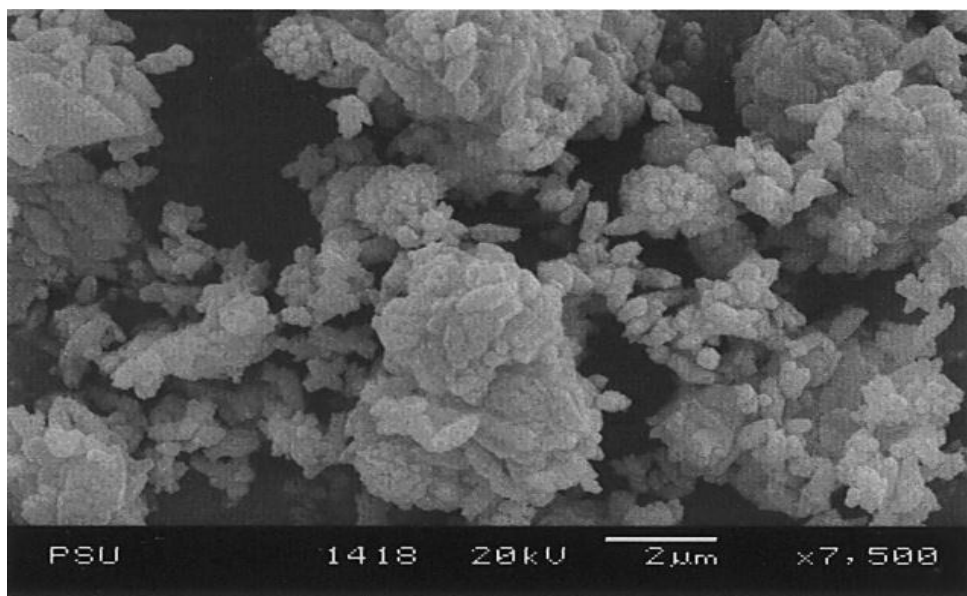**Figure 3.2.2.10** SEM image of TiO$_2$-BT at 2,000X magnification

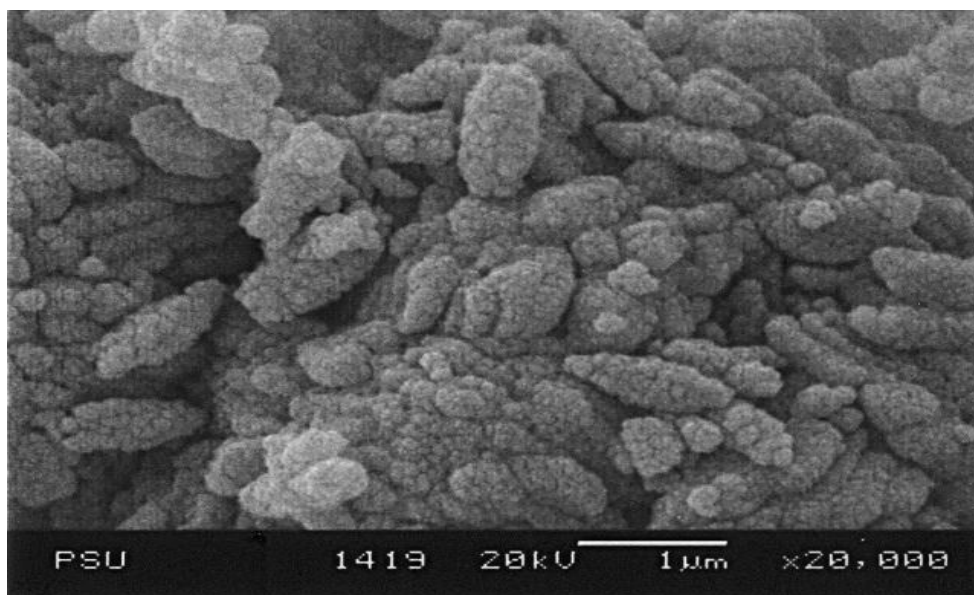**Figure 3.2.2.11** SEM image of TiO$_2$-BT at 7,500X magnification

Figure 3.2.2.12 SEM image of TiO$_2$-BT at 20,000X magnification

3.2.3 BET specific surface area

The specific surface area of sample was determined by physical adsorption of nitrogen gas on the surface of the solid and by calculating the amount of adsorbate gas corresponding to a monomolecular layer on the surface. Physical adsorption results from relatively weak forces (van der Waals forces) between the adsorbate gas molecules and the adsorbent surface area of the test powder. The determination is usually carried out at the temperature of liquid nitrogen. The amount of gas adsorbed can be measured by either volumetric or continuous flow procedure.

The data are treated according to the Brunauer, Emmett and Teller (BET) adsorption isotherm equation:

$$\frac{1}{\left[V_a \left(\frac{P_0}{P} - 1 \right) \right]} = \frac{C-1}{V_m C} \times \frac{P}{P_0} + \frac{1}{V_m C} \qquad 3.2.3$$

P = partial vapour pressure of adsorbate gas in equilibrium with the surface at 77.35 K (b.p. of liquid nitrogen), in pascals

P_o = saturated pressure of adsorbate gas, in pascals

V_a = volume of gas adsorbed at standard temperature and pressure (STP) [273.15 K and atmospheric pressure (1.013 × 10^5 Pa)], in milliliters

V_m = volume of gas adsorbed at STP to produce an apparent monolayer on the sample surface, in milliliters

C = The adsorbate gas on the powder sample

A value of Va is measured at each of not less than 3 values of P/Po. Then the BET value is plotted against P/P_o according to equation. This plot should yield a straight line usually in the approximate relative pressure range 0.05 to 0.3. The data are considered acceptable if the correlation coefficient, r, of the linear regression is not less than 0.9975; that is, r^2 is not less than 0.995. From the resulting linear plot, the slope, which is equal to $(C − 1)/V_mC$, and the intercept, which is equal to $1/V_mC$, are evaluated by linear regression analysis. From these values, V_m is calculated as $1/(slope + intercept)$, while C is calculated as $(slope/intercept) + 1$. From the value of V_m so determined, the specific surface area, S, in $m^2{\cdot}g^{-1}$, is calculated by the equation:

N = Avogadro constant (6.022×10^{23} mol^{-1})

a = effective cross-sectional area of one adsorbate molecule, in square meters (0.162 nm^2 for nitrogen and 0.195 nm^2 for krypton)

m = mass of test powder, in grams

22400 = volume occupied by 1 mole of the adsorbate gas at STP allowing for minor departures from the ideal, in milliliters

A minimum of 3 data points is required. Additional measurements may be carried out, especially when non-linearity is obtain at a P/Po value close to 0.3. Because non-linearity is often obtain at a P/Po value below 0.05, values in this region are not recommend. The test for linearity, the treatment of the data, and the calculation of the specific surface area of the sample are describe above (http://particle.dk/methods-analytical-laboratory/surface-area-bet/surface-area-bet-theory/).

The BET plot between P_0/P and specific surface area shown in Figure 3.2.3.1-3.2.3.3. The specific area of BTO, TiO_2-BaC_2O_4, and TiO_2-BT are 26.63, 3.32, and 3.55 m^2/g, respectively. The values of specific surface area are low corresponding to high crystalinity nature of the products.

Table 3.2.3 specific surface areas, correlation coefficient values, and C-values

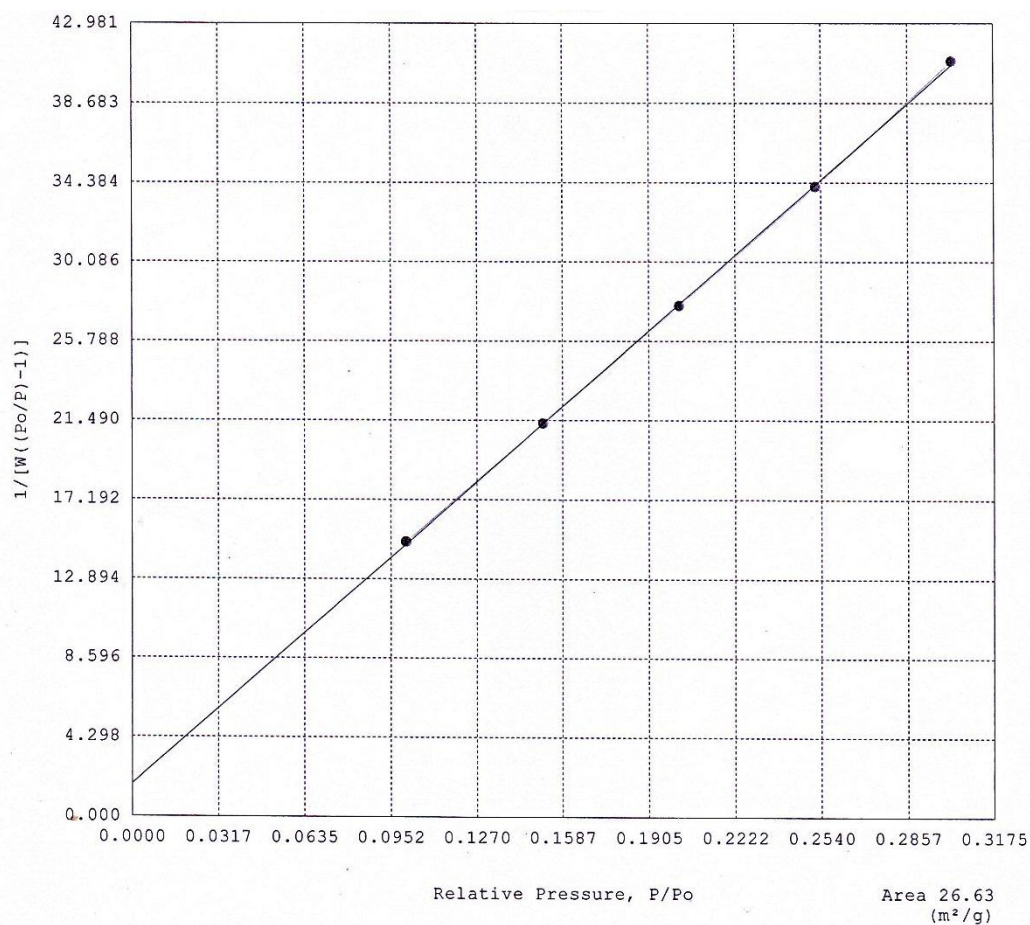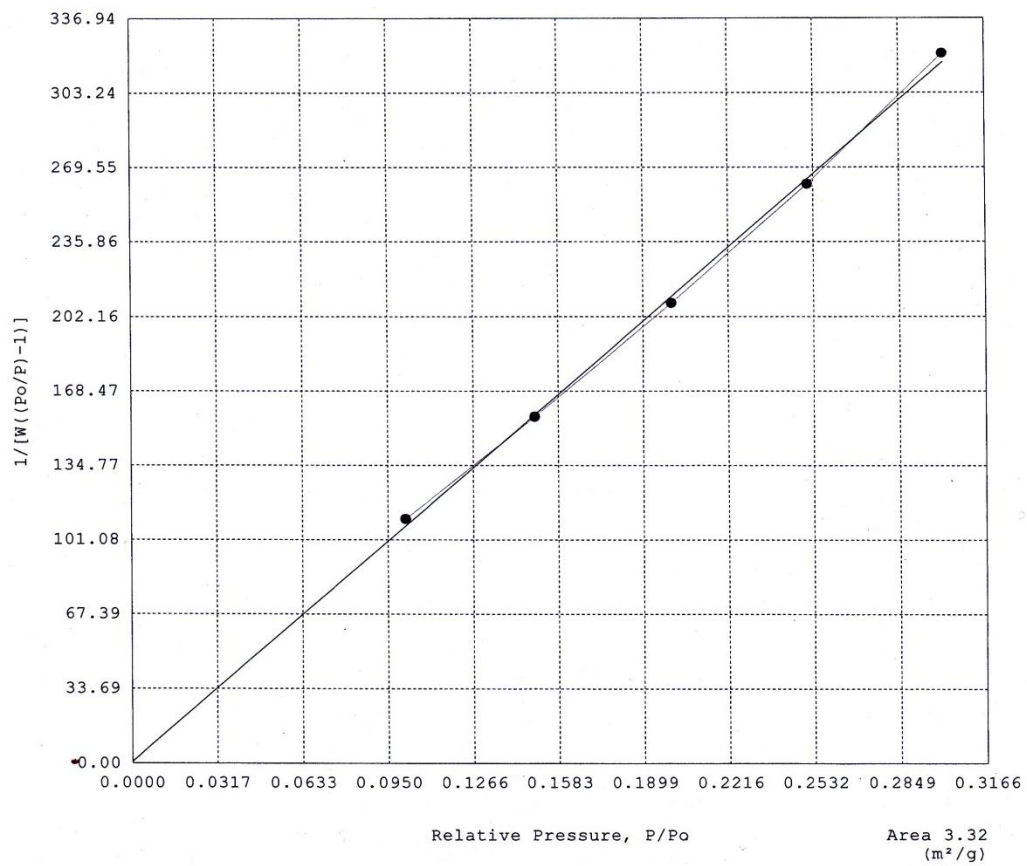| Sample	Specific surface area (m^2/g)	Correlative coefficient values	C-values
BTO	26.63	0.999909	74.52
TiO_2-BaC_2O_4	3.32	0.999240	1581.00
TiO_2-BT	3.55	0.999728	117.70

Figure 3.2.3.1 The BET plot of BTO
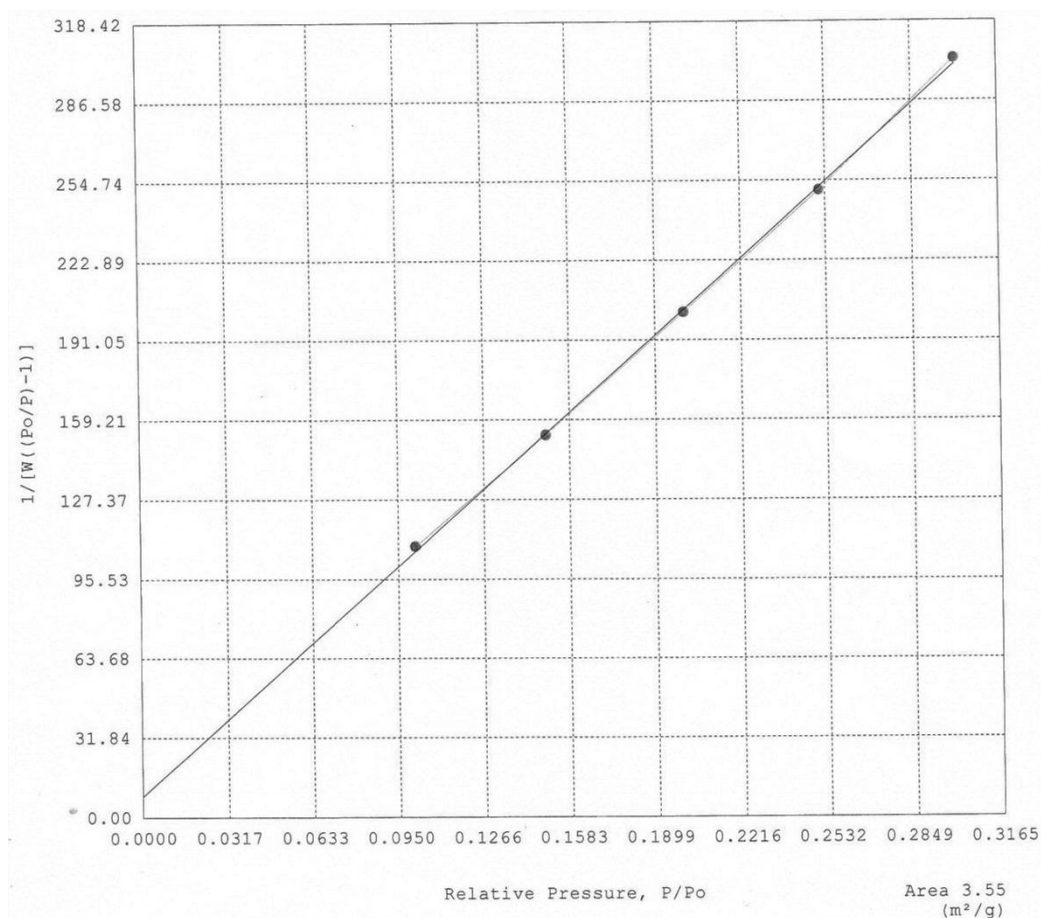
Figure 3.2.3.2 The BET plot of TiO_2-BaC_2O_4

Figure 3.2.3.3 The BET plot of TiO$_2$-BT

3.2.4 Diffused reflectance UV-Vis spectroscopy (DRS)

Diffused reflectance studies were performed on a UV-vis absorption spectrophotometer (Shimadzu UV-2401) in the scan range 200-800 nm with a 2.0 nm slit width using BaSO$_4$ as reference sample. UV-vis diffused reflectance spectroscopy is used to probe the band structure or molecular energy levels in the materials since UV-vis light excitation creates photo-generated electron and holes (Reddy, *et al.,* 2001). The band gap energies of all samples were determined from their diffused reflectance spectra and calculated using the Plank's equation (Eq. 2.4). The BTO showed edge of absorption band at 382 nm corresponding to the band gap energy of 3.26 eV. Diffused reflectance UV-Vis spectra of BTO is shown in Figure 3.2.4.1. The commercial anatase TiO$_2$ has band gap energy 3.20 eV (Suwanchawalit, 2008).

BaC$_2$O$_4$ and BT (or BaTiO$_3$) have band gap energy 4.0 and 3.20 eV (Cox, 1995), respectively. The UV-visible DRS spectra of TiO$_2$-BaC$_2$O$_4$ is shown in Figure 3.2.4.2 showing edge of absorption band at 390 nm corresponding to the band gap energy 3.18 eV. The UV-visible DRS spectrum of TiO$_2$-BT is shown in Figure 3.2.4.3. The edge of absorption band of TiO$_2$-BT appear at 395 nm corresponding to the band gap energy 3.14 eV.
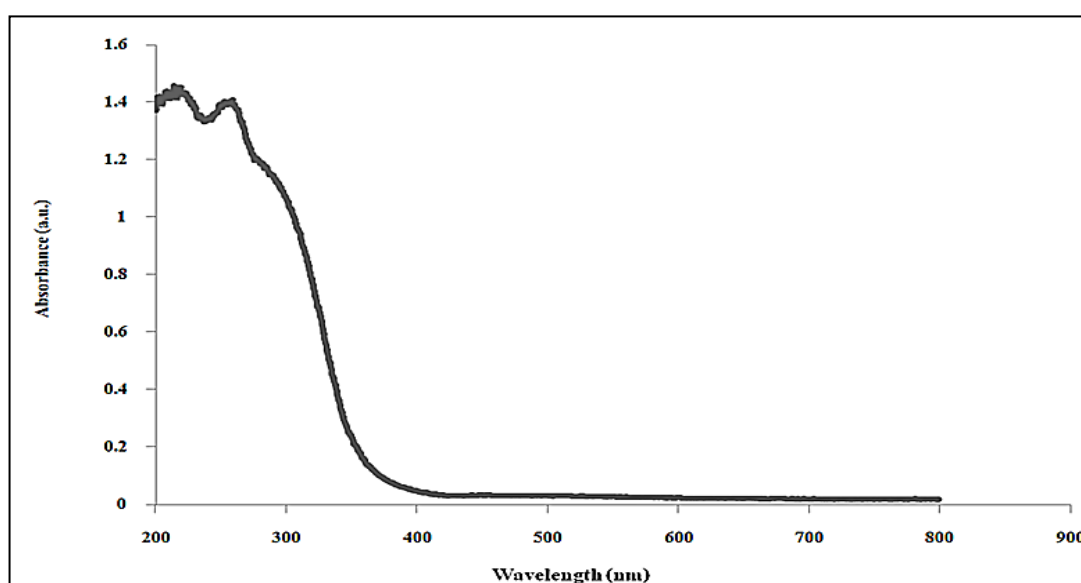

Figure 3.2.4.1 Diffused reflectance UV-Vis spectra of BTO

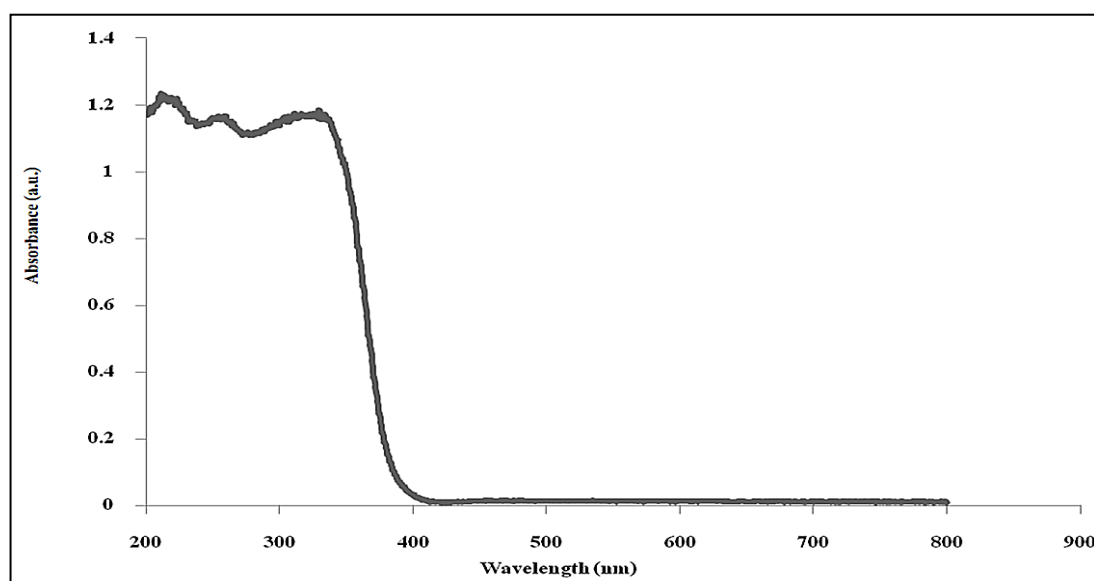**Figure 3.2.4.2** Diffused reflectance UV-Vis spectra of TiO$_2$-BaC$_2$O$_4$

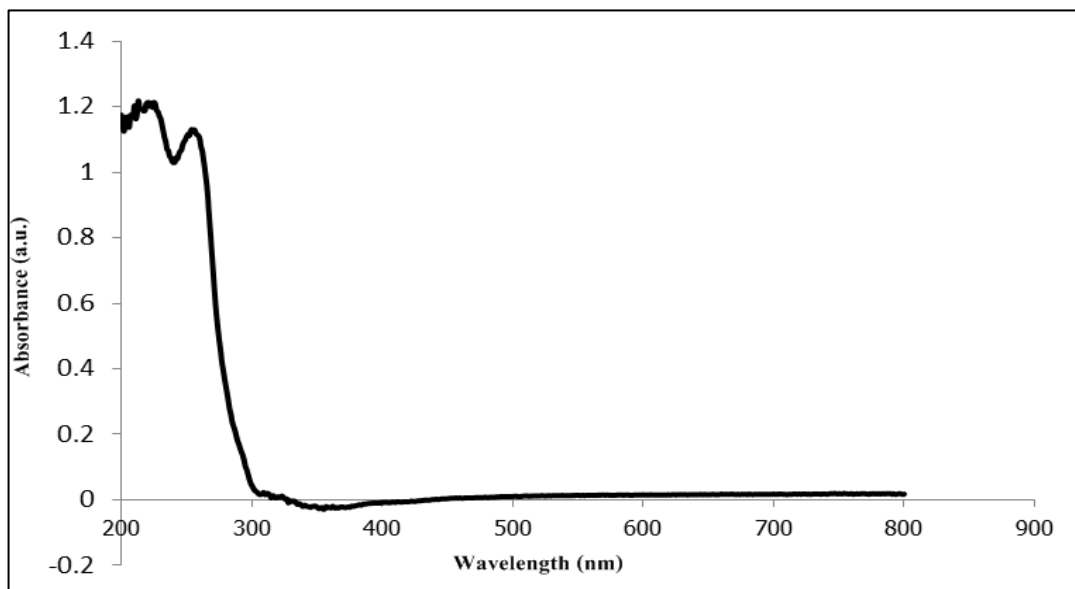**Figure 3.2.4.3** Diffused reflectance UV-Vis spectra of BaC_2O_4

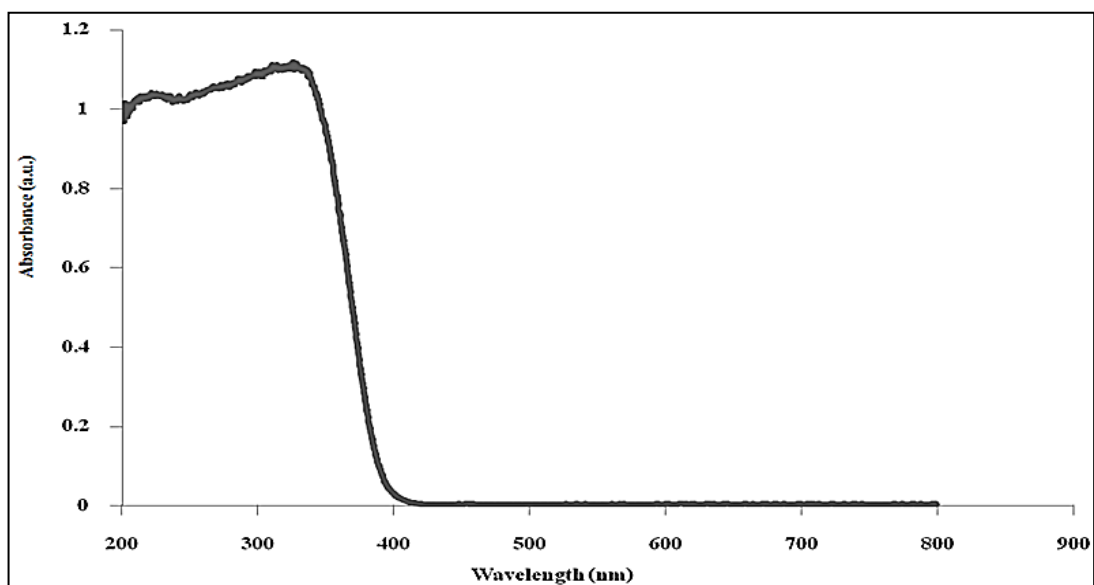**Figure 3.2.4.4** Diffused reflectance UV-Vis spectra of TiO_2-BT
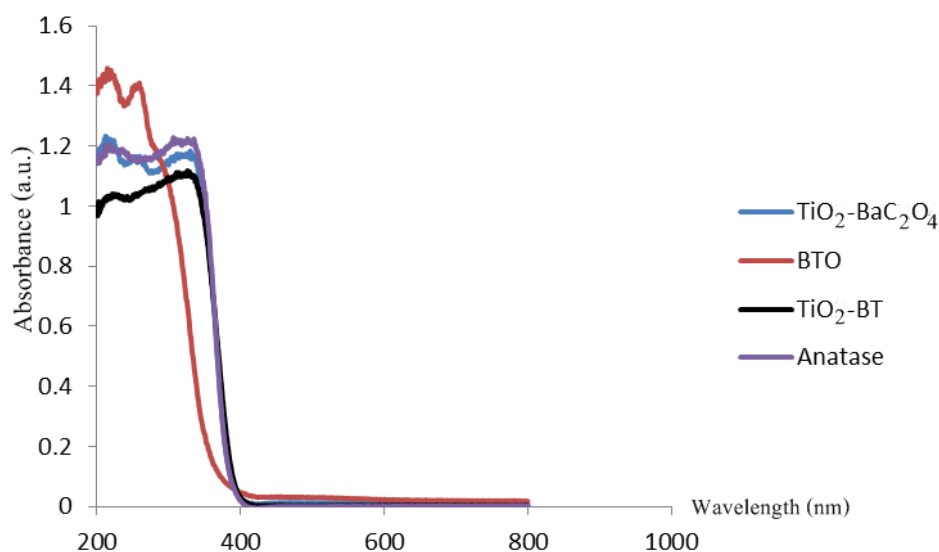
Figure 3.2.4.5 The compared DRS spectra of BTO, TiO_2-BaC_2O_4, TiO_2-BT, and anatase TiO_2

Table 3.2.4.2 Band gap energies of related compounds

Sample	Absorption edge (nm)	Band gap energy (eV)
BTO	382.0	3.26
TiO_2-BaC_2O_4	390.0	3.18
TiO_2-BT	395.0	3.14
TiO_2 (Anatase)	387.5	3.20
BaC_2O_4	310.0	4.00 [a]
BT or $BaTiO_3$	387.5	3.20[a]

[a]Cox, 1995

From the DRS results, the band gap of BTO is larger than the other two samples. The commercial anatase TiO_2 has band gap energy 3.20 eV (Suwanchawalit, 2008). Hence, we can see that coupling of TiO_2 with BaC_2O_4 and BT decreased band gap energy of sample as shown in Table 3.2.4.2.

The results showed that coupling of different semiconductor oxides can reduce its band gap energy, extend its adsorption range to visible light region, promote electron-hole pair separation under irradiation, and, consequently, achieve a higher photocatalytic activity (Chao, *et al*., 2010).

3.2.5 Fourier-transformed infrared spectroscopy (FT-IR)

Fourier-transformed spectroscopy is a measurement technique whereby spectra are collected based on measurement of the temporal coherence of radiative source, using time-domain measurement of electromagnetic radiation or other type of radiation. It can be applied to variety of types of spectroscopy including optical spectroscopy, infrared spectroscopy (FT-IR), and electron spin resonance spectroscopy. Infrared spectroscopy is a technique for determining the functional groups within the compounds. The FT-IR spectrum range of the usage is in the mid infrared region which covers the frequency from 400 to 4000 cm^{-1} (Skoog and Leary, 1992). The FT-IR spectrum of BTO is shown in Figure 3.2.5.1. The assigned modes of functional groups corresponding to Figure are listed in Table 3.2.5.1.

The broad band centered around 3550 cm^{-1} may be assigned to anti-symmetric and symmetric stretching vibration of OH group and at 1600 cm^{-1} may be assigment to H-O-H bending of coordinated water (Wang, *et al.*, 2000; Kangle, *et al.*, 2009). The band around 1600 cm^{-1} is overlapped with that of ν_{asy} (C= O) of oxalate group (Khollam, *et al.,* 2002). The band around 1471 cm^{-1} is ν_{C-O} of CO_2, and around 1328 cm^{-1} is ν_{C-O} of oxalate ligand (Sharma, *et al.,* 2009). The sharp band appearing around 772 cm^{-1} is characteristic of ν_{Ba-O} (Khollam, *et al.,* 2002) and around 532 cm^{-1} is ν_{Ti-O} of BTO (Rhine, *et al.,* 1992).
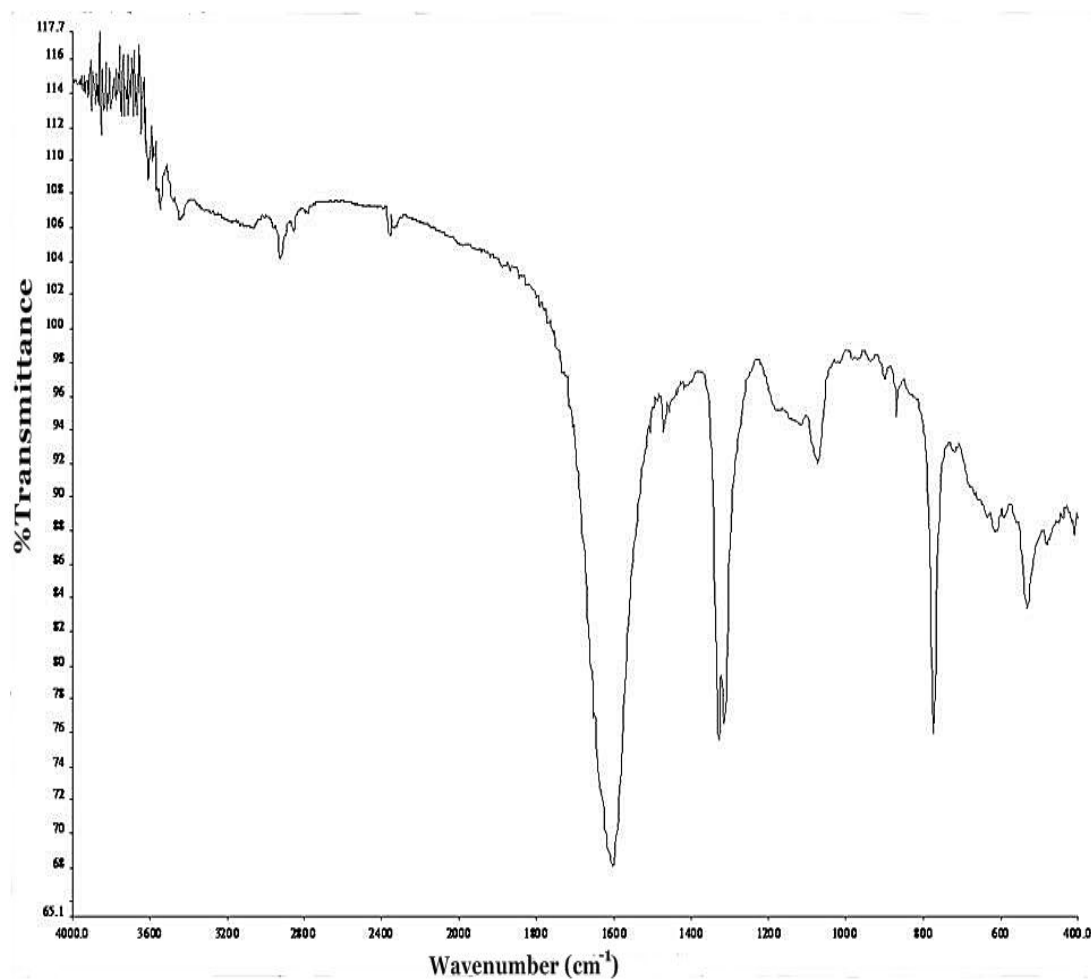
Figure 3.2.5.1 FT-IR spectrum of BTO

Table 3.2.5.1 Assignment of the FT-IR band of BTO.

Sample	Wavenumber (cm^{-1})	Assignment	Functional group/molecule	Reference
BTO	3433	ν_{OH}	H_2O	Wang, *et al.,* 2000
	1600	ν_{OH}, ν_{CO}	OH group overlap with νC-O of oxalate ligand	Khollam, *et al.,* 2002 and Kangle, *et al.*, 2009

Sample	Wavenumber (cm^{-1})	Assignment	Functional group/molecule	Reference
	1471	ν_{C-O}, ν_{C-C}	CO_2 overlap with ν_{C-C} of oxalate ligand	Sharma, *et al.,* 2009
	1328	ν_{CO}	Oxalate ligand	Sharma, *et al.,* 2009
	772	δ_{Ba-o}	BTO	Khollam, *et al.,* 2002
	532	ν_{Ti-o}	BTO	Rhine, *et al.,* 1992

The FT-IR spectrum of the TiO_2-BaC_2O_4 is shown in Figure 3.2.5.2 which can provide the information of functional groups on the surface of materials. The broad band centered around 3425 cm^{-1} may be assigned to anti-symmetric and symmetric stretching vibration of OH group and that at 1630 cm^{-1} may be assigned to H-O-H bending of coordinated water (Wang, *et al.,*2000; Kangle, *et al.,* 2009).

These results confirm the presence of hydroxyl group in the structure of all synthetic samples. The adsorbed water and hydroxyl group are crucial to the photocatalytic reactions since they react with photo-excited holes on the catalyst surface to produce hydroxyl radicals which are powerful oxidant (Kangle, *et al.,* 2009).

The broad band below 800 cm^{-1} is attributed to the Ti-O stretching vibration of TiO_2 phase. For commercial anatase TiO_2 a broad band at 710 cm^{-1} is the confirmation of anatase phase (Zhang, *et al.,* 2001). The band around 2350 cm^{-1} is CO_2 (Belver, *et al.,* 2006). The bands around 1600 and 1329 cm^{-1} are characteristic of oxalate ligand (Khollam, *et al.,* 2002), and 1471 cm^{-1} is ν_{C-O} of CO_2 (Sharma, *et al.,* 2009). The ν_{Ti-O} of TiO_2 appears around 667 and 532 cm^{-1} (Zhang, *et al.,* 2003). The sharp band appearing around 772 cm^{-1} characteristic of ν_{Ba-O} (Khollam, *et al.,* 2002). The assigned modes of functional groups are listed in Table 3.2.5.2.
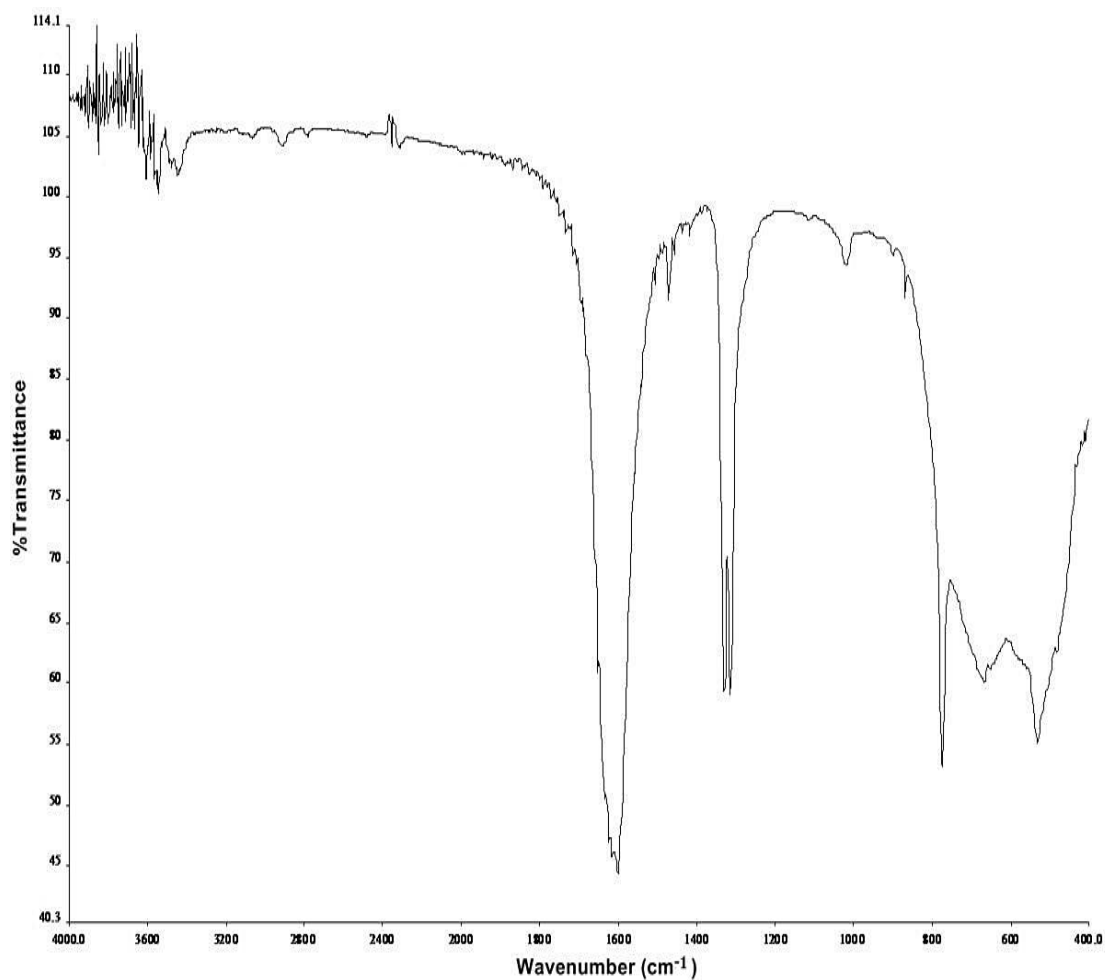
Figure 3.2.5.2 FT-IR spectrum of TiO_2-BaC_2O_4

Table 3.2.5.2 Assignment of the FT-IR band of commercial TiO_2 (anatase) and TiO_2-BaC_2O_4

Sample	Wavenumber (cm^{-1})	Assignment	Functional group/molecule	Reference
TiO_2	3500-3200	ν_{OH}	H_2O	Wang, *et al.*, 2000
	2375	ν_{CO}	CO_2	Belver, *et al.*, 2006

Sample	Wavenumber (cm^{-1})	Assignment	Functional group/molecule	Reference
	1633	δ_{OH}	OH group	Wang, *et al.*, 2000
	710	ν_{m-o}	TiO_2	Zhang, *et al.*, 2001
	503	ν_{m-o}	TiO_2	Zhang, *et al.*, 2001
TiO_2-BaC_2O_4	3455	ν_{OH}	OH	Wang, *et al.*, 2000
	2351	ν_{CO}	CO_2	Belver, *et al.*, 2006
	1600	ν_{OH}, ν_{CO}	OH group overlap withνC-O of oxalate ligand	Khollam, *et al.*, 2002 and Kangle, *et al.*, 2009
	1471	ν_{C-O}, ν_{C-C}	CO_2 overlap with ν_{C-C} of oxalate ligand	Sharma, *et al.*, 2009
	1329	ν_{CO}	Oxalate ligand	Sharma, *et al.*, 2009
	772		BTO	Khollam, *et al.*, 2002
	667		TiO_2	Zhang, *et al.*, 2001
	532		TiO_2	Zhang, *et al.*, 2001

The FT-IR spectrum of the TiO_2-BT is shown in Figure 3.2.5.3. The band around 2451, 1749, 1453, and 1019 cm^{-1} corresponding to ν_{C-O} of CO_2 (Khollam, *et al.,* 2002; Rhine, *et al.,* 1992). The ν_{Ti-O} of TiO_2 appears around 693 and 541 cm^{-1} (Zhang, *et al.*, 2003). The band appearing around 857 cm^{-1} is characteristic of ν_{Ba-O} in $BaTiO_3$ (Xia, *et al.,* 1995). The assigned modes of functional groups are listed in Table 3.2.5.3.
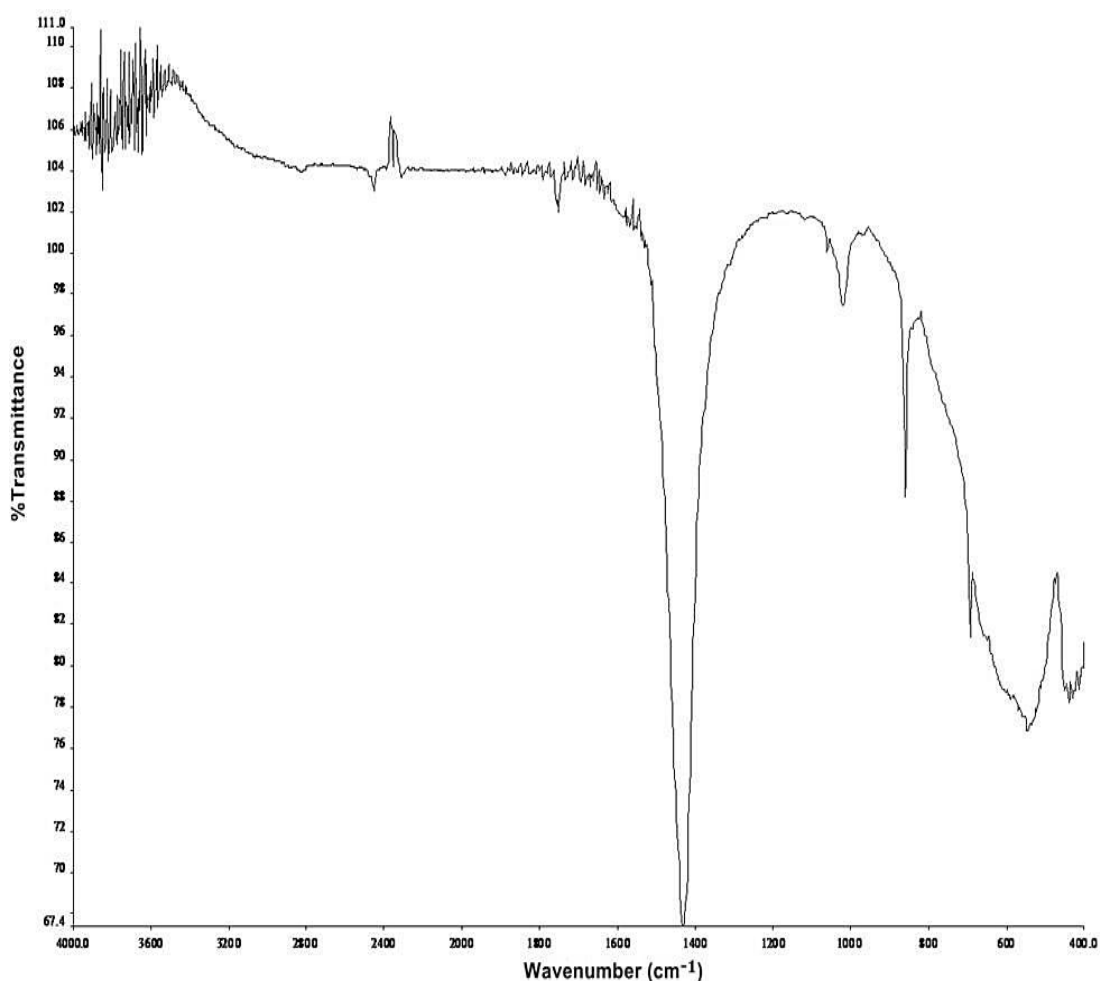

Figure 3.2.5.3 FT-IR spectrum of TiO_2-BT

Table 3.2.5.3 Assignment of the FT-IR band of TiO_2- BT

Sample	Wavenumber (cm^{-1})	Assignment	Functional group/molecule	Reference
TiO_2-BT	2451	ν_{CO}	CO_2	Khollam, *et al.,* 2002
	1750	ν_{OH}	H_2O	Khollam, *et al.,* 2002
	1453	ν_{CO}	CO_2	Sharma, *et al.*, 2009
	857	ν_{Ba-o}	$BaTiO_3$	Xia, *et al.*, 1995
	693	ν_{Ti-o}	TiO_2	Zhang, *et al.*, 2003
	541	ν_{Ti-o}	TiO_2	Zhang, *et al.*, 2003

3.3) The pH at the point of zero charge

The suspensions were prepared by adding 0.05 g of TiO_2 sample into 50 mL of 0.01 M NaCl solution and stirred for 3h. The pH of 0.01 M NaCl solution was adjusted using either 0.1 M HCl or 0.1M NaOH. The point of zero charge (pH_{pzc}) of samples were determined by measuring the final pH and plotted as a function of initial pH. The experimental results of pH_{pzc} determination were carried out using the pH drift method (Bessekhouad, *et al.,* 2004 and Nandi, *et al.,* 2009). The TiO_2 anatase phase has pH_{pzc} about 5.8 (Tan, *et al.*, 2009), TiO_2 rutile phase about 5.4 (Parfitt., 1976), TiO_2 Degussa P25 about 6.8 (Konstantinou, *et al.*, 2004). The experimental data and treatment to obtain pH_{pzc} of commercial TiO_2 of Degussa P25, anatase, and rutile yielded 8.0, 6.7, and 6.2 as shown in Figure 3.3.1, 3.3.2, and 3.3.3, respectively.
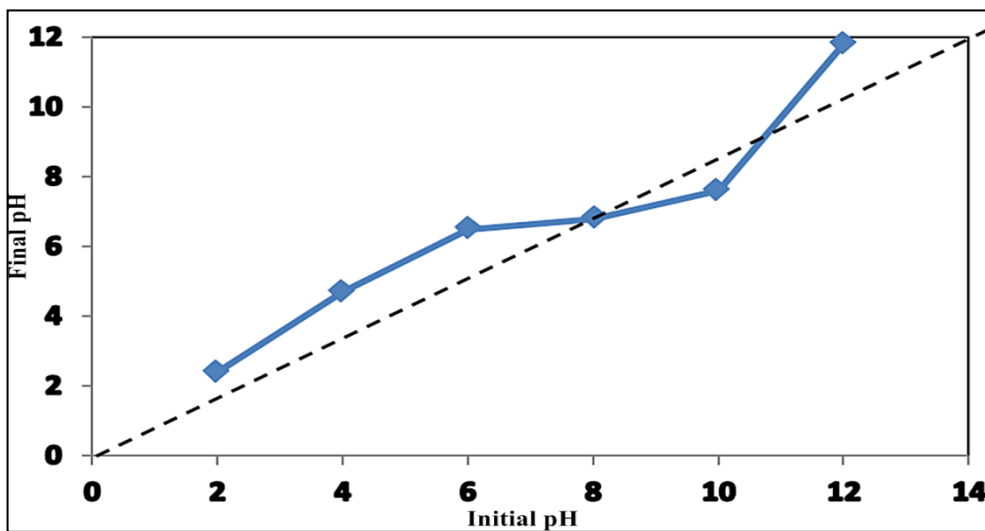
Figure 3.3.1 The plot of equilibrated pH (pH$_f$) vs. initial pH (pH$_i$) of Degussa P25 for determining pH$_{pzc}$ from the crossover point
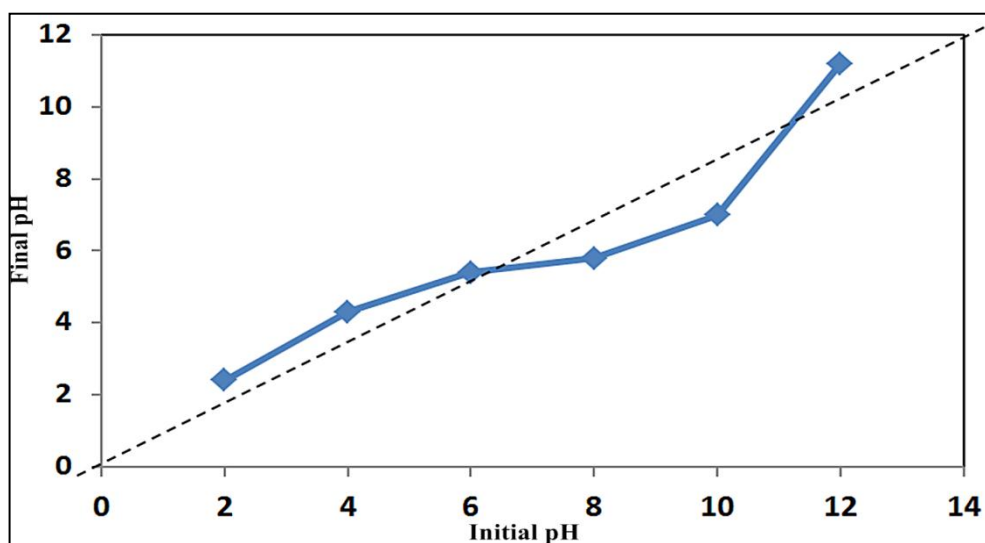

Figure 3.3.2 The plot of equilibrated pH (pH$_f$) vs. initial pH (pH$_i$) of anatase for determining pH$_{pzc}$ from the crossover point
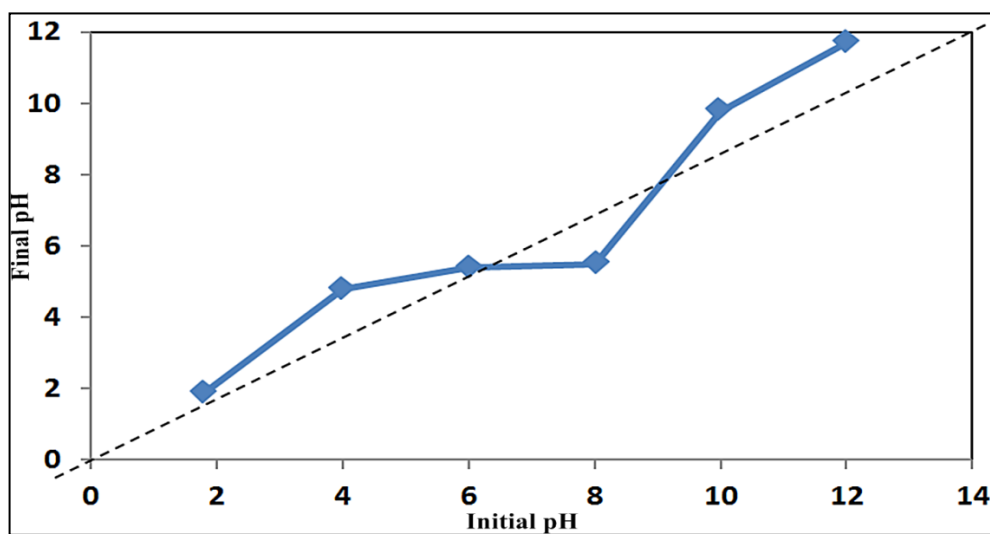
Figure 3.3.3 The plot of equilibrated pH (pH_f) vs. initial pH (pH_i) of rutile for determining pH_{pzc} from the crossover point

Table 3.3.1 pH_{pzc} of commertial TiO_2 and synthesized samples

Sample	pH_{pzc}	pH_{pzc} (Ref.)
Degussa P25	8.0	6.8 [a]
Anatase	6.2	5.8 [b]
Rutile	6.2	5.4 [c]
BTO	8.2	-
coupled TiO_2-BaC_2O_4	5.9	-
coupled TiO_2-BT	9.5	-

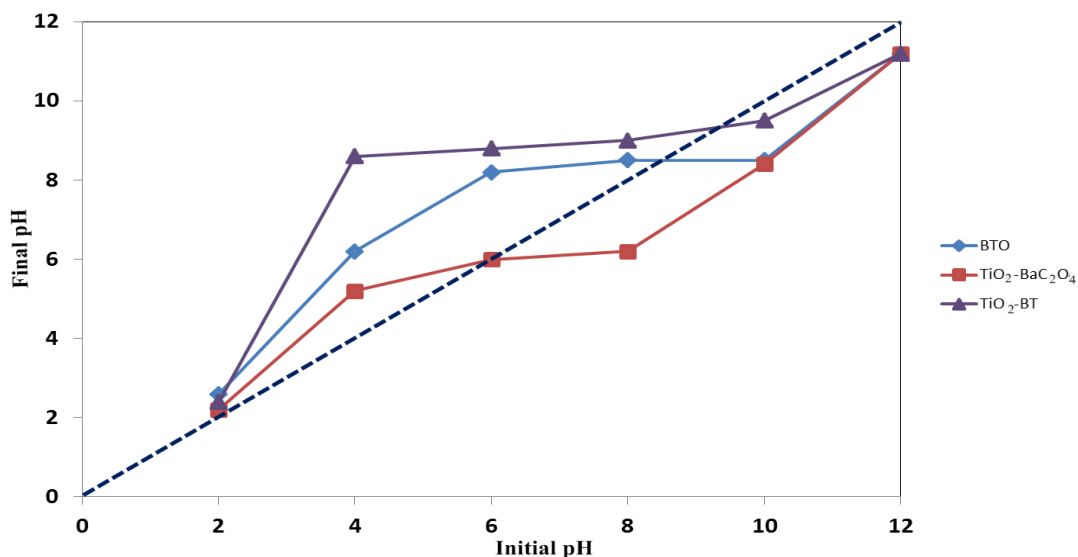[a]Konstantinou, *et al.*, 2004: [b]Tan, *et al.*, 2009: [c]Parfitt, 1976

Figure 3.3.4 The plots of equilibrated pH (pH_f) vs. initial pH (pH_i) of BTO, TiO_2-BaC_2O_4, and TiO_2-BT for determining pH_{pzc} from the crossover points

The pH_{pzc} of BTO, TiO_2-BaC_2O_4, and TiO_2-BT was measured in the same way as above and the graphs are given in Figure 3.3.4. The pH_{pzc} of BTO, TiO_2-BaC_2O_4, and TiO_2-BT then was obtained from the crossover points in the graphs as 8.2, 5.9, and 9.5, respectively.

The BTO prepared in this work was characterized to be BTO.$5H_2O$ identical to that reported by Rhine, *et al,* 1992 but with different starting material. In this work, the less prevail $TiO(SO_4)$ was used as the starting material. The XRD pattern of this BTO agreed with that reported by Potdar, *et al*., 1999. The surface and textural morphology (by SEM) appear like leaves of tree. The UV-visible DRS spectrum shows edge of absorption band at 382 nm corresponding to the band gap energy of 3.26 eV.

In the coupled TiO_2-BaC_2O_4, the XRD pattern was matched with TiO_2 (anatase) and $BaC_2O_4.10.5H_2O$ in the XRD library. For BaC_2O_4, the 2θ values agreed with that reported by Sharma, *et al*., 2009, 2θ: 18.5, 23.4, 26.2, 28.2, 29.0, 35.5, 39.6, 42.0, 43.6^o with the most prominent peak at 28.2^o. This peak correlated to (200) hkl indices, predicting a monoclinic structure of BaC_2O_4 and growth of monoparticles along the face (200) (Poonam, *et al*., 2009). The SEM images of coupled TiO_2-

BaC_2O_4 revealed the morphology of BaC_2O_4 appear as long rod or micelle (Sharma, *et al*., 2009) with its surface covered with TiO_2. The UV-visible DRS spectrum of TiO_2-BaC_2O_4 showing edge of absorption band at 390 nm corresponding to the band gap energy of 3.18 eV which is lower than the commercial anatase TiO_2 3.20 eV (Suwanchawalit, 2008) and that of BaC_2O_4 with edge of absorption band at 310 nm corresponding to the band gap energy of 4.00 eV.

In the coupled TiO_2-BT, BT or $BaTiO_3$ showed XRD pattern agreeing with that by Potdar, *et al*., 2001 and Thonsang, 2002. TiO_2 in this coupled sample showed anatase phase agreeing with that reported by Wongkaew, *et al*., 2010. The SEM images of the coupled TiO_2-BT revealed spherical BT agglomerated with spherical TiO_2 anatase. The pure BT particles have been shown to be spherical with size about 100 nm (Khollam, *et al*., 2002). The UV-visible DRS spectrum of TiO_2-BT showed edge of absorption band at 395 nm corresponding to the band gap energy of 3.14 eV which is lower than the commercial anatase TiO_2 of 3.20 eV (Suwanchawalit, 2008) and that of $BaTiO_3$ at 3.20 eV (Cox, 1995).

The results showed that coupling of different semiconductor oxides can reduce its band gap energy, extend its adsorption range to visible light region, promote electron-hole pair separation under irradiation, and, consequently, achieve a higher photocatalytic activity (Chao, *et al*., 2010).

3.4) Photocatalytic degradation studies of orange II sodium salt by commercial titanium dioxide (anatase), BTO, TiO_2-BaC_2O_4, and TiO_2-BT under UV and visible irradiation

In this work, the photocatalytic activities of all samples were evaluated using orange II sodium salt as a model organic dye compound under UV and visible light irradiation. The experimental set up for photocatalytic degradation consisted of 50 mL of the dye solution (orange II sodium salt) in a beaker and to it was added catalyst at a dose of 0.08 g. The solution was stirred in the dark for 30 minutes to establish the adsorption equilibrium. The mixture was stirred in the closed wooden compartment to avoid interference from ambient light until the end of experiment, 7 h.

At each time intervals (every 1 h), 5 mL of orange II sodium salt solution samples was collected. The degradation of orange II sodium salt solutions was analyzed from the changes in absorbance of the maximum absorption (λ_{max}) at 487 nm using UV-vis spectrophotometer.

Controlled experiments, without the catalyst, were performed to demonstrate that the degradation of the dye was dependent on the presence of the catalyst.

3.4.1 Preparation of calibration graph

The concentration of standard orange II sodium salt solutions was prepared in the range of $1.0 \times 10^{-6} - 1.0 \times 10^{-4}$ M. In order to construct reliable standard calibration graph of dye, the concentrations were divided into two ranges: 1.0×10^{-6} M to 1.0×10^{-5}M and 1.0×10^{-5}M to 1.0×10^{-4} M. The absorbance of dye solution was measured with SPECORD S100. The two ranges of standard calibration graphs are shown in Figures 3.4.1.1 and 3.4.1.2, respectively.
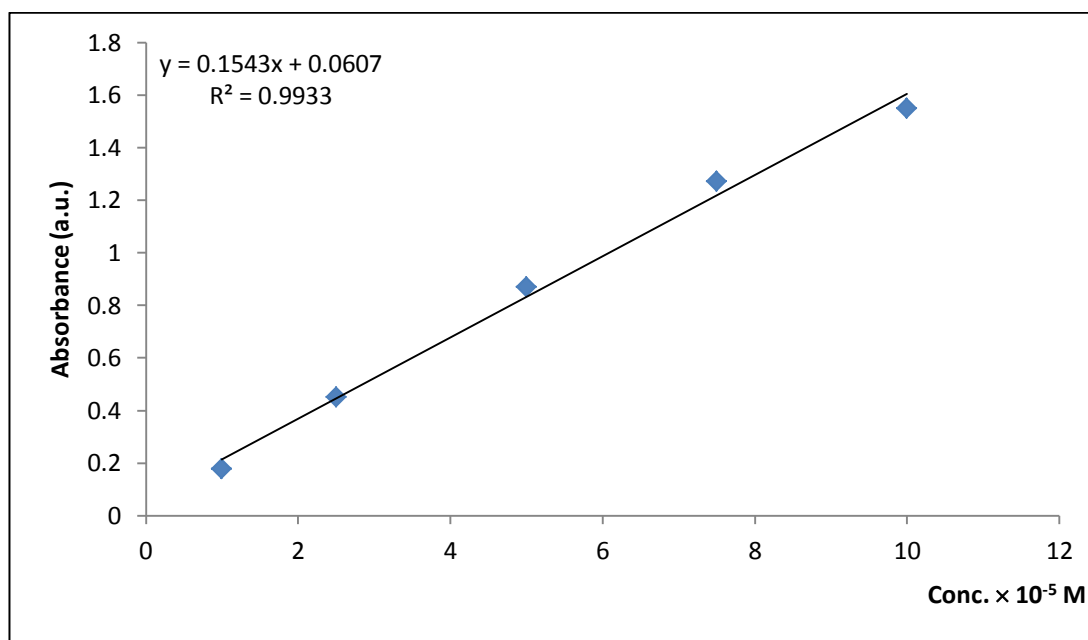

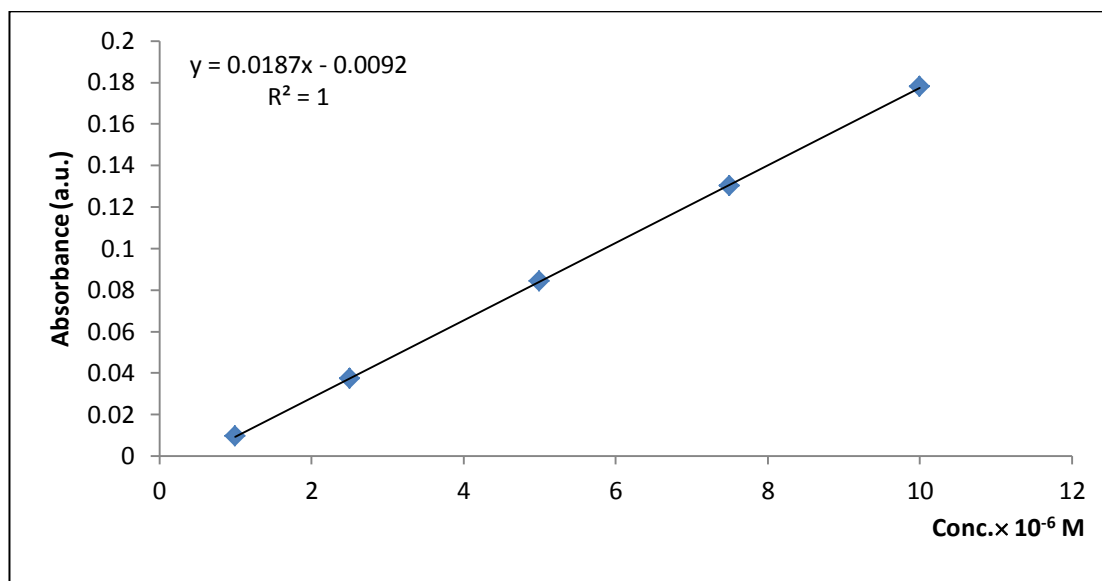**Figure 3.4.1.1** The standard calibration graph of orange II sodium salt solution in the range of 1.0×10^{-5}M to 1.0×10^{-4} M

Figure 3.4.1.2 The standard calibration graph of orange II sodium salt solution in the range of 1.0×10^{-6} M to 1.0×10^{-5} M

3.4.2 Effect of dye concentrations under UV and visible irradiation

The graphical comparison of commercial TiO_2 anatase phase with BTO, TiO_2-BaC_2O_4, and TiO_2-BT under UV and visible light are shown in Figure 3.4.2.1-3.4.2.6 with dye at various concentrations. Under UV irradiation the commercial anatase exhibited the highest degradation efficiencies at every concentration. However, under visible irradiation reversal of results were observed, that is, the synthesized coupling catalyst performed better than the commercial anatase with the general trend as: TiO_2-BT> BTO> anatase> TiO_2-BaC_2O_4.

Under visible light, anatase generally showed poor degradation performance since the light energy is not sufficient to create the e^- - h^+ pair. Among the three synthesized coupling catalyst, TiO_2-BT and BTO showed higher degradation efficiency than TiO_2-BaC_2O_4.

The three samples in our studies (BTO, TiO_2-BaC_2O_4, and TiO_2-BT) had two advantages over the commercial sample (anatase). The first is that their surfaces remained clean after use while the anatase surface was dirty due to dye

adsorption. The second is that the colloid containing anatase had to be spun at least 15 minutes to obtained clear solution for spectrophotometric measurement while that containing BTO (or TiO_2-BaC_2O_4 or TiO_2-BT) did not need centrifugation as the particles settled down quickly.
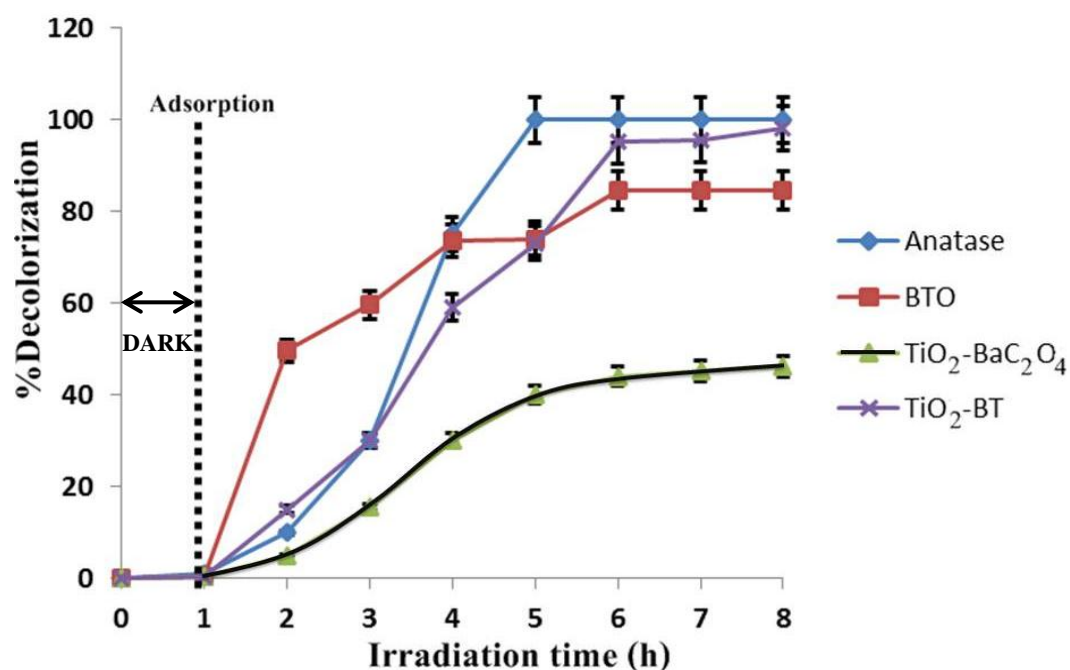

Figure 3.4.2.1 The effect of concentration under UV of anatase, BTO, TiO_2-BaC_2O_4, and TiO_2-BT at 2.0×10^{-5} M (n=3)
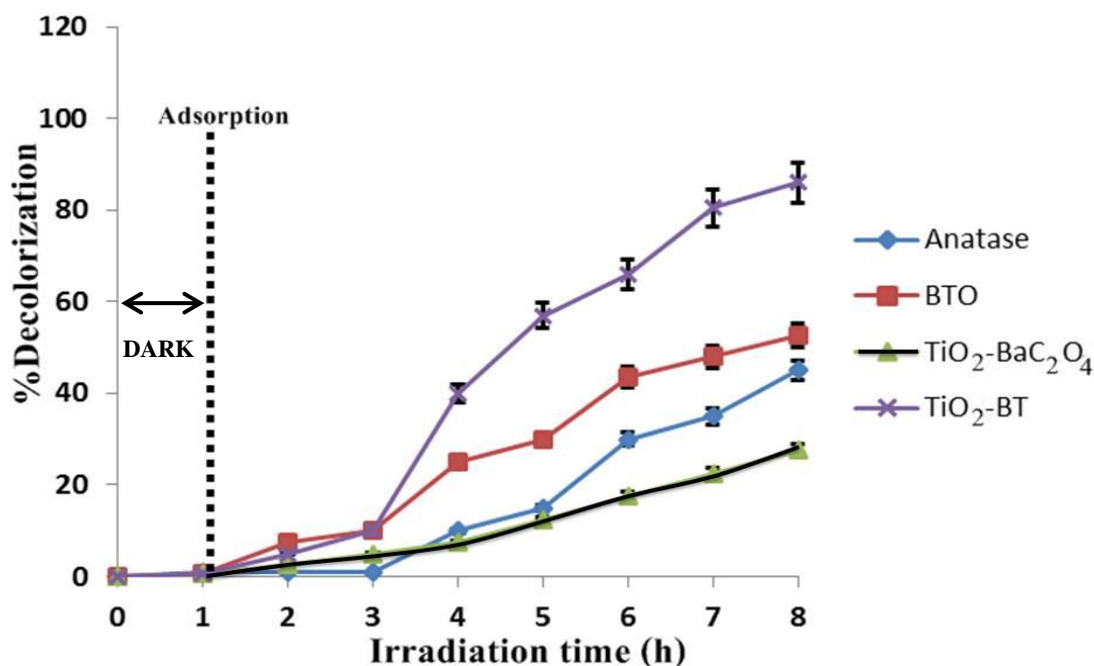
Figure 3.4.2.2 The effect of concentration under visible of anatase, BTO, TiO_2-BaC_2O_4, and TiO_2-BT at 2.0×10^{-5} M (n=3)

In the case of dye concentration at 2.5×10^{-5} M, Degussa P25 was included in the degradation experiment for comparison purpose. This is because this concentration (2.5×10^{-5} M) is the prevailing concentration. Most of the reported results employing Degussa P25 with other dyes were carried out at this concentration. The results in this series can serve as a link from our result to works reported by others. The % decolorization of Degussa P25 under UV irradiation was the highest among all samples in the study as shown in Figure 3.4.2.3 Under visible irradiation the reverse was observed as shown in Figure 3.4.2.4 (Degussa P25 was used only at 2.5×10^{-5} M but anatase was used in all concentrations due to the readily availability of anatase combined with the prior knowledge that anatase is almost equal but only slightly less active than Degussa P25 (Kanna, *et al*., 2010).)
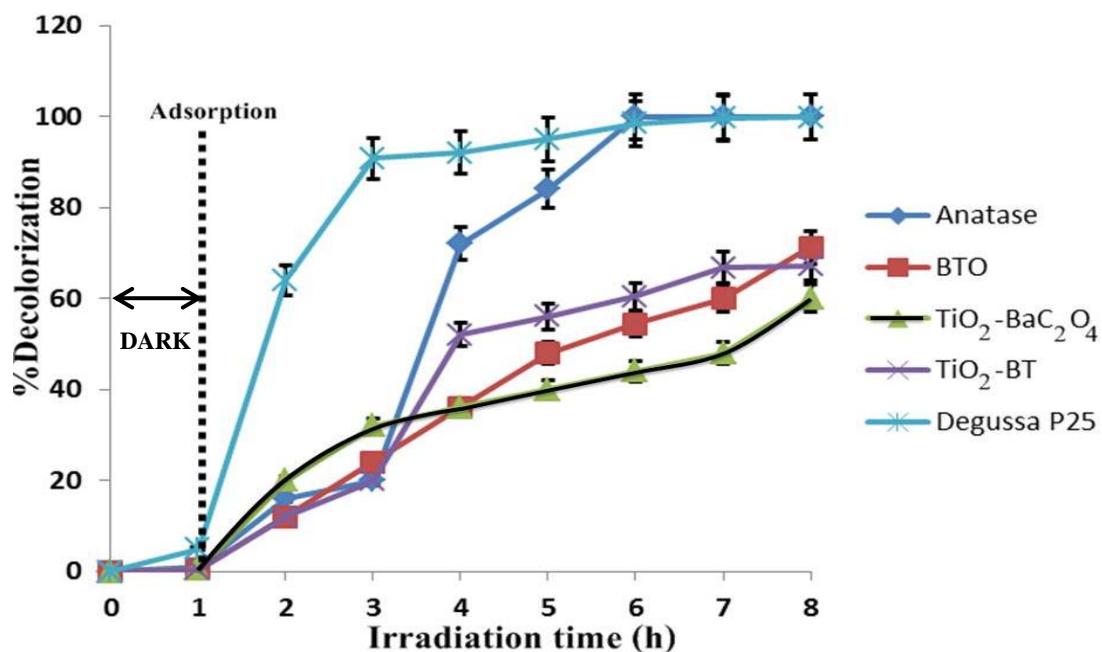
Figure 3.4.2.3 The effect of concentration under UV of Degussa P25, anatase, BTO, TiO$_2$-BaC$_2$O$_4$, and TiO$_2$-BT at   2.5×10^{-5} M (n=3)
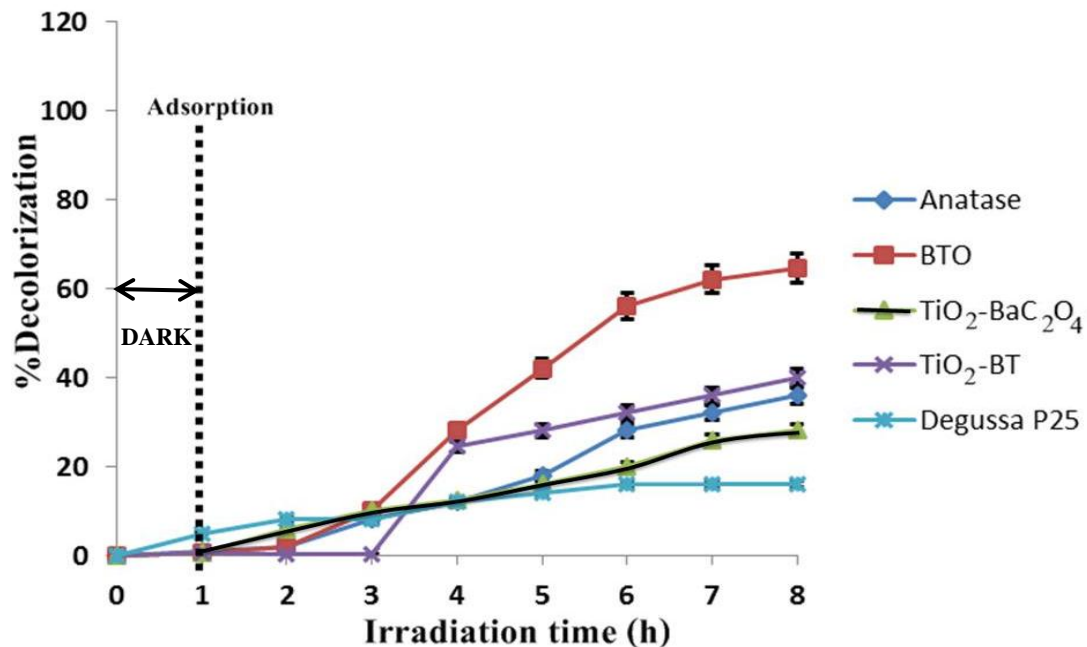
Figure 3.4.2.4 The effect of concentration under visible of Degussa P25, anatase, BTO, TiO$_2$-BaC$_2$O$_4$, and TiO$_2$-BT at 2.5×10^{-5} M (n=3)
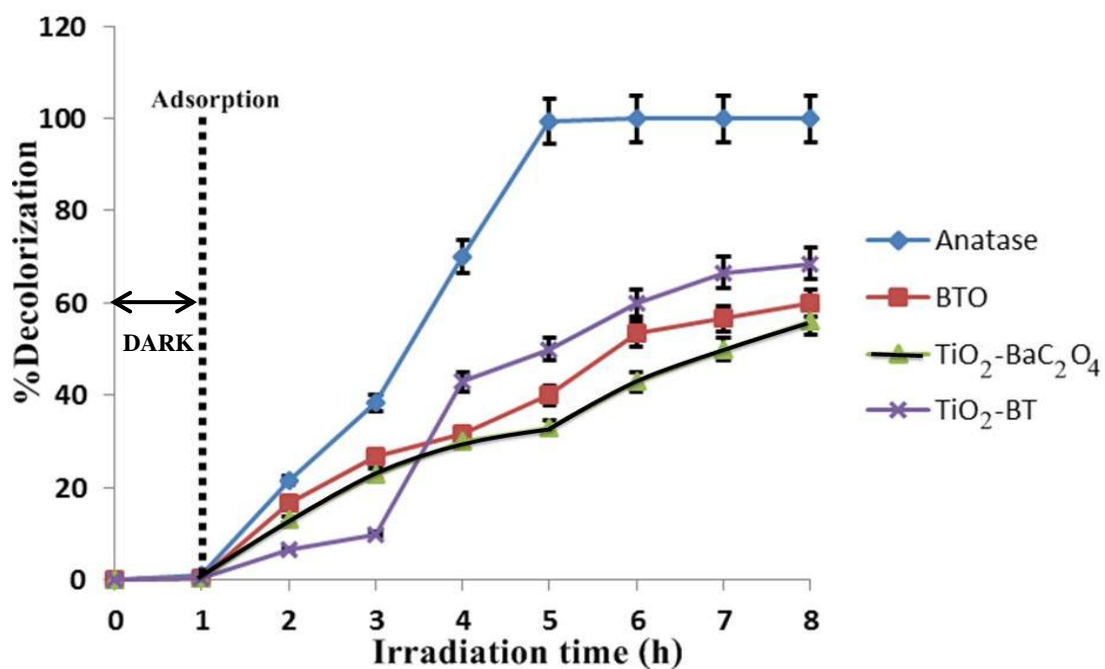
Figure 3.4.2.5 The effect of concentration under UV of anatase, BTO, TiO_2-BaC_2O_4, and TiO_2-BT at 3.0×10^{-5} M (n=3)
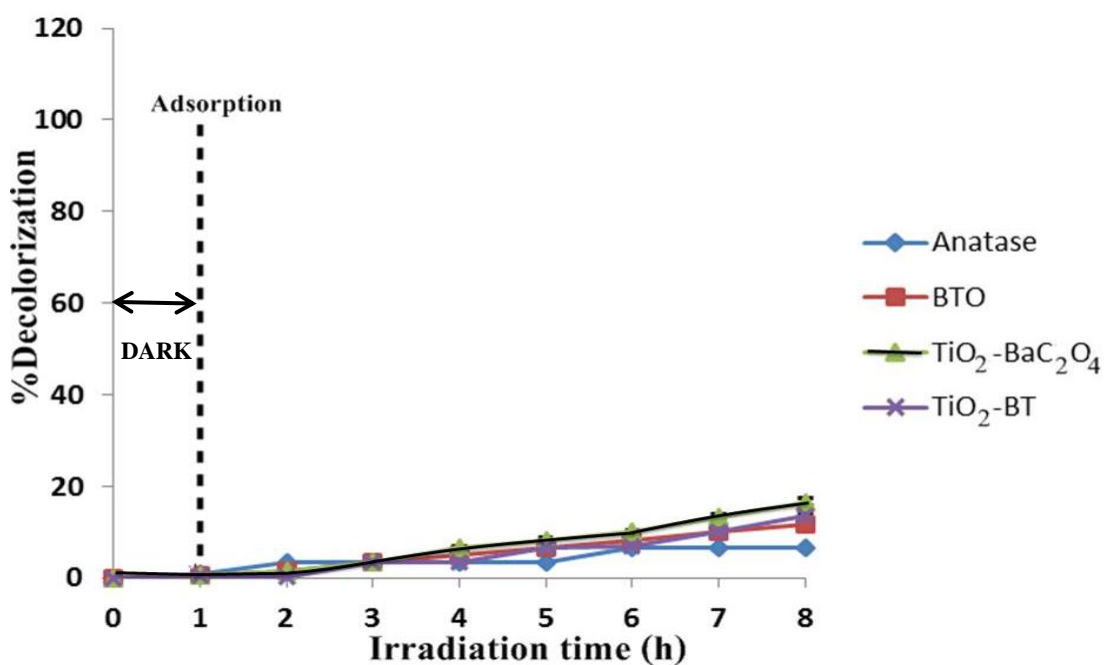
Figure 3.4.2.6 The effect of concentration under visible of anatase, BTO, TiO_2-BaC_2O_4, and TiO_2-BT at 3.0×10^{-5} M (n=3)

The comparison of degradation of BTO, TiO$_2$-BaC$_2$O$_4$, and TiO$_2$-BT

    The degradation efficiencies of BTO, TiO$_2$-BaC$_2$O$_4$, TiO$_2$-BT under UV and visible irradiation are comparatively displayed as bar chart for clarity in Figure 3.4.2.9, 3.4.2.10, and 3.4.2.11 for the three concentrations of dye (2.0×10^{-5} M, 2.5×10^{-5} M, 3.0×10^{-5} M), respectively. We can see that in all cases the performances under UV light were always better than visible light. Two samples (BTO and TiO$_2$-BT) worked the best at low concentration (2.0×10^{-5} M) of dye under UV light. At higher concentration, the efficiencies decreased and there was almost no differences among the three samples.
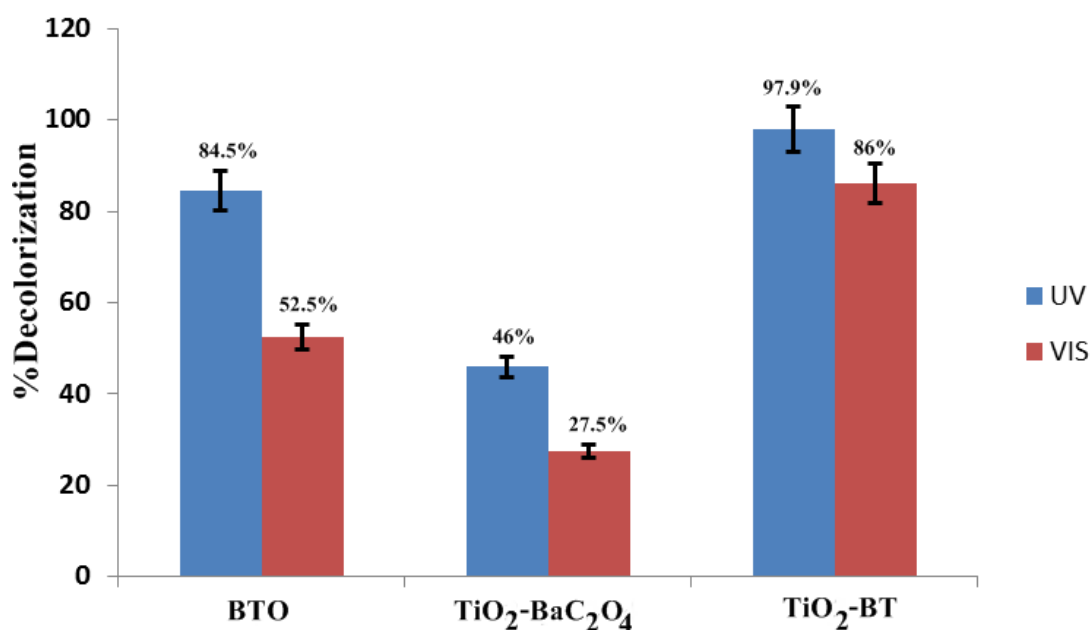
Figure 3.4.2.9 Photodegradation of Orange II sodium salt solution with BTO, TiO$_2$-BaC$_2$O$_4$, and TiO$_2$-BT under UV and visible irradiation at 7h (2.0x10^{-5}M) (n=3)
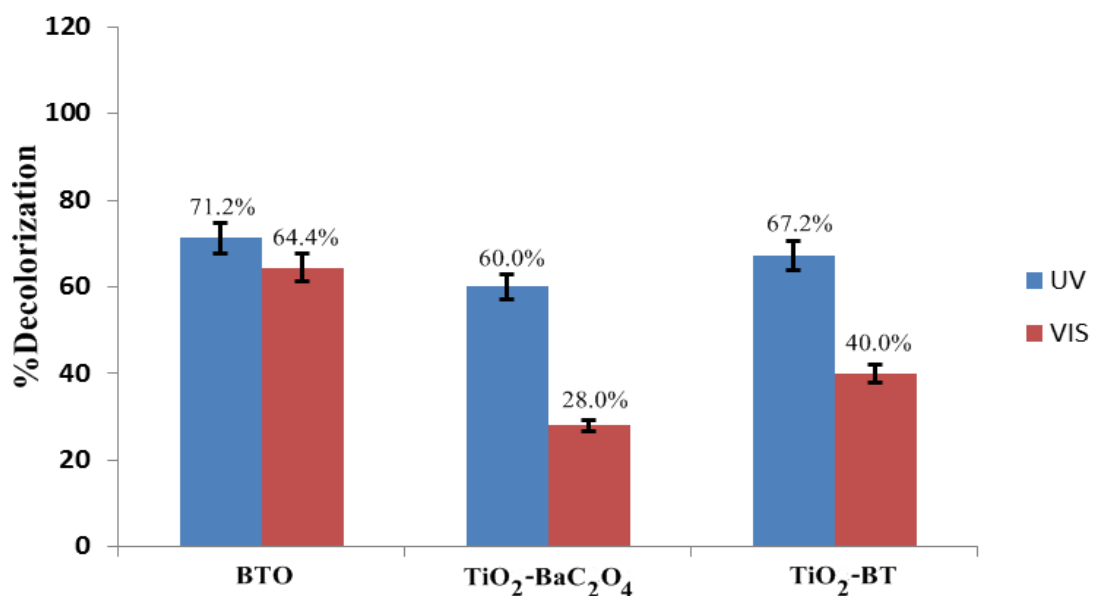
Figure 3.4.2.10 Photodegradation of Orange II sodium salt solution with BTO, TiO_2-BaC_2O_4, and TiO_2-BT under UV and visible irradiation at 7h (2.5×10^{-5}M) (n=3)
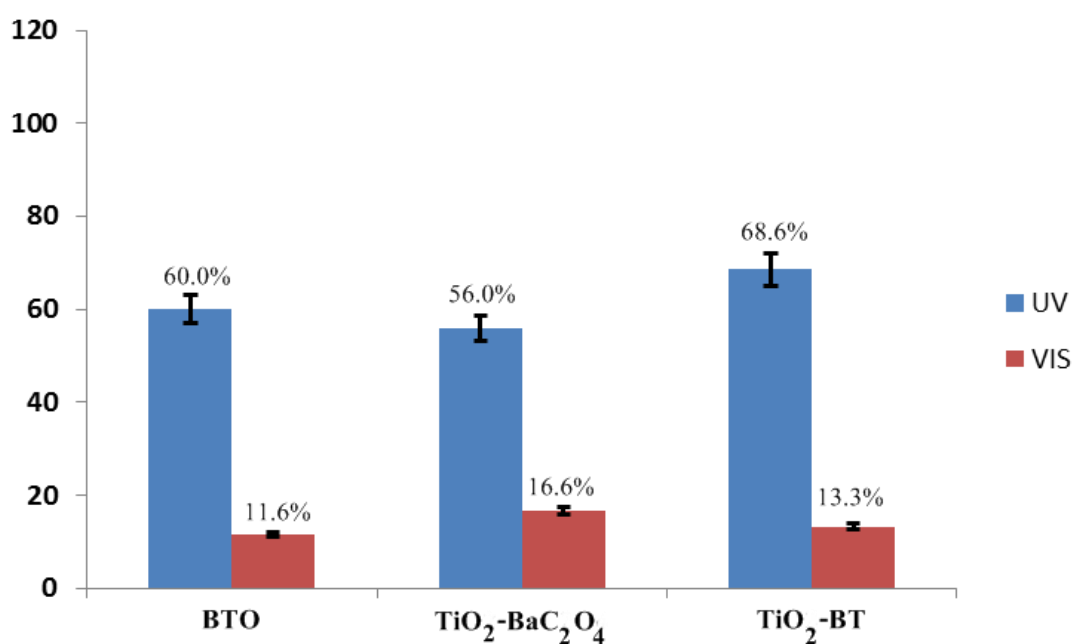
Figure3.4.2.11 Photodegradation of Orange II sodium salt solution with BTO, TiO_2-BaC_2O_4, and TiO_2-BT under UV and visible irradiation at 7h (3.0×10^{-5}M) (n=3)

3.4.3 Effect of pH

The effect of pH under UV and visible irradiation was studied at pH 2, 4, 6, 8, 10, and 12 in the period of 7 h. Figure 3.4.3.1 and 3.4.3.2 show the influence of pH on the degradation of orange II sodium salt dye in the pH range 2-12 under UV and visible light (7h), respectively. The natural pH of orange II sodium salt dye was 5.9. The optimum result was found at pH 12 which showed the highest percent decolorization under UV and visible irradiation.
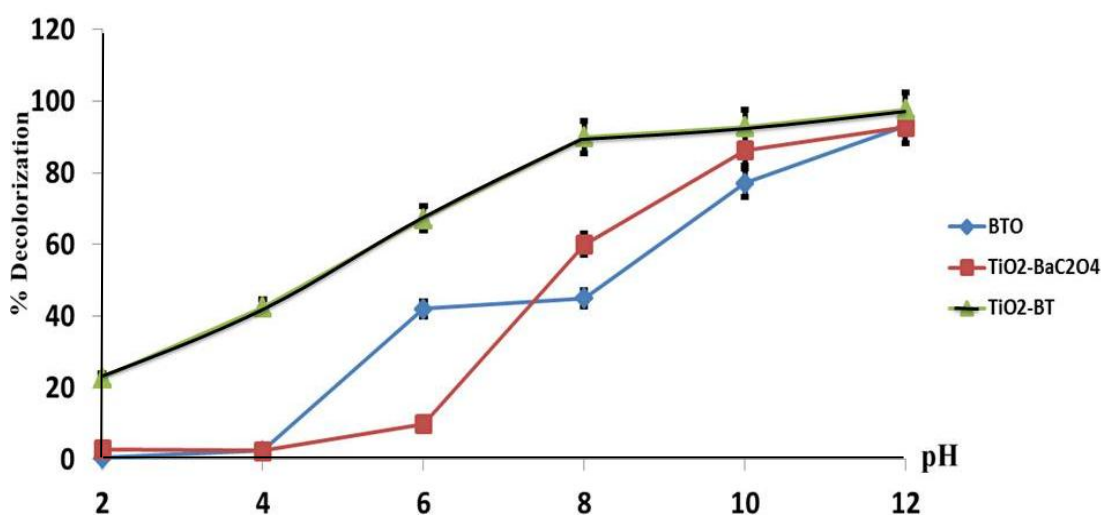
Figure 3.4.3.1 The effect of pH under UV irradiation of BTO, TiO_2-BaC_2O_4, and TiO_2-BT at 2.5×10^{-5} M (n=3)
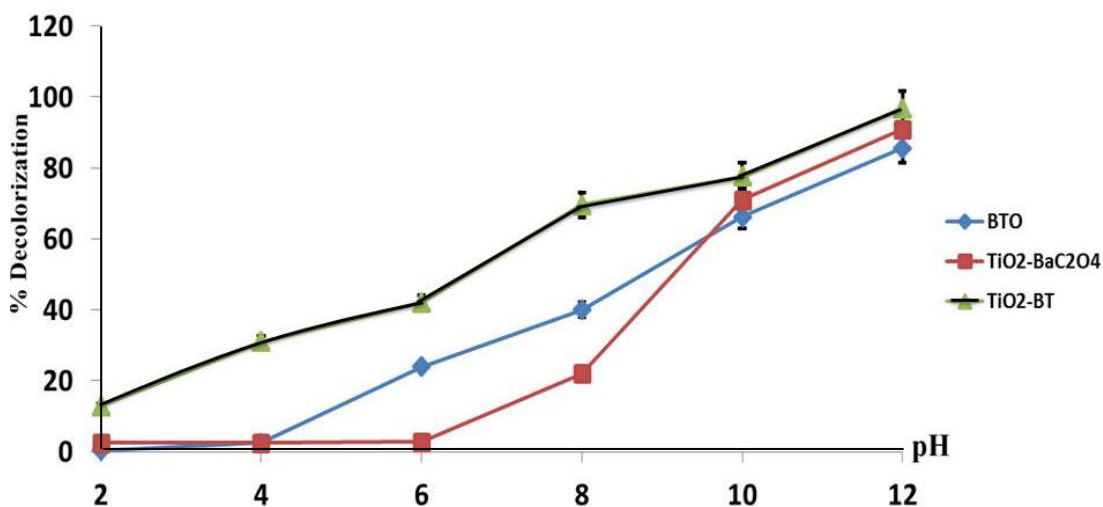
Figure 3.4.3.2 The effect of pH under visible irradiation of BTO, TiO_2-BaC_2O_4, and TiO_2-BT at 2.5×10^{-5} M (n=3)

Among all samples, TiO_2-BT showed highest %decolorization. Under UV irradiation, BTO and TiO_2-BaC_2O_4 were inactive if pH lower than 4, and under visible light irradiation if pH lower than 4 and 6, respectively. Orange II sodium salt dye was stable under both light sources as long as 7 h even at pH12. Figure 3.4.3.3 and 3.4.3.4 are evidences that this dye remained unchanged under the same condition as that used in the experiment of Figure 3.4.2.1-3.4.2.6. So we can conclude that the degradation of dye was from the photocatalytic property of all three samples (BTO, TiO_2-BaC_2O_4, TiO_2-BT) under studied.
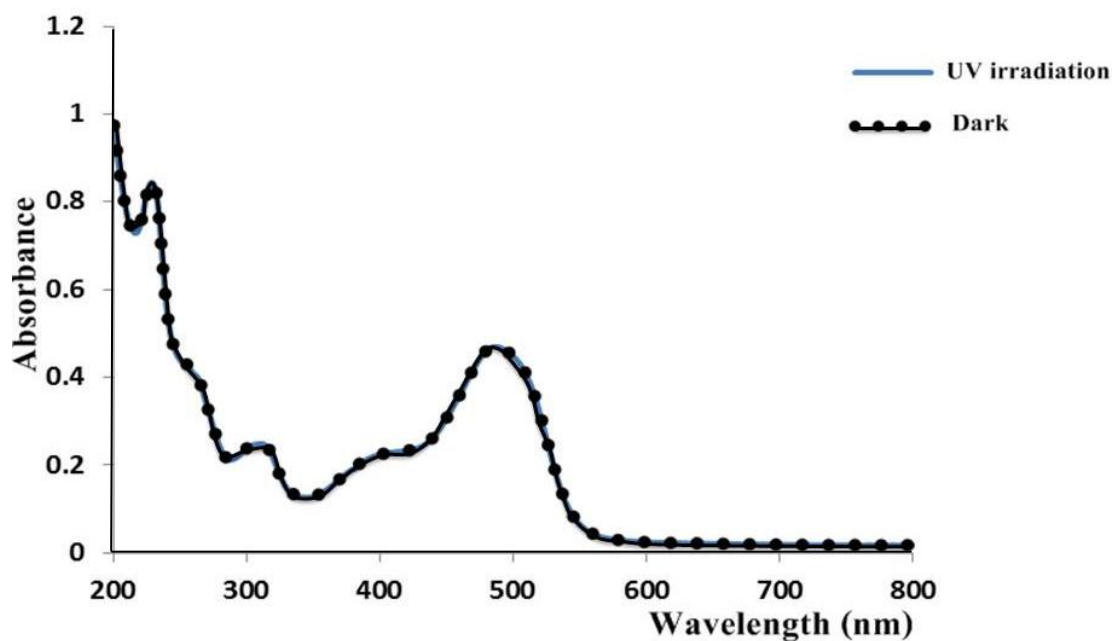
Figure 3.4.3.3 Absorption spectrum of orange II sodium salt solution (2.5×10^{-5} M, pH=12) under UV irradiation 7 h

Figure 3.4.3.4 Absorption spectrum of orange II sodium salt solution (2.5×10^{-5} M, pH=12) under visible irradiation 7 h

The wastewater from textile industries usually has a wide range of pH values. Generally, the pH of the solution is an important parameter in the photocatalytic process, since it not only plays an important role in the characteristics of textile wastewater, but also determines the surface charge properties of catalyst, the size of aggregates formed, the charge of dye 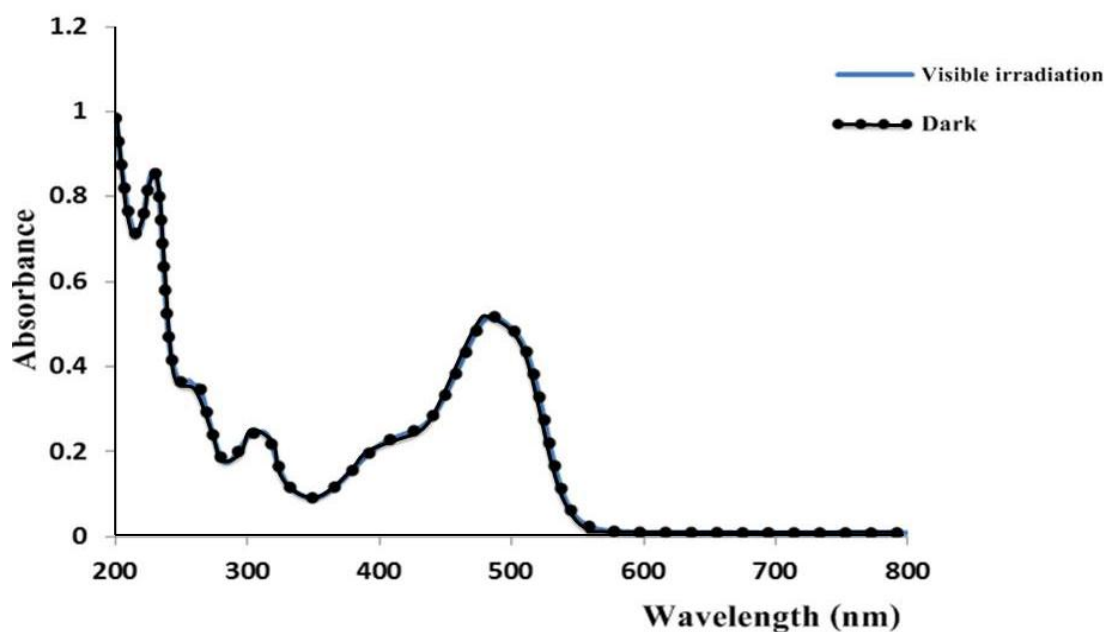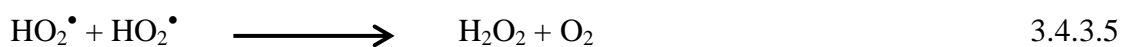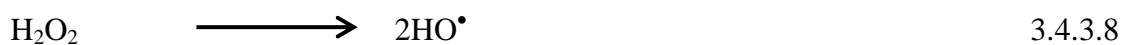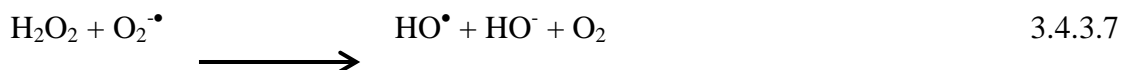molecules, adsorption of dyes onto catalyst sample surface and concentration of hydroxyl radicals. According to the point of zero charge (pzc), the surface charge property of catalyst sample changes with the change of solution pH such as TiO_2 surface is presumably positive charged in acidic solution (pH<pH_{pzc}) and negatively charged in alkaline solution (pH>pH_{pzc}) as given in Eqs. (3.4.3.1) and (3.4.3.2)(Sun, *et al.*, 2008).

$$TiOH + H^+ \rightleftharpoons TiOH_2^+ \qquad (3.4.3.1)$$

$$TiOH + OH^- \rightleftharpoons TiO^- + H_2O \qquad (3.4.3.2)$$

The orange II sodium salt dye in solution is negatively charged as the sulphonated group existing in its structure is hydrolyzed. Due to the electrostatic attraction, the acidic solution favors adsorption of dye onto catalyst sample (BTO has pH_{pzc}=8.2, TiO_2-BaC_2O_4 has pH_{pzc}=5.9, and TiO_2-BT has pH_{pzc} =9.5). It was found that the photocatalytic degradation of dye solution could be enhanced by both H^+ and OH^- ion formation. Under acidic conditions, the perhydroxyl radical is formed by the protonation of superoxide radical. These perhydroxyl radicals combine together to form hydrogen peroxide, which in turn dissociates to give hydroxyl radical (Eqs (3.4.3.3-3.4.3.9)).

$$O_2 + e^- \longrightarrow O_2^{-\bullet} \qquad\qquad 3.4.3.3$$

$$O_2^{-\bullet} + H^+ \longrightarrow HO_2^{\bullet} \qquad\qquad 3.4.3.4$$

$$HO_2^{\bullet} + HO_2^{\bullet} \longrightarrow H_2O_2 + O_2 \qquad\qquad 3.4.3.5$$

$$H_2O_2 + e^-_{cb} \xrightarrow{h\nu} HO^{\bullet} + HO^- \qquad\qquad 3.4.3.6$$

$$H_2O_2 + O_2^{-\bullet} \longrightarrow HO^{\bullet} + HO^- + O_2 \qquad\qquad 3.4.3.7$$

$$H_2O_2 \longrightarrow 2HO^{\bullet} \qquad\qquad 3.4.3.8$$

Therefore, in the alkaline pH range, the concentration of hydroxyl radicals increases (3.4.3.9) (Kumar, *et al.,* 2010).

$$O_2 + HO^- \longrightarrow O_2^{-\bullet} + HO^{\bullet} \qquad\qquad 3.4.3.9$$

3.5) The kinetics study

In the kinetics study, the apparent rate constant (k_{app}) has been chosen as the basic kinetics parameter for all the sample under investigation. The apparent first-order kinetics equation is (Silva, *et al*., 2006; Baiju, *et al*., 2007; Ao, *et al*., 2008.)

$$\ln \frac{C_o}{C} = K_{app} \times t \qquad\qquad (3.5.1)$$

where *Co* is the initial concentration of dye, *C* is the concentration at time *t*, and K_{app} is the apparent rate constant. The straight lines obtained when ln(Co/C) is plotted against *t* is an indication that dye degradation proceeds by the first-order kinetics. The kinetic plots rate of BTO, TiO_2-BaC_2O_4, and TiO_2-BT at 2.0×10^{-5} M under UV irradiation are shown in Figure 3.5.1. The rate constant, i.e., the slope of the line of BTO, TiO_2-BaC_2O_4, and TiO_2-BT are 0.1275, 0.0459, and 0.2064 h^{-1}, respectively.
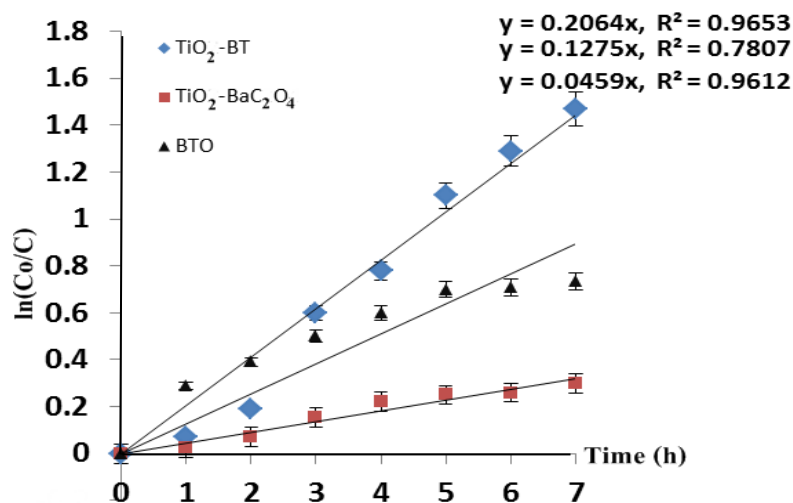
Figure 3.5.1 The kinetic plots of BTO, TiO_2-BaC_2O_4 and TiO_2-BT at 2.0×10^{-5} M under UV irradiation, n=3

Likewise the kinetic plots of BTO, TiO_2-BaC_2O_4, and TiO_2-BT at 2.0×10^{-5} M under visible irradiation are shown in Figure 3.5.2 the rate constant 0.0438, 0.0165, and 0.1071 h^{-1} for BTO, TiO_2-BaC_2O_4, and TiO_2-BT, respectively.
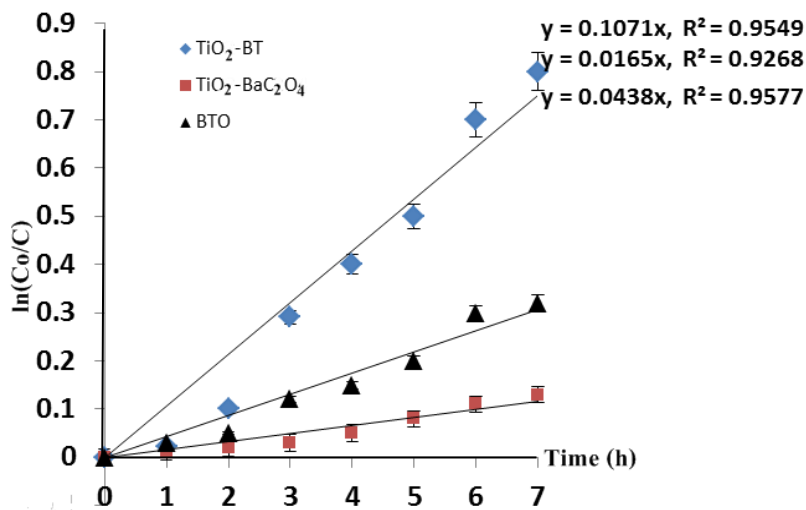
Figure 3.5.2 The kinetic plots of BTO, TiO_2-BaC_2O_4 and TiO_2-BT at 2.0×10^{-5} M under visible irradiation, n=3

The kinetic plots of BTO, TiO_2-BaC_2O_4, and TiO_2-BT at 2.5×10^{-5} M under UV are shown in Figure 3.5.3. The rate constant, i.e., the slope of the line of BTO, TiO_2-BaC_2O_4, and TiO_2-BT are 0.0730, 0.0533, and 0.0776 h^{-1}, respectively.
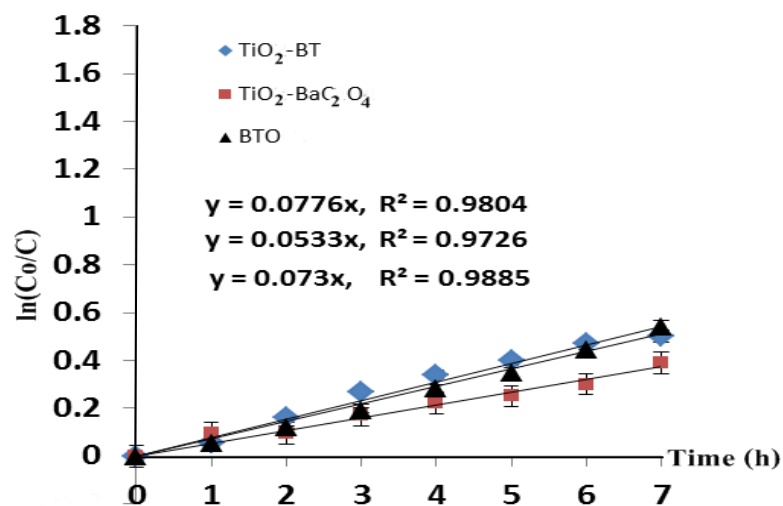
Figure 3.5.3 The kinetic plots of BTO, TiO_2-BaC_2O_4 and TiO_2-BT at 2.5×10^{-5} M under UV irradiation, n=3

The kinetic plots of BTO, TiO_2-BaC_2O_4, and TiO_2-BT at 2.5×10^{-5} M under visible irradiation are shown in Figure 3.5.4. The rate constant, i.e., the slope of the line of BTO, TiO_2-BaC_2O_4, and TiO_2-BT are 0.0663, 0.0198, and 0.0329 h^{-1}, respectively.
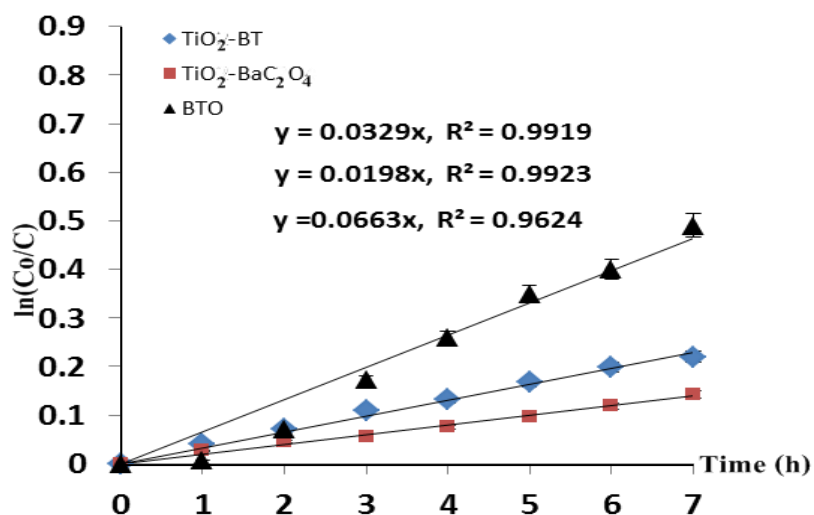
Figure 3.5.4 The kinetic plots of BTO, TiO_2-BaC_2O_4 and TiO_2-BT at 2.5×10^{-5} M under visible irradiation, n=3

The kinetic plots of BTO, TiO_2-BaC_2O_4, and TiO_2-BT at 3.0×10^{-5} M under UV irradiation are shown in Figure 3.5.5. The rate constants, i.e., the slope of the line of BTO, TiO_2-BaC_2O_4, and TiO_2-BT are 0.0646, 0.0502, and 0.0773 h^{-1}, respectively.
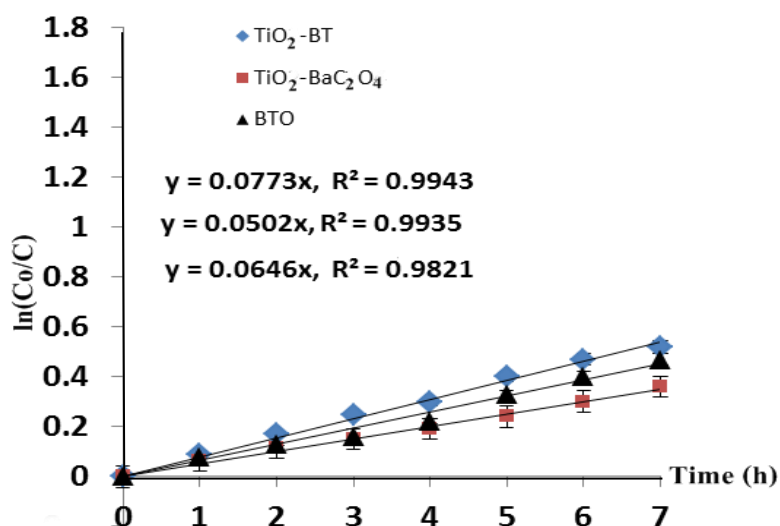
Figure 3.5.5 The kinetic plots of BTO, TiO_2-BaC_2O_4 and TiO_2-BT at 3.0×10^{-5} M under UV irradiation, n=3

The kinetic plots of BTO, TiO_2-BaC_2O_4, and TiO_2-BT at 3.0×10^{-5} M under visible irradiation are shown in Figure 3.5.6. The rate constant, i.e., the slope of the line of BTO, TiO_2-BaC_2O_4, and TiO_2-BT are 0.0075, 0.0102, and 0.0075 h^{-1}, respectively.
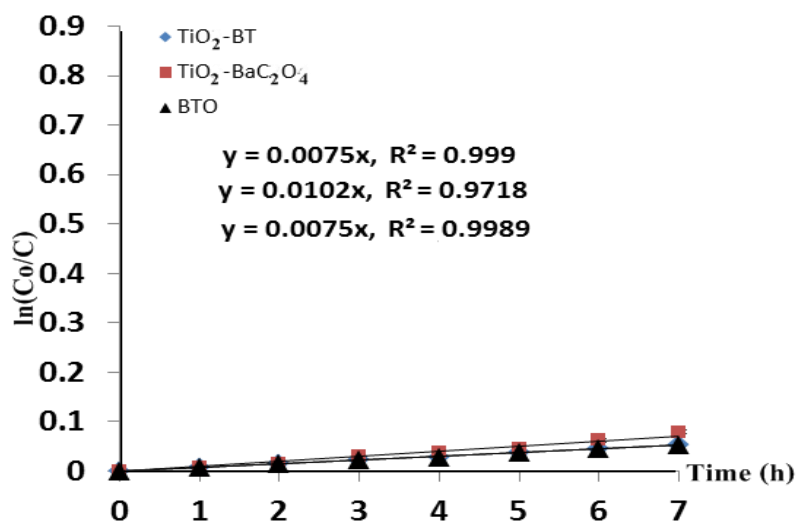
Figure 3.5.6 The kinetic plots of BTO, TiO_2-BaC_2O_4 and TiO_2-BT at 3.0×10^{-5} M under visible irradiation, n=3

Table 3.5.1 The rate constant (K_{app}) of sample under UV and visible irradiation at 2.0×10^{-5} M, 2.5×10^{-5} M, and 3.0×10^{-5} M

Sample	K_{app} under UV irradiation (h^{-1})	K_{app} under visible irradiation (h^{-1})
At 2.0×10^{-5} M		
BTO	0.1275	0.0438
TiO_2-BaC_2O_4	0.0459	0.0165
TiO_2-BT	0.2298	0.1071
At 2.5×10^{-5} M		
BTO	0.0730	0.0663
TiO_2-BaC_2O_4	0.0533	0.0198
TiO_2-BT	0.0776	0.0329
At 3.0×10^{-5} M		
BTO	0.0646	0.0075
TiO_2-BaC_2O_4	0.0502	0.0102
TiO_2-BT	0.0773	0.0075

3.6) Recyclability of BTO, TiO_2-BaC_2O_4, and TiO_2-BT

In the recyclability study, the three synthesized photocatalysts were investigated in the repeating uses up to 6 times. The photocatalysts powder was collected after each use and washed few times with DI water before reuse. (Surfaces of catalysts were clean since almost no surface adsorption of dye was detected. Washing was through the filtering funnel and water aspirator). The dye concentration used in this part was 2.5×10^{-5} M. The investigation was carried out with both light sources (UV and visible) for 7h.
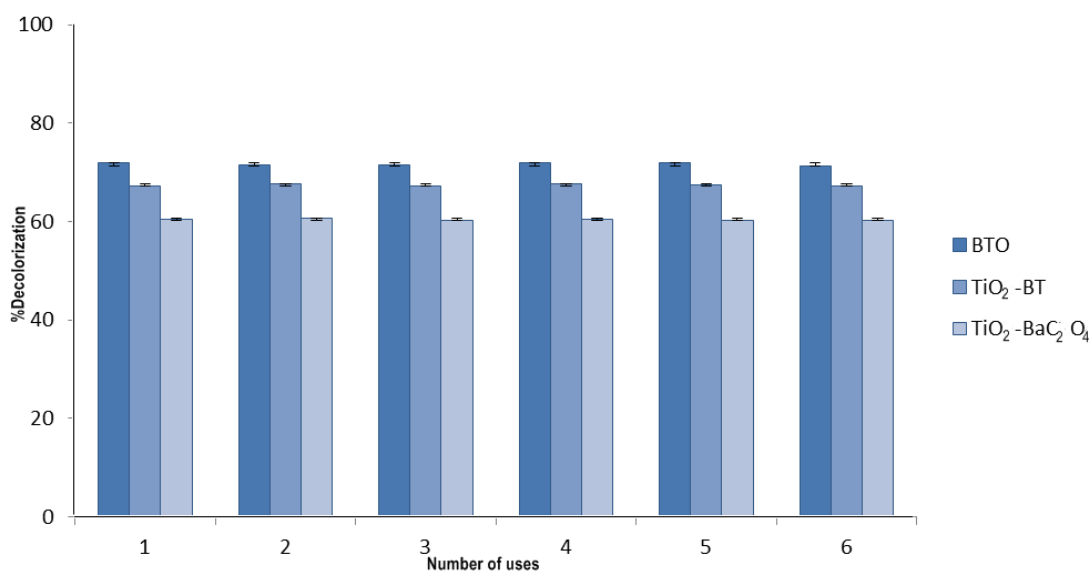
Figure 3.6.1 The photodecolorization efficiencies of BTO, TiO_2-BaC_2O_4, and TiO_2-BT from the recyclability test (under UV light, 7 h, 2.5×10^{-5} M), n=3
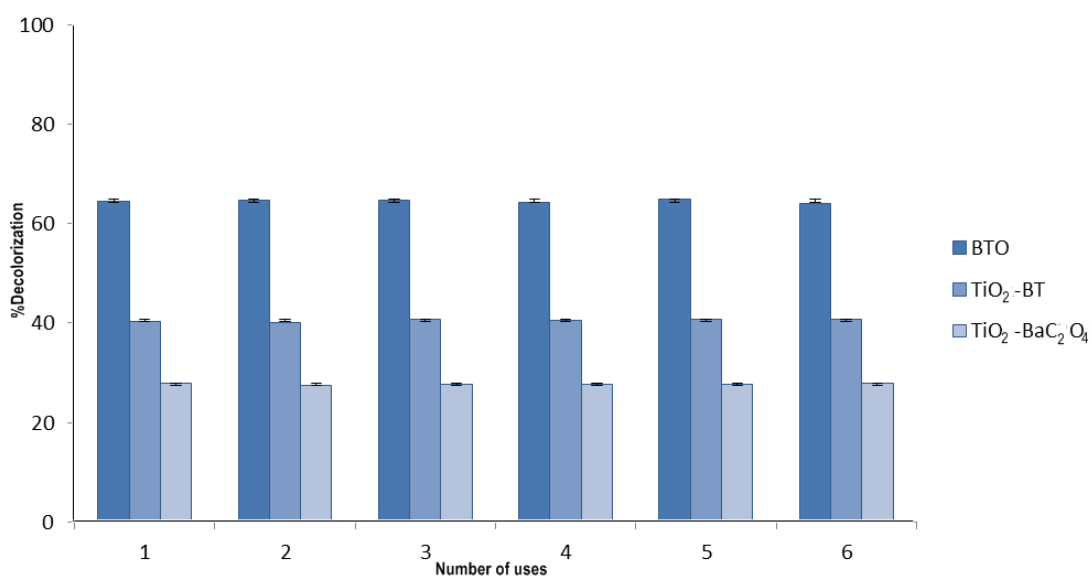
Figure 3.6.2 The photodecolorization efficiencies of BTO, TiO_2-BaC_2O_4, and TiO_2-BT from the recyclability test (under visible light, 7 h, 2.5×10^{-5} M), n=3

The results from recyclability test of $BTO, TiO_2 - BaC_2O_4$, and TiO_2-BT under UV and visible light are shown in Figure 3.6.1 - 3.6.2, respectively. From these graphical results we can see that:

(1) The degradation efficiencies of the 1st use to the 6th use remained unchanged. This means that there was no different between the freshly prepared sample and the used sample.

(2) The efficiency of BTO under visible light was only slightly less than that under UV light while TiO_2-BaC_2O_4 and TiO_2-BT showed large different in efficiency between visible and UV sources. This means that BTO should be a better choice since it can work almost equally well under either light source.

After 6 times of recycle test which yielded similar degradation efficiencies, the three catalysts did not show any sign of physical changes significantly. Although the investigation was performed only 6 times in the laboratory scale, from the physical stability of the catalysts it seems that these catalysts should have long service time.

CHAPTER 4

Conclusions

Barium titanium oxalate (BTO) in this study was synthesized from reaction between titanium oxysulfate ($TiOSO_4$), oxalic acid ($H_2C_2O_4$), and barium chloride ($BaCl_2$) (adapted from Fang, *et al*., 1989 and Khollam, *et al*., 2002). BTO exists as a white powder solid. Typically BTO was prepared by using $TiCl_4$ as source of Ti atom but in this research it was replaced by $TiOSO_4$ as source of Ti atom. The use of $TiOSO_4$ is scarce and less prevail than $TiCl_4$.

BTO was characterized by several techniques such as XRD, DRS, SEM, FT-IR, and UV-vis spectroscopy. The XRD patterns of BTO matched with the XRD library. The band gap energy was measured to be 3.26 eV. The SEM image revealed the morphology of BTO having the shape of tree leaves.

In the study of the effect of dye concentration under UV and visible irradiation with BTO we found that at higher concentration the percent decolorization decreased. The recyclability of BTO was tested 6 times. There was no different in efficiency before and after reuses.

In the case of TiO_2-BaC_2O_4 and TiO_2-BT they can be considered as mixed catalyst or cocatalyst between TiO_2 with BaC_2O_4 and TiO_2 with BT. The precursor to prepare cocatalyst is TiO_2 anatase phase. The advantage of using cocatalyst, which was no colloidal mixture, was formed thus the sample was collected with ease after the photocatalytic study. The solution was cloudy due to colloid formation if not using cocatalyst.

TiO_2-BaC_2O_4 and TiO_2-BT were characterized by several techniques, such as XRD, DRS, SEM, FT-IR, and UV-vis spectroscopy. The SEM image revealed the morphologies of TiO_2-BaC_2O_4 as long rods of BaC_2O_4 cover with TiO_2 on the

surface. The TiO_2-BT powder was obtained by calcination of TiO_2-BaC_2O_4. The pure BT particles are spherical in nature, TiO_2-BaC_2O_4 after calcination at 800 °C for 3h changed to BT with excess TiO_2 agglomerated TiO_2 particles.

The photocatalytic degradation of TiO_2-BaC_2O_4 and TiO_2-BTwere carried out under UV and visible light irradiation. It was found that on increasing concentration of dye the degradation efficiency decreased. The decolorization efficiencies of catalysts under studied were compared with commertial TiO_2 anatase and Degussa P25. The percent decolorization of commertial TiO_2 anatase and Degussa P25 under UV irradiation were higher than others but under visible irradiation the reverse was observed.

The effect of pH was studied under UV and visible irradiation using dye concentration $2.5x10^{-5}$M. The pH range under studied was 2-12 and the reaction time was 7h. The optimum result was found at pH 12 which showed highest % decolorization under UV and visible irradiation. Among all samples, TiO_2-BT showed highest % decolorization. Under UV irradiation, TiO_2-BaC_2O_4 was inactive if pH was lower than 4. Under visible light irradiation, TiO_2-BaC_2O_4 was inactive if pH lower than 6. In case of BTO under UV irradiation and visible irradiation inactivity was observed if pH lower than 4.

The pH_{pzc} of BTO, TiO_2-BaC_2O_4, and TiO_2-BT were determined to be 8.2, 5.9, and 9.5, respectively. The surface charge property of catalyst sample changes with the change of solution pH. The surface is presumably positively charged in acidic solution (pH<pH_{pzc}) and negatively charged in alkaline solution (pH>pH_{pzc}).

The orange II sodium salt dye in solution is negatively charged as the sulphonated group in its structure is hydrolyzed. Due to the electrostatic attraction, the acidic solution favors adsorption of dye onto catalyst sample (It was found that the photocatalytic degradation of dye solution could be enhanced by both H^+ and OH^- ion formation. Under acidic conditions, the perhydroxyl radical is formed by the protonation of superoxide radical. These perhydroxyl radicals combine together to form hydrogen peroxide, which in turn dissociates to give hydroxyl radical. On the other hand, under alkaline conditions, the hydroxide ions (OH^-) are abundant and can

react with oxygen molecules (O_2) to give hydroxyl radicals. Therefore, in the alkaline pH range, the concentration of hydroxyl radicals increases.

The recyclability test of TiO_2-BaC_2O_4, and TiO_2-BT showed no different in efficiencies before and after reuses.

REFERENCES

Acid-dye from Wikipedia, the free encyclopedia : http://en.wikipedia.org./wiki/acid-dye (accessed 3/01/10).

Al-Rasheed, R. (2005). "Water treatment by heterogeneous photocatalysis an overview". *Presented at 4th SWCC acquired experience symposium held in jeddah.*

Ao, Y., Xu, J., Fu, D. and Yuan, C. (2008). "Preparation of porous titania thin film and its photocatalytic activity", *Appl. Surf. Sci.* 255, 3137-3140.

Azam, A. and Hamid, A. (2006). "Effects of gap size and UV dosage on decolorization of C.I. Acid Orange 7 by UV/H$_2$O$_2$ process", *J. Hazard. Mater.* 133, 167-171.

Baiju, K. V., Shukla, S., Sandhya, K. S., James, J. and Warrier, K. G. K. (2007). "Photocatalytic activity of sol-gel derived nanocrystalline titania", *J. Phys. Chem. C.* 111, 7612-7622.

Baolong, Z., Baishun, C., Keyu, S., Shangjin, H., Xiaodong, L., Zongjie, D. and Kelian, Y. (2003). "Preparation and characterization of nanocrystal grain TiO$_2$ porous microsheres", *Appl. Catal. B: Environ.* 40, 253-258.

Bassiad, s., Robert, D. and Chaib, M. (2009). "Use of oxalate sacrificial compounds to improve the photocatalytic performance of titanium dioxide", *Appl. Catal. B: Environ.* 86, 93-97.

Basic dyes : http://www.jagson.com/paper-dyes.htm (acessed 3/01/10).

Belver, C., Bellod, R., Fuerte, A. and Ferendez-Garcia, M. (2006). "Nitrogen containing TiO_2 photocatalyst part1: synthesis and solid characterization", *Appl. Catal. B: Environ.* 65, 301-308.

Bera, J. and Sarkar, D. (2003). "Formation of $BaTiO_3$ from barium oxalate and TiO_2", *Pub. J. Electro.* 11, 131-137.

Bessekhouad, Y., Robert, D., Weber, J. V. and Chaoui, N. (2004). "Effect of alkaline doped TiO_2 on photocatalytic efficiency", *J. Photoch. Photobio. A.* 65, 49-57.

BET surface area theory : http://particle.dk/methods-analytical-laboratory/surface-area-bet-theory/ (accessed 24/07/13)

Bhatkhande, D. S., Pangarkar, V. G. and Beenackers, A. A. (2001). "Photocatalytic degradation for environmental application", *Chem, Thechn. Biotechn.* 77, 102-116.

Bizani, E., Fytianos, K., Poulios, I. and Tsiridis, V. (2006). "Photocatalytic decolorization and degradation of dye solutions and waste water in the presence of titanium dioxide" , *J. Hazard. Mater.* 136, 85-94.

Chao, H. Y., Cheng, J. H., Lu, J. Y., Chang, Y. H., Cheng, C. L. and Chen, Y. F. (2010). "Growth and characterization of type-II ZnO/ZnTe core-shell nanowire arrays for solar cell applications", *Superlatt. Micro.* 47, 160-164.

Chatterjee, D. and Saraf, K. B. (2002). "Visible light induced photodegradation of organic pollutants on dye adsorbed TiO_2 surface", *J. Photoch. Photobio. A: Chem.* 153, 199-204.

Christensen, A. N. (1992). "Hydrogen bonds in the structure of $BaC_2O_4.D_2O$", *Acta. Chemica. Scandinavica.* 46, 240-243.

Christensen, A. N., Hazell, R.G., Bell, A. M. T. and Altomare, A. (1994). "Precision of a crystal structure derived from A syncrotron X-ray powder pattern. The structure of barium oxalate hydrate, $BaC_2O_4.2H_2O$", *J. Phys. Chem. Solids.* 56, 1359-1362.

Clabough, W. S., Swiggard, E. M. and Gilchrist, R. (1956). "Preparation of barium titanyl oxalate tetrahydrate for conversion to barium titanate of high purity", *J. Research. Nation. Bureau. Stand.* 56, 2677.

Clark, R. J. H. (1968). "The chemistry of titanium and vanadium", *Amsterdam: Elsevier.*

Cox, P. A. (1995). "Transition metal oxides: an introduction to their electronic structure and properties", *Clardon Press, Oxford.* Page 105.

Dalal, P. V. and Saraf, K. B. (2006). "Growth and study of barium oxalate single crystal in agar gel", *Ind. Aca. Sci.* 29, 421-425.

Deneshvar, N., Aber, S. and Hosseinzadeh, F. (2003). "Study of C.I. acid orange 7 removal in contaminated water by photo oxidation processes", *Glob. Nest. J.* 10, 16-23.

Direct dyes : http://www.pburc.net/dyeing/directdyes.html (accessed 3/01/10).

Fang, T. T. and Lin, H. B. (1989). " Factor affecting the preparation of barium titanyl oxalate tetrahydrate", *J. Am. Ceram. Soc.* 72, 1899-1906.

Ferendez-Ibanez, P., Blanco, J., Malato, S. and Nieves, F. J. (2002). "Application of the colloidal stability of TiO_2 particles for recovery and reuse in solar photocatalysis", *Water Res.* 37, 3180-3188.

Ferendez, J., Kiwi, J., Beaza, J., Freer, J., Lizama, C. and Mansilla, H. D. (2004). "Orange II photocatalysis on immobilised TiO_2: effect of the pH and H_2O_2", *Appl. Catal. B.* 48, 205-211.

Fox, M. A. and Dulay, M. T. (1993). "Heterogeneous photocatalysis", *Chem. Reviews.* 93, 341-357.

Fujishima, A. and Honda, K. (1972). "Electrochemical photolysis of water at a semiconductor electrode", *nature.* 238.

Golubko, N. V. and Yanovskaya, M. I. (2000). "preparation of barium titanate and related materials by the alkoxide-hydroxide route", *J. Sol-Gel. Sci. Tech.* 20, 135-143.

Gomes da silva, S., Freire, R. S., and Duran, N. (2003). "Degradation and toxicity reduction of textile effluent by combined photocatalytic and ozonation processes", *Chemospere.* 40, 369-373.

Gotar, F. S., Perez-Maqueda, L. A. and Crido, J. M. (2003). "Synthesis of $BaTiO_3$ by applying the sample controlled reaction temperature(SCRT) method to the thermal decomposition of barium titanyl oxalate", *J. Euro. Ceramic. Soc.* 23, 505-513.

Grzechulska, J. and Morawski, A. W. (2002). "Photocatalytic decomposition of azo-dye acid black 1 in water over modified titanium dioxide" *Appl. Catal. B: Environ.* 36, 45-51.

Hammami, S., Bellakhal, N., Oturan, N., Oturan, M. A. and Dachraoui, M. (2008). " Degradation of acid orange 7 by electrochemically generated •OH radicals in acidic aqueous medium using boron-doped or platinum anode : A mechanistic study", *Chemosphere.* 73, 678-684.

Hachem, C., Bocquillon, O., Zahraa, O. and Bouchy, M. (2001). "Decolourization of textile industry wastewater by the photocatalytic degradation process", *Dye. Pigm.* 49, 117-125.

Houas, A., Lachheb, H., Ksibi, M., Elaloui, E., Guillard, C. and Herman, J. M. (2001). "Photocatalytic degradation pathway of methylene blue in water", *Appl. Catal. B: Environ.* 31, 145-157.

Hu, M. Z. C., Kurian, V., Payzant, E. A., Rawan, C. J. and Hunt, R. D. (2000). "Wet-chemical synthesis of monodispersed barium titanate particles hydrothermal conversion of TiO_2 microsheres to nanocrystalline $BaTiO_3$", *Powder. Technol.* 110, 2-14.

Jiehui, X., Wang, W., Sun, S. and Wang, L. (2012). "Enhancing visible-light-induced photocatalytic activity by coupling with wide-band-gap semiconductor : A case study on Bi_2WO_6/TiO_2", *Appl. Catal. B: Environ.* 111, 126-132.

Jung, W. S., Min, B. K., Park, J. and Yoon, D. H. (2011). "Formation mechanism of barium titanate by thermal decomposition of barium titanyl oxalate", *Ceramics. Inter.* 37, 669-672.

Kabra, K., Chaudhary, R. and Sawhney, L. (2004). "Treatment of hazardous organic and inorganic compounds through aqueous-phase photocatalysis ", *Ind. Eng. Chem. Res.* 43, 7683-7696.

Kangle, L., Zuo, H., Sun, J., Deng, K., Liu, S., Li, X. and Wang, D. (2009). "Bi, C and N codoped TiO_2 nanoparticles", *J. Hazard. Mater.* 161, 396-401.

Kanna, M., Wongnawa, S., Budde, S. and Dilokkhunakol, K. (2010). "Amorphous titanium dioxide: a recyclable dye remover for waste treatment", *J. Sol-Gel. Sci. Technol.* 53, 162-170.

Kawahara, T., Ozawa, T., Iwasaki, M., Tada, H. and Ito, S. (2003). "Photocatalytic activity of rutile-anatase coupled TiO_2 particles prepared by a dissolution-reprecipitation method", *J. Colliod. Interface. Sci.* 267, 377-381.

Keller, V. and Garin, F. (2003). "Photocatalytic behavior of a new composite ternary system: WO_3/SiC-TiO_2. Effect of the coupling of semiconductors and oxides in photocatalytic oxidation of methylethyl ketone in the gas phase", *Catal. Commun.* 4, 377-383.

Khollam, Y. B., Deshpande, A. S., Potdar, H. S., Deshpande, S. B., Date, S. K. and Patil, A. J. (2002). "A self-sustaining acid-base reaction in semi-aqueous media for synthesis of barium titanyl oxalate leading to $BaTiO_3$ powder", *J. Mater. Lett.* 55, 175-181.

Kim, H. R., Lee, T. G. and Shul, Y. G. (2007). "Photoluminescence of La/Ti mixed oxides prepared using sol-gel process and their PCBA photocomposition", *J. Photoch. Photobio. A: Chem.* 185, 156-160.

Konstantinou, I. K. and Albanis, T. A. (2004). "TiO_2-assisted photocatalytic degradation of azo dyes in aqueous solution: kinetic and mechanistic investigations", *Appl. Catal. B: Environ.* 49, 1-14.

Kumar, B. V. S., Sajan, C. P., Rai, K. M. L. and Byrappa, K. (2010). "Photocatalytic activity of TiO_2 : $AlPO_4$-5zeolite for dehradation of indigo carmine dye", *Indian. J. Chem. Techn.* 17, 191-197.

Lakshiminarasimhan, N., Bae, E. and Choi, W. (2007). "Enhanced photocatalytic production of H_2 on mesoporous TiO_2 prepared by template-free method: role of interparticle charge transfer", *J. Phys. Chem. C.* 111, 15244-15250.

Louer, M., Louer, D., Gotar, F. J., Criado, J. M. (1992). "Crystal structure of barium titanyl oxalate $BaTiO(C_2O_4)_2.4.5H_2O$", *J. Solids. Chem.* 92, 565-572.

Malghe, Y. S., Gujar, A. V. and Dharwadkar, S. R. (2004). "Synthesis of $BaTiO_3$ powder from barium titanyl oxalate (BTO) precursor employing microwave heating technique", *Bull. Mater. Sci.* 3, 217-220.

Maolin, Z., Sheng, G., Fu, J., An, T., Wang, X. and Hu, X. (2005). "Novel preparation of nanosized $ZnO-SnO_2$ with high photocatalytic activity by homogeneous co-precipitation method", *Mater. Lett.* 59, 3641-3644.

Maruska, H. P. and Ghosh, A. K. (1978). "Photocatalytic decomposition of water at semiconductor electrodes", *Solar. Energy.* 20, 443-458.

Mordant-dye : http://www.jagson.com/mordant-dye.htm (acessed 3/01/10).

Murunganandham, M., Shobana, N. and Swaminathan, M. (2005). "Optimization of solar photocatalytic degradation conditions of reactive yellow 14 azo dye in aqueous TiO_2", *J. Molecular. Catal. A: Chem.* 246, 154-161.

Nagaveni, K., Sivalingam, G. and Heged, M. S. (2004). "Photocatalytic degradation of dyes: high activity of combustion synthesized nano TiO_2", *Appl. Catal. B: Environ.* 48, 83-93.

Nandi, B. K., Goswani, A. and Purkait, M. K. (2009). "Removal of cationic dyes from aqueous solutions by kaolin: kinetic and equilibrium studies", *Appl. Clay. Sci.* 42, 583-590.

Nayak, H. and Bhatta, D. (2000). "Influence of γ-irradiation and Dy_2O_3 on the decomposition of barium oxalate: a thermogravimetric study", *Thermo. Chemica. Acta.* 362, 99-105.

Nur, H., Misnon, I. I. and Wei, L. K. (2007). "Stannic oxide-titanium dioxide coupled semiconductor photocatalyst loadded with polyaniline for enhanced photocatalytic oxidation of 1-octane", *Hindawi. Pub. Corp. Inter. J. Photoenergy.* 7, 1-6.

Orange II sodium salt dye : http://www.sigmaaldrich.com (accessed 3/01/10).

Osseoasare, K. and Arriagada, F. J. (1990). "Preparation of SiO_2 Nanoparticles in nonionic reverse miceller system", *Colloids. Surf.* 50, 321-339.

Parfitt, G. D. (1976). "Surface chemistry of oxides", *Pure. Appl.* 48, 415-418.

Potdar, H. S., Deshpande, S. B. and Date, S. K. (1999). "Chemical coprecipitation of mixed (Ba+Ti) oxalates precursor leading to $BaTiO_3$ powders ", *Mater. Chem. Phy.* 58, 121-127.

Potdar, H. S., Deshpande, S. B., Deshpande, A. S., Khollam, Y. B., Patil, A. J. and Pradham, S. D. (2001). "Simplified chemical route for the synthesis of barium titanyl oxalate (BTO)", *Int. J. Inorg. Mater.* 3, 613-623.

Randon, C., Wongnawa, S. and Boonsin, P. (2004). "Bleaching of methylene blue by hydrated titanium dioxide", *Sci. Asia.* 30, 149-156.

Reactive dye from Wikipedia, the free encyclopedia : http://en.wikipedia. org/wiki/ reactive _dye (accessed 3/01/10).

Reddy, K. M., Reddy, R. C. V. and Manorama, S. V. (2001). "Preparation characterization, and spectra studies on nanocrystalline anatase TiO_2", *J. Solids. Chem.* 30. 149-156.

Rhine, W. E., Hollock, R. B., Davis, W. M. and Wong-Ng, W. et al. (1992). "Synthesis and crystal structure of barium titanyl oxalate, $BaTi(O)(C_2O_4)_2.5H_2O$: A molecular precursor for barium titanate ($BaTiO_3$)" *Chem. Matter.* 4, 1208-1216.

Sauer, T., Neto, G. C., Jose, H. J. and Moreira, R. F. P. M. (2002). "Kinetic of photocatalytic degradatio of reactive dyes in a TiO_2 slurry reactor", *J. Photoch. Photobio. A: Chem.* 149, 147-154.

Senthilkumarr, S. and Porkodi, K. (2006). "Heterogeneous photocatalytic decomposition of crystal violet in UV-illuminated sol-gel derived nanocrystalline TiO_2 suspensions", *J. Colliod. Interface. Sci.* 288, 184-189.

Sharma, P. and Virk, H. S. (2009). "Fabrication of nanoparticles of barium carbonate/oxalate using reverse micelle technique", *Open. Surf. Sci. J.* 1, 34-39.

Sharma, Y. K., Kharkwal, M., Uma, S. and Nagarajan, R. (2009). "Synthesis and characterization of titanates of the formula $MTiO_3$ (M = Mn, Fe, Co, N and Cd) by co-precipitation of mixed metal oxalates", *Polyhedron.* 28, 579-585.

Shifu, C., Lei, C., Shen, G. and Genyu, C. (2005). "The preparation of coupled WO_3/TiO_2 photocatalyst by ball milling", *Powder. Techn.* 160, 198-202.

Shut, V., Kostomarov, S. and Gavrilov, A. (2008). "PTCR barium titanate ceramics obtained from oxalate-derived powder with varying crystallinity", *J. Matter. Sci.* 43, 5251-5257.

Silva, V. G., Wang, W. and Faria, J. L. (2006). "Photocatalytic and photochemical degradation of monm-, di-, and tri-azo dyes in aqueous solution under UV irradiation", *J. Photoch. Photobio. A: Chem.* 181, 314-324.

Skoog, D. A. and Leary, J. J. (1992). "Principle of instrumental analysis", *Philadelphia: Saunders collage publishing.*

Sreekantan, S., Noor, A. F. M., Ahmad, A. Z., Othman, R. and West, A. (2008). "Structural and electrical characteristic of crystalline barium titanate synthesized by low temperature aqueous method", *J. Mater. Process. Techn.* 195, 171-177.

Stylidi, M., Kondarides, D. I. and Verykios, X. E. (2004). "Pathways of solar light induced photocatalytic degradation of azo dyes in aqueous TiO_2 suspensions", *Appl. Catal. B: Environ.* 40, 271-286.

Sulfur dye : http://www.dyeman.com/dye%20summary.html (acessed 3/01/10).

Sun, C., Wang, N., Zhou, S., Hu, X., Zhou, S. and Chen, P. (2008). "Preparation of self-supporting hierarchical nanostructured anatase/rutile composite TiO_2 film", *Chem. Commun.* 28, 3293-3295.

Suwanchawalit, C. and Wongnawa, S. (2008). "Influence of calcination on the microstructures and photocatalytic activity of potassium oxalate-doped TiO_2 powders ", *Appl. Catal. A: Gen.* 338, 87-99.

Tan, X., Fan, Q., Wang, X. and Grambow, B. (2009). "Eu(III) sorption to TiO_2 (anatase and rutile): batch, XPS and EXAFS studies", *Environ. Sci. Technol.* 43, 3115-3121.

Thongsang, B. (2002). "The preparations and physical properties of barium titanate", *Master of science thesis of physics, Prince of songkla university.*

Trotman, E. R. (1975). "Dyeing and chemical technology of textile fibers", *Fifth edition, Charles Griffine, Co.ltd.*

Torr, A. P., Verma, A., Jotshi, C. K., Bajpai, P. K. and Singh, V. (2006). "Photocatalytic degradation of direct yellow 12 day using UV/TiO_2 in shallow pond slurry reactor", *Dyes. Pigm.* 68, 53-60.

Utrilla, J. R., Toledo, I. B., Garcia, M. A. F. and Castilla, C. M. (2001). "Activated carbon surface modifications by adsorption of becteria and their effect on aqueous lead adsorption", *J. Chem. Techn. Biot.* 16, 1209-1215.

Vat-dyes : http://en.wikipedia.org/wiki/vat-dyes (acessed 3/01/10).

Venkatachalam, N., Palanichamy, M. and Murugesan, V. (2007). "Sol-gel preparation and characterization of nanosize TiO_2: its photocatalytic performance", *Mater. Chem. Phys.* 104, 454-459.

Wang, H., Wu, Z., Liu, Y. and Sheng, Z. (2008). "The characterization of ZnO-anatase-rutile three-component semiconductor and enhanced photocatalytic activity of nitrogen oxides", *J. Molec. Catal. A: Chem.* 287, 176-181.

Wang, Z. C., Chen, J. F. and Hu, X. F. (2000). "Preparation of nanocrystalline TiO_2 powders at near room temperature from peroxide-polytitanic acid gel", *Mater. Lett.* 43, 87-90.

Wongkaew, A., Jansome, W. and Khemchan, S. (2010). "Synthesis of nanoparticles of mixed oxides containing titanium cerium silver and silicon: phase transformation", *Energy. Research. J.* 1, 73-77.

Xia, C. T., Shi, E. W., Zhong, W. Z. and Guo, J. K. (1995). "Preparation of $BaTiO_3$ by the hydrothermal method", *J. Europ. Ceram. Soc.* 15, 1171-1176.

Xie, Y. and Yuan, C. (2003). "Photocatalytic activity and recycle application of titanium dioxide sol for X-3B Photodegradation", *J. Molecul. Catal. A: Chem.* 206, 419-428.

Yanqing, Z., Erwel, S., Zhinzhan, C., Wenjun, L. and xingfang, H. (2001). "Influence of solution concentration on the hydrothermal preparation of titania crystalline", *J. Mater. Chem.* 11, 1547-1551.

Yin, H., Danzhen, L., Yi, Z., Wei, C., Yunhui, H., Yu, S., Xianzhi, F. and Guangcan, X. (2011). "BiVO$_4$/TiO$_4$ nanocrystalline heterostructure: a wide spectrum responsive photocatalyst towards the highly efficient decomposition of gaseous benzene", *J. Appl. Catal. B: Environ.* 104, 30-36.

Yu, C., Yang, K., Shu, Q., Yu, J., Cao, F. and Li, X. (2011). "Preparation of WO$_3$/ZnO composite photocatalyst and its photocatalytic performance", *J. Chin. J. Catal.* 32, 555-565.

Zainal, Z., Hui, L. H., Hussein, M. Z. and Ramli, I. (2005). "Removal of dyes using immobilized titanium dioxide illuminated by fluorescent lamps", *J. Hazards. Mater.* 125, 113-120.

Zhang, F., Zhao, J., Shen, T., Hidaka, H., Pelizzetti, E. and Serpone, N. (1998). "TiO$_2$-assisted photodegradation of dye pollutants II adsorption and degradation kinetics of Eosin in TiO$_2$ dispersions under visible light irradiation", *Appl. Catal. B.* 45, 147-156.

Zhang, J., Li, M., Feng, Z., Chen, J. and Li, C. (2006). "UV Raman spectroscopic study on TiO$_2$ phase transformation at the surface and in bulk", *J. Phys. Chem. B.* 110, 297-935.

Zhang, L. and Wan, M. (2003). "Polyaniline/TiO$_2$ composite nanotubes", *J. Physics. Chem. B.* 107, 6748-6753.

Zhang, Q., Gao, L. and Guo, J. (2000). "Effect of hydrolysis conditions on morphology and crystallization of nanosized TiO$_2$ powders", *J. Eur. Ceram. Soc.* 20, 2153-2158.

Zhang, X., Sun, D. D., Li, G. and Wang, Y. (2008). "Investigation of the roles of active oxygen species in photodegradation of azo dye AO7 in TiO$_2$ photocatalysis

illuminated by micro wave electrodeless lamp", *J. Photoch. Photobio. A: Chem.* 199, 311-315.

Zhang, Y. H. and Reller, A. (2001). "Nanocrystalline iron-doped mesoporous titania and its phase transition", *J. Mater. Chem.* 11, 2537-2541.

Zhao, W., Chen, C., Li, X., Zhao, J., Hidaka, H. and Serpone, N. (2002). "Photodegradation of sulforrhodamine-B dye in platinized titania dispersions under visible light irradiation : Influence of platinum as functional co-catalyst", *J. Phys. Chem. B.* 106, 5022-5028.

Zhu, C., Wang, L., Kong, L., Yang, X., Wang, L., Zheng, S., Chen, F., Maizhi, F. and Zong, H. (2000). "Photocatalytic degradation of azo dyes by supported TiO_2+UV in aqueous solution", *Chemoshere.* 41, 303-309.

VITAE

Name   Miss Petdaw Karoh

Student ID   5210220054

Birth Data   24 July 1985

Educational Attainment

Degree	Name of Institution	Year of Graduate
Bachelor of Science (Chemistry)	Prince of Songkla University	2008

Scholarship Awards during Enrollment

1. Center of Excellence for Innovation in Chemistry (PERCH-CIC)

2. Teaching Assistant, Department of Chemistry, Prince of Songkla University

List of Publication and Proceedings

1. Karoh, P. and Wongnawa, S. "Degradation of Dye Using M(II)-Titanium Compound Photocatalyst". International Congress for Innovation in Chemistry (PERCH-CIC Congress VII), Jomtien Palm Beach Hotel & Resort, Pattaya, Thailand, 4-7 May 2011.

2. Karoh, P. and Wongnawa, S. "Degradation of Dye Using Barium Titanium Oxalate Compound Photocatalyst" 14th Asian Chemical Congress 2011 (14 ACC), Queen Sirikit National Convention Center, Bangkok, Thailand. 5-8 September 2011.